Lehrstuhl für Fertigungstechnik und Betriebsorganisation

Peter A. Arrabiyeh

Electroless Plated Micro Pencil Grinding Tools: Conception, Manufacturing, and Application

Produktionstechnische Berichte aus dem FBK
Band 02/2021
Herausgeber: Prof. Dr.-Ing. Jan C. Aurich

TECHNISCHE UNIVERSITÄT
KAISERSLAUTERN

Lehrstuhl für Fertigungstechnik und Betriebsorganisation

Peter A. Arrabiyeh

Electroless Plated Micro Pencil Grinding Tools: Conception, Manufacturing, and Application

Produktionstechnische Berichte aus dem FBK
Band 02/2021
Herausgeber: Prof. Dr.-Ing. Jan C. Aurich

TECHNISCHE UNIVERSITÄT
KAISERSLAUTERN

Bibliografische Information Der Deutschen Bibliothek
Die Deutsche Bibliothek verzeichnet diese Publikation in der Deutschen Nationalbibliografie; detaillierte bibliografische Daten sind im Internet über **http://dnb.ddb.de** abrufbar.

Bibliographic information published by Die Deutsche Bibliothek
Die Deutsche Bibliothek lists this publication in the Deutsche Nationalbibliografie; detailed bibliographic data is available in the Internet at **http://dnb.ddb.de.**

Produktionstechnische Berichte aus dem FBK

Wissenschaftliche Schriftenreihe des
Lehrstuhls für Fertigungstechnik und Betriebsorganisation
der Technischen Universität Kaiserslautern

Herausgeber: Lehrstuhl für Fertigungstechnik und Betriebsorganisation
Prof. Dr.-Ing. Jan C. Aurich
Postfach 3049
Technische Universität Kaiserslautern
67653 Kaiserslautern

Verlag: Technische Universität Kaiserslautern

Druck: Technische Universität Kaiserslautern
Hauptabteilung 5
Abteilung 5.6 Foto-Repro-Druck

D-386

ISBN 978-3-95974-158-3
ISSN 0937-9061

Electroless Plated Micro Pencil Grinding Tools: Conception, Manufacturing, and Application

A dissertation approved by
the Department of Mechanical and Process Engineering
at Technische Universität Kaiserslautern
for the award of the doctoral degree
Doctor of Engineering (Dr. –Ing.)

to

Peter Amer Arrabiyeh

from Bamberg

Oral exam was held at the 9th of April 2021

Promotion committee:

Chairman:	Prof. Dr. –Ing. Peter Mitschang
1st rapporteur:	Prof. Dr. –Ing. Jan C. Aurich
2nd rapporteur:	Prof. Dr. –Ing. Jörg Seewig

Kaiserslautern, 2021

D 386

Preface

"Courage is the magic that turns dreams into reality."
Richter Abend in Tales of Symphonia: Dawn of a New World

This dissertation contains the results that I attained during my employment period at the Institute for Manufacturing Technology and Production Systems Kaiserslautern (FBK) between the December of 2014 and March 2020. I had to research the process from the ground up to improve upon the tools previously manufactured at our institute. What really struck a chord with me is that no one is documenting the basics of micro grinding with micro pencil grinding tools in a way that allows a newcomer to grasp the essence of the process; which is why the subject matter in this Dissertation is aimed to help newcomers get into the manufacturing and application of micro pencil grinding tools, while at the same time advancing the state of the art to the next level.

I first and foremost need to thank Professor Jan C. Aurich for taking a gamble on an engineer who has never worked in the field manufacturing science before and for believing in me wholeheartedly through my employment period at FBK, it was an absolute honor working for you. To Professor Jörg Seewig, I thank you for taking on the request of becoming my 2nd rapporteur, it meant a lot to me. Knowing that you were part of the committee, made me work twice as hard, preparing for the oral exam because I know that you are a tough examiner and I did not want to embarrass myself too much. I also thank Professor Peter Mitschang for taking the role of chair of the committee, the exam went extra smoothly thanks to your involvement. I am also honored to say, that as of the moment I am writing this, you are my new boss.

I thank Marius Heintz, Martin Bohley, and Hendrik Hotz for taking the time to discuss the results of this dissertation with me and to give me the criticism needed for me to improve this dissertation. I also thank the technical personnel Michael Lutzke, Henry Welz, Oliver Benz, Philipp Schmittat, and Lucas Hartmann for making sure that I always had what I needed for my research. In addition, I would also like to thank Rosemarie Schleret for all the help I received over the years and especially at the final stages of the dissertation – you are truly a treasure to the employees of FBK.

To Benjamin Kirsch, with whom I had critical discussions regarding almost all of my results and discoveries, who endured my persistence whenever I had a hunch, and who improved my scientific writing over the years, you have my gratitude.

To my dear senior colleagues Martin Bohley, Ingo Gustav Reichenbach, and Christopher Müller, who showed me the ropes around the lab, who knew how to deal with my hot tempered-personality, who were always kind and supportive of me, who were always there when things didn't go as smoothly as I envisioned. I owe each of you a great debt of gratitude.

I also owe a huge debt of gratitude to the numerous students who supported me throughout the years, especially towards Marius Heintz, who helped me push the boundaries of the process to the next level, and who ultimately became one of best micro grinders out there.

To my first roommate Lukas Heberger. You were generally perhaps the purest soul of all of us; you were always kind and helpful. I really enjoyed our brief time together in what we called "The Nintendo Club" back in the day. To my other roommates Vandeet Raval, Stefan Gutwein,

and Daniel Weber, I had a great although brief time with each of you. I apologize to all three of you because you had to endure the low-volume music, constantly coming out of my speakers.

Finally, I would like to thank my parents Mahmoud and Elke Monika Arrabiyeh for supporting me on this long journey. I was born in Bamberg, Germany; I grew up in Nazareth, Israel and returned as an immigrant. My journey started on the night of the 3rd of September 2005. It was a long and tough journey, but my parents were always there to aid me with everything they could from a large distance, making sure I always had a roof above my head and an ear that listens. Now that I am writing this preface, my journey ends and I can finally embark on a new journey with my beautiful wife Asil and hopefully little Mahmoud and his siblings soon.

August 2021, Kaiserslautern Peter A. Arrabiyeh

Abstract

Modern microtechnology has the central task of ensuring technological progress through the miniaturization and reduction of component dimensions. Micro grinding with micro pencil grinding tools (MPGTs) has established itself as a manufacturing process in microtechnology, especially for the machining of hard and brittle materials. The process has been investigated by numerous researchers. Yet, tools with diameters of <100 µm, could not satisfy the needs of the industry. The tool life of MPGTs was insufficient, their feed rates were too slow for a meaningful application and both the MPGTs, and their microstructures were not reproducible. Therefore, this dissertation is dedicated to the task of investigating and revising the complete manufacturing process and application methodology of these tools. New substrate geometries and materials are investigated. Surface treatment methods are investigated to increase adhesion between the abrasive layer and the substrate. In addition, conventional coating processes like electroplating are replaced by an autocatalytic electroless plating process, that has a much higher reproducibility rate of MPGTs with diameters of about 50 µm and less. The micro grinding methodology is optimized by parameter studies, and new coolant supplying methods with new metalworking fluids, which are introduced to achieve the best possible result when machining 16MnCr5.

Kurzfassung

Die moderne Mikrotechnik hat die zentrale Aufgabe, den technologischen Fortschritt durch die Miniaturisierung und Reduzierung von Bauteildimensionen zu gewährleisten. Besonders für die spanende Bearbeitung von sprödharten Werkstoffen hat sich das Mikroschleifen mit Mikroschleifstiften als ein Fertigungsverfahren in der Mikrotechnik etabliert. Das Verfahren ist von zahlreichen Forschern untersucht worden. Jedoch konnten Werkzeuge mit Durchmessern von <100 µm, die Bedürfnisse der Industrie nicht befriedigen. Die Standzeit der Mikroschleifstifte war unzureichend und die Vorschubsgeschwindigkeiten waren zu langsam für eine sinnvolle technische Anwendung. Sowohl die Mikroschleifstifte als auch die mit Ihnen geschliffenen Mikrostrukturen waren nicht oder nur bedingt reproduzierbar. Deswegen widmet sich diese Dissertation der Aufgabe, den kompletten Herstellungsprozess und die Anwendungsmethodik dieser Werkzeuge zu untersuchen und zu überarbeiten. Dabei werden auch neue Rohlingsgeometrien und -werkstoffe untersucht. Oberflächenbehandlungsmethoden werden untersucht, um die Haftfestigkeit zwischen Abrasivschicht und Rohling zu erhöhen. Zudem werden konventionelle Beschichtungsverfahren wie das galvanische Beschichtungsverfahren durch ein autokatalytische ablaufendes chemisches Beschichtungsverfahren ersetzt, dass eine viel höhere reproduzierbare Herstellung für Mikroschleifstifte mit Durchmesser von ca. 50 µm (oder weniger) hat. Die Methodik des Mikroschleifens wird durch Parameterstudien, neue KSS-Zuführmethoden mit neuen KSS optimiert, um bei der Bearbeitung von 16MnCr5, die bestmöglichen Ergebnisse zu erzielen.

Table of Contents

Deutsche Zusammenfassung – German Summary

Der Trend zur Miniaturisierung von Bauteilen ist ein zentrales Thema in der Produktentwicklung, das zahlreiche neue Fertigungsprozesse ins Leben gerufen hat. Zu diesen Herstellungsverfahren gehören berührungslose Verfahren wie die Laserbearbeitung, die Funkenerosion oder lithografische Verfahren, bei denen Werkstücke mit einer lichtempfindlichen Resistschicht bedeckt und mit Hilfe von ultraviolettem Licht oder Elektronenstrahlen mikrostrukturiert werden. Der mikrostrukturierte Bereich auf der Resistschicht dient entweder dazu, Material durch Nassätzen vom Werkstück zu entfernen oder Material über Galvanikprozesse aufzutragen.

Mit der Verbesserung der Fertigungstechniken entstand ein weiterer Trend: die Herstellung neuer Mikrowerkzeuge für die Mikrobearbeitung. Mit Mikrowerkzeugen können komplexe Mikrokanäle mit Hilfe von CNC-gesteuerten Werkzeugmaschinen bei minimaler Probenvorbereitung direkt hergestellt werden. Mikrobearbeitungsprozesse eignen sich daher für die Fertigung von Kleinserien und Prototypen. Zu diesen Mikrowerkzeugen gehören Mikrofräser, Mikrobohrer, Dicing Blades und Mikroschleifstifte.

Mikroschleifstifte bestehen aus einem zylindrischen Schaft sowie Schleifmittel aus Diamant oder kubisches Bornitrid (cBN) und einer Metallmatrix aus Nickel, die mit dem Schaft verbunden werden. Diese Mikrobearbeitungswerkzeuge nutzen sowohl ihren Umfang als auch ihre Stirnseite bei der Herstellung von Mikrokanälen in sprödharten Werkstoffen. Mikroschleifstifte sind in der Lage jede Art von geschlossener Struktur herzustellen. Dabei können Mikroschleifstifte benutzt werden, die Mikrokanäle mit verschiedenen Querschnittsgeometrien herstellen können. Diese Queschnittsgeometrien können auch Hinterschneidungen ermöglichen.

Aufgrund ihrer kleinen Durchmesser haben Mikroschleifstifte relativ niedrige Schnittgeschwindigkeiten, die ihre erreichbaren Vorschubsgeschwindigkeiten und ihre Werkzeugstandzeiten im Vergleich zu größeren Schleifwerkzeugen, wie Dicing Blades oder konventionellen Schleifscheiben begrenzen. Ziel dieser Dissertation war es, Methoden zu entwickeln, um sowohl die Werkzeugstandzeit als auch die Vorschubgeschwindigkeiten deutlich zu verbessern. Um dieses Ziel zu erreichen, erforderte der auf Vorarbeiten basierende Werkzeugherstellungsprozess eine umfassende Überarbeitung, die den Substratwerkstoff, der Substratherstellungsprozess, die Substratgeometrie und den Beschichtungsprozess umfasste. Darüber hinaus wurden aus dem Stand der Technik, Kühlschmierstoff-(KSS) Zuführmethoden und KSS adaptiert und eingesetzt, um sowohl eine höhere Werkzeugstandzeit als auch eine höhere Oberflächenqualität zu erreichen. Es wurden neue Bearbeitungsmethoden sowie zahlreiche Parameterstudien durchgeführt.

Ein chemisches Beschichtungsverfahren wurde entwickelt, um das galvanische Beschichtungsverfahren zu ersetzen, das vorwiegend zur industriellen Herstellung von Mikroschleifstiften eingesetzt wird. Zusätzlich wurde ein neues Oberflächenbehandlungsverfahren entwickelt, das aus elektrolytischer Entfettung, elektrochemischen Abtragen, einem Beizverfahren und einer galvanischen Vorbeschichtung besteht. Der Hauptbeschichtungsprozess wurde auf einer Heizplatte mit Magnetrührer durchgeführt, der die Beschichtungslösung auf eine Temperatur von 87 °C ± 1 °C erwärmte. Die Schleifmittel wurden der Lösung zugegeben. Durch ein konstantes Nickelwachstum wird das Schleifmittel während des Prozesses in die Schleifschicht eingebettet. Die Schleifmittel erreichen die Oberfläche des Substrats durch Aufwirbelung der Lösung

durch den Rührmagneten – gleichzeitig, dreht sich der Rohling über einen kleinen Elektromotor. Die Lösung besteht aus 30 g/L Nickel(II)-sulfat-Hexahydrat, 20 g/L Natriumhypophosphit, 20 g/L Natriumacetat, 0,4 mg/L Thioharnstoff und Salzsäure.

Die Thioharnstoffkonzentration wurde in einer Parameterstudie bestimmt. Es stellte sich heraus, dass ein Bereich von 0,4-0,5 mg/L die größte Prozesssicherheit und das höchste Nickelwachstum gewährleistet; ein Nickelwachstum von 21 µm/h wurde bei einer Thioharnstoffkonzentration von 0,4 mg/L gemessen. Die Einbettungszeit für diverse Korngrößen und die Rohlingsdrehzahlen wurden ebenfalls untersucht – eine zu hohe Drehzahl erzeugt ein ungleichmäßiges Nickelwachstum. Mit diesem Verfahren wurden Schleifstifte mit verschiedenen Durchmessern und unterschiedlichen Korngrößen beschichtet; wobei für die Zerspanuntersuchungen lediglich ein Werkzeugdurchmesser von 50 µm verwendet wurde.

Bei den Bearbeitungsversuchen wurden gehärtete Stahlproben aus 16MnCr5 mit einer Härte von ca. 665 HV30 verwendet. Es wurde festgestellt, dass die Trockenbearbeitung nahezu unmöglich ist, weshalb eine KSS-Studie erforderlich war. Es wurde ein MQL-System mit einem KSS aus destilliertem Wasser und Natriumdodecylsulfat (SDS) entwickelt. Zunächst, wurde im KSS nur eine SDS-Konzentration von 0,02 g/L verwendet. Im Gegensatz zu Versuchen mit Trockenbearbeitung und der Bearbeitung mit destillierten Wasser, gelang es mit Hilfe des neuen KSS, 0,5 mm lange und 5 µm tiefe Mikrokanäle bei einer Drehzahl von 30.000 U/min bei Vorschubgeschwindigkeiten von 0,05 mm/min und 0,1 mm/min herzustellen – die Mikroschleifstifte hatten eine Korngröße von 2-4 µm. Aufbauend auf diesen ersten Ergebnissen wurde eine größere Parameterstudie durchgeführt und mittels Varianzanalyse (ANOVA) bewertet. Diese Parameterstudie bestand aus einer vollfaktoriellen Parameterstudie, bei der die Parameter Vorschubgeschwindigkeit (0,1 mm/min und 0,2 mm/min), Drehzahl (30.000 min^{-1} und 50.000 min^{-1}), Korngröße (1-2 µm und 3-6 µm) und Werkzeugneigungswinkel (0° und 2°) untersucht wurden. Im KSS wurde eine SDS-Konzentration von 1% verwendet, die Mikrokanäle waren dieses Mal 1 mm lang und 5 µm tief. Die wichtigsten Ergebnisse waren:

- Eine größere Korngröße erhöht die Werkzeugstandzeit, während sowohl höhere Drehzahlen als auch das einstellen eines Neigungswinkels die Werkzeugstandzeit reduziert. Eine höhere Drehzahl bedeutet, dass jedes Korn an der Stirnseite des Werkzeugs, weniger Material pro Umdrehung entfernt, die Prozesskräfte reduziert und somit die Werkzeugstandzeit erhöht. Im vorliegenden Fall wurde jedoch durch die Analyse der verwendeten Mikroschleifstifte mittels Rasterelektronenmikroskop (REM) und energiedispersiver Röntgenspektroskopie (EDX) bestimmt, dass die Stirnseite der Schleifstifte mit Eisenanhaftungen bedeckt sind. Die Werkzeuge versagen somit wegen erhöhter Reibungstemperaturen bei höheren Drehzahlen. Anhaftungen sind ein Zeichen für mangelnde Schmierung, daher ist das verwendete KSS für den Prozess nicht ausreichend.
- Die Oberflächenqualität der Mikrokanäle schwankte durch die Bildung sogenannter Substrukturen. Substrukturen sind kleinere Mikrokanäle, die sich am Nutgrund eines Mikrokanals bilden. Unterschiedliche Kornverteilungen, Werkzeugveschleiß und Maschinenfehler werden als die Ursache für Substrukturen erkannt. Die Bildung von Substrukturen könnte die Funktion der Mikrokanäle beeinträchtigen, da sie die Gesamtkanaltiefe reduziert.

Um das Substrukturenproblem zu beheben, wurde ein am FBK entwickeltes Funkenerosionsverfahren eingesetzt, um kleine Kavitäten an der Stirnseite von Mikroschleifstiften aufzubringen – Kavitäten mit Durchmessern von 20-25 µm. Dadurch wird die minimale Breite der Substrukturen erhöht und deren Tiefe verringert. Dadurch wird zugleich der Einfluss von Substrukturen auf die Rauheitswerte reduziert. Die Ergebnisse wurden auch mit Mikroschleifversuchen die mit um 2° geneigter Spindel durchgeführt worden sind verglichen. Schleifstifte mit Kavitäten erzeugten breite Substrukturen, die nur wenige hundert Nanometer tief waren. Geneigte Schleifstifte hingegen, produzierten konkave Mikrokanäle. Die während des Prozesses entstandenen Adhäsionen konzentrierten sich großteils in der Kavität. Zusätzlich konnte die Werkzeugstandzeit verbessert werden, da sich Adhäsionen eher in der Kavität ansammelten und nicht auf der Schleifschicht.

Um die Werkzeugstandzeit der Werkzeuge weiter zu erhöhen, wurde eine neue KSS-Zuführmethode eingeführt: das Tauchkühlschmieren. Die Bearbeitung erfolgte in einem Becken, dass mit KSS gefüllt war. Eingebaute Mikrometerschrauben wurden verwendet, um den Montagewinkel des Werkstücks so einzustellen, dass die Werkstückoberseite planparallel zum Achsverlauf des Kreuztisches liegt. Mit dieser KSS-Zuführmethode wurde eine weitere Fallstudie initiiert, in der sieben verschiedene KSS getestet wurden. Mikroschleifstifte mit einer Korngröße von 5-10 µm wurden zur Herstellung von 3 mm langen und 5 µm tiefen Mikrokanälen eingesetzt. Die Durchführung erfolgte bei einer Drehzahl von 30.000 min^{-1} und einer Vorschubsgeschwindigkeit von 1 mm/min. Das Bewertungskriterium der Experimente war die Menge an Anhaftungen an der Stirnseite der Mikroschleifstifte. Die KSS "Twinmax" und "Lubrimax Edel C", zwei pflanzliche, hochviskose Schneidöle der Firma Steidle GmbH, lieferten die besten Ergebnisse und erreichten Anhaftungenskonzentrationen von weniger als 5%.

Ein Pendelschleifverfahren wurde auf das Mikroschleifverfahren adaptiert. Bei diesem Pendelschleifverfahren wurde die erforderliche Mikrokanaltiefe durch eine stufenweise Zustellung von 0,5 µm erreicht. Die Vorschubgeschwindigkeit wurde für Mikroschleifstifte mit einer Korngröße von 5-10 µm auf Werte von 30-60 mm/min bei einer Drehzahl von 30,000 min^{-1} erhöht. Gleichzeitig wurde die Grabenbreite erhöht, um mehr Durchfluss von KSS in den Bearbeitungsbereich zu garantieren. Nachdem das Werkzeug die gesamte Grabenlänge erreicht hat, trägt es 4 µm mehr in der Breite ab und fährt in Gegenrichtung wieder zurück zum Startpunkt. Die Z-Achse bewegt sich während des Prozesses nur nach unten, um Positionierfehler die als Folge eines Umkehrspiels entstehen zu vermeiden. Es wurde ein Standzeituntersuchungsverfahren entwickelt, bei dem das Pendelschleifen in Kombination mit dem Tauchkühlschmierverfahren eingesetzt wurde. In dieser Standzeituntersuchung wurden 5 mm lange und 50 µm tiefe Mikrokanäle mit verschiedenen Parameterkombinationen geschliffen. Jeder Versuch wurde achtmal wiederholt, da frühere Experimente eine recht hohe Standardabweichung zeigten. Es wurde eine kleine Versuchsreihe mit den Basisparametern: Drehzahl 30.000 min^{-1}, Korngröße 5-10 µm, Vorschub 30 mm/min und dem KSS "Twinmax" durchgeführt. Die folgenden Experimente wurden mit dieser Methode durchgeführt:

- Die KSS "Twinmax" und "Lubrimax Edel C" wurden ein zweites Mal gegenübergestellt. Die erreichten Mittelwerte lagen bei 35,9 µm ± 13,2 µm für "Twinmax" und 33,3 µm ± 10,4 µm für "Lubrimax Edel C". Die Differenz der Mittelwerte galt als sta-

tistisch unbedeutend, allerdings waren vier der Werkzeuge, die mit "Twinmax" eingesetzt worden sind, nach den Versuchen noch einsetzbar und nur ein Werkzeug das mit "Lubrimax Edel C" eingesetzt wurde.

- Der Einfluss der Drehzahlen 10.000 min^{-1}, 30.000 min^{-1} und 50.000 min^{-1} auf die Standzeit wurde in Mikroschleifversuchen verglichen. Die Ergebnisse zeigten deutlich, dass die höchste Drehzahl am besten geeignet ist.
- Die Korngrößen 4-8 µm, 5-10 µm und 6-12 µm wurden gegenübergestellt. Das Ergebnis war, dass für einen Durchmesser von 50 µm die Korngröße 5-10 µm am besten geeignet ist.
- Es wurden Mikroschleifstifte mit einer Kavität und Mikroschleifstifte ohne Kavität in Mikroschleifversuchen verglichen. Die Ergebnisse zeigten, dass eine Kavität die Werkzeugstandzeit auf etwa ein Drittel (14,5 µm ± 9,8 µm) reduziert.

In einer darauffolgenden Untersuchung wurde eine andere Werkzeugmaschine mit einer Spindel verwendet, die höhere Drehzahlen ermöglicht. Mit einer Drehzahl von 120.000 min^{-1} wurden Mikroschleifversuche mit Vorschubgeschwindigkeiten von 120 mm/min und 240 mm/min durchgeführt. Die Ergebnisse die mit einer Vorschubgeschwindigkeit von 120 mm/min erzielt worden sind wurden zunächst mit denen die mit einer Vorschubsgeschwindigkeit von 120 mm/min bei einer Drehzahl von 30,000 min^{-1} verglichen, um zu untersuchen, ob das Verhältnis zwischen Vorschubsgeschwindigkeit und Drehzahl hochskaliert werden kann; die Hochskalierung konnte zwar nicht vollständig erreicht werden, aber die Ergebnisse lagen von einem zum anderen innerhalb der Fehlertoleranzgrenze. Beim Vergleich von den Grabentiefen die mit Vorschubgeschwindigkeiten von 120 mm/min und 240 mm/min erreicht worden sind, konnte ein fast linearer Zusammenhang zwischen Vorschubsgeschwindigkeit und erreichte Grabentiefe festgestellt werden.

Symbols and Abbreviations

Roman alphabet

2D	Two dimensional
3D	Three dimensional
a	Cutting depth in µm
A	Rotational axis
Acc. to	According to
a_e	Width of cut in µm
AISI	American Iron and Steel Institute
Al_2O_3	Aluminum oxide
ANOVA	Analysis of variance
a_p	Depth of cut in µm
b	Edge breakout width in µm
C	Carbon
C_1	Static cutting-edge density
C_{60}	Unalloyed steel with about 0.6% carbon
CAD	Computer aided design
CADCAM	Computer aided manufacturing
cBN	Cubic boron nitride
CCD	Charge-coupled device
CE	Capillary electrophoresis
CIRP	The international academy for production engineering
Cl	Chlorine
CNC	Computerized numerical control
Co. KG.	Compagnie Kommanditgesellschaft
Cr	Chrome
CRC	Collaborative research center
CVD	Chemical vapor deposition
D	Diameter in mm
d_E	Diameter of µelectrode in µm
DIN	Deutsche Institut für Normung
d_M	Diameter of cavity in µm
DNA	Deoxyribonucleic acid
d_s	Substrate tooltip diameter in µm
e^-	Electron
E	Modulus of elasticity in N/mm^2
EBSD	Electron backscatter diffraction
ECM	Electrochemical machining
EDM	Electrical discharge machining
EDX	Energy dispersive X-ray
E.g.	Example given
Et al.	And the other authors
Etc.	Et cetera
f	Frequency in Hz
Fe	Iron
FIB	Focused ion beam
FBK	Institute for Manufacturing Technology and Production Systems Kaiserslautern
F_N	Normal force in N
F_t	Tangential force in N
F_c	Cutting force in N
F_f	Feed force in N
f_z	Feed per rotation in mm
GmbH	Gesellschaft mit beschränkter Haftung
H	Hydrogen
H	Hardness
H_D	Depth of thermally damaged zone in µm
h_{cu}	Chip thickness in µm
$h_{cu,crit}$	Critical chip thickness in µm
$h_{cu,eff}$	Effective chip thickness in µm

$h_{cu,max}$	Maximum undeformed chip thickness in µm
h_M	Depth of cavity in µm
HSS	High speed steel
HV30	Vickers hardness with an experimental load of 30 kg
i_e	Peak current in mA
IRTG	International research training group
IWF	Institut für Werkzeugmaschinen und Fertigungstechnik in Braunschweig
j	Number of grits on circumference
K_c	Critical fracture toughness in $Pa \cdot m^{0.5}$
L	Length in mm
Laser	Light amplification by stimulated emission of radiation
LBM	Laser beam machining
LED	Light emitting diode
LIGA	Lithography, electroplating and molding
l_s	Substrate tooltip length in µm
m	Average shape of cutting edges
Mn	Manganese
Mo	Molybdenum
MPGT	Micro pencil grinding tool
MQL	Minimum quantity lubrication
MWF	Metal working fluid
n	Rotational speed in rpm
Na	Sodium
NA	Numerical aperture
Ni	Nickel
Ni-P	Phosphorous nickel
No.	Number
O	Oxygen
OptiAdi	Project: Optimierung der Werkzeugstandzeit bei der Zerspanung duktiler ADI-Werkstoffe
p	Static cutting-edge density in cutting edges/mm^2
P	Phosphor
P_k	Working plane
PMMA	Polymethylmethacrylate
PTFE	Polytetrafluoroethylene
R_a	Arithmetic mean roughness value in nm
R_z	Mean roughness depth value in nm
s	Distance grit travels each rotation in µm
S	Sulfur
SDS	Sodium dodecyl sulfate
SEM	Scanning electron microscope
Si	Silicon
S_G	Spark gap in µm
t_e	Discharge duration in s
t_i	Pulse duration in s
TIR	Total indicated run-out in µm
Tµ	Grit cutting depth in nm
u_o	Supply voltage in V
u_e	Discharge voltage in V
$\dot{V}$	Liquid flow rate in ml/h
v_c	Cutting speed in mm/s
v_f	Feed rate in mm/min
v_e	Effective cutting speed in mm/s
v_E	Feed rate in EDM process in µm/min
W_e	Discharge energy in Watt
WEDG	Wire electrical discharge grinding
Wt.%	Weight percentage

z	Grit size in µm

Greek alphabet

α	Tool angle in °
α_k	Contact angle in °
η	Cutting angle of grits in °
κ	Electrical conductivity value in $S \cdot m^{-1}$
λ	Distance between grits on circumference of grinding wheel in µm
µ	Micro
µEDM	Micro electrical discharge machining
µTAS	Micro total analysis systems
ψ	Correction factor
ϑ	Form factor of grits

1 Introduction into the Art of Micro Grinding

„There's Plenty of Room at the bottom," words made famous in a lecture held by physicist Richard Feynman at the annual American Physical Society meeting at Caltech in 1959 [Feyn91]. In his speech, he speculated reconstructing materials on an atomic level and challenged researchers around the world to find ways to manipulate and control mater on a small scale [Godd12]. FEYNMAN offered a prize of 1000 $ to the first person to show him a rotating electric motor that is not larger than $1/64^{th}$ $inch^2$ (0.3968 mm^2), a challenge completed in November 1960 by craftsman William McLellan (Figure 1-1) [Worl60]. MCLELLAN spent his lunch breaks for 2.5 months, building the motor with the help of a microscope, a watchmaker's lathe and a toothpick [Tiny86].

A second prize was offered to the first person to show him the entire Encyclopedia of Britannica fit on the head of a pin – a feat that requires a scaling 1/25000 [Feyn95]. A Stanford graduate student named Tom Newman collected the prize money in 1985. NEWMAN used an electron beam lithography process to etch the opening page of Charles Dickens' A Tale of Two Cities on an area of 5.9 µm x 5.9 µm (Figure 1-1) [Tiny86]. Each character was about 50 nm wide [Grig09].

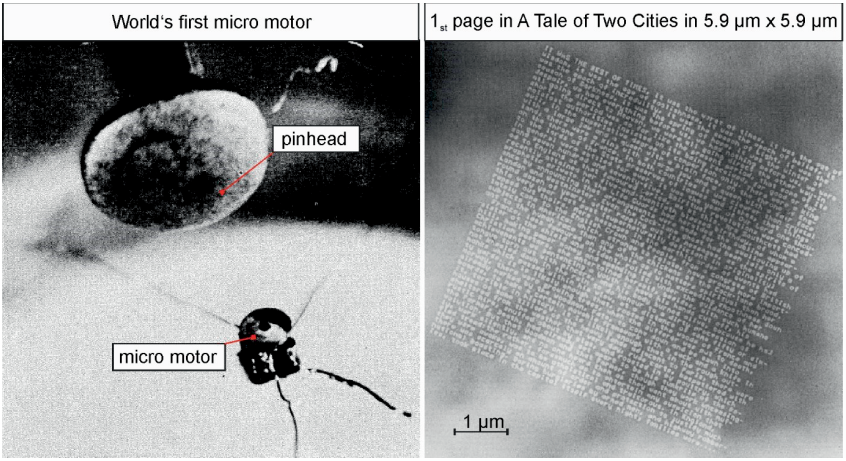

Figure 1-1: World's first micro motor [Worl60] and text etched in an area of 5.9 µm x 5.9 µm [Tiny86]

Since then, a global trend in miniaturization has become a central topic in product development. An increasing necessity to reduce the size of mechanical and electrical components has emerged, making micro and nano production, critical technologies of the 21st century [Engm11]. The progression of the semiconductor, telecommunication and biotech industries required new manufacturing methods to miniaturize products while adding new and improved functions [Liao05]. An example from the micro total analysis systems (µTAS) is the emergence of capillary electrophoresis (CE) microchips. CE chips are establishing themselves as essential microfluidic components in the field of deoxyribonucleic acid (DNA) sequencing [Schl01]. These microchips demonstrate superior performance over conventional systems for high

throughput capillary DNA analysis that accelerates research and new drug discoveries [Lach06]. All done by a miniaturized lab that fits in the palm of one's hand [Arra19c].

A common method to manufacture microstructured parts is using photolithographic techniques, similar to the one NEWMAN used to complete FEYNMAN's challenge in 1985. In these techniques, a light-sensitive resist layer is applied to the workpiece surface. A precise ultraviolet light beam [Wens02] or an electron beam used by NEWMAN [Feyn95], removes parts of the resist, forming nano- or microchannels on the applied layer. Following that, material can be removed from the workpiece through these channels, using processes like isotropic wet etching [Sait08] or powder blasting [Schl01]. Material can also be added using an electroplating process – a process commonly known as LIGA (Lithography, Electroplating, and Molding). After either adding material to or removing material from the channels, the resist layer is removed [Sail09]. These processes are suitable for both mass production and hybrid applications.

Alternatively, processes that employ Laser (light amplification by stimulated emission of radiation) [Schw03] or focused ion beam (FIB) [Pica03] have been used to selectively melt material, producing micro/nanostructured surfaces. Micro electrical discharge machining (µEDM) uses a microelectrode to conduct spark impulses to a workpiece surface, melting selected areas with temperatures of up to 40000 K [DiBi89]. Micro molding as the name states is a process in which micro molds are manufactured using a different micro manufacturing process. Micro components like microlenses can then be produced via casting [Suzu01].

A recent emerging trend is using micromachining processes like micro milling [Auri12], micro drilling [Aziz12b], and micro grinding [Auri09], in combination with highly precise machine tools to manufacture microchannels/holes in a broad range of materials [Dorn06]. These three processes are suitable to produce unique microstructures as well as small batch production cycles. Micro grinding via dicing blades, for example, a process that uses thin grinding wheels is often used in the semiconductor industry to cut silicon wafers and to produce open-textured surfaces [Park10].

Shaft tools like micro end mills or micro drills can be manufactured using processes like µEDM [Egas11a] or dicing [Auri12]. The tool manufacturing methods are fast and allow for tailormade micro cutting tools that can be used to manufacture microchannels with unique cross-sections. A CNC (computerized numerical control) based control system enables the user to scribe any structure desired and allows for quick program optimizations, enabling rapid prototyping [Arra17b]. One of these micro cutting processes is micro grinding with micro pencil grinding tools (MPGTs) micro tools that have a cylindrical micro tip that consists of a cemented carbide or steel base body and an abrasive layer; this abrasive layer comprises of superabrasives like diamond and cBN (cubic boron nitride) grits and a metallic binder [Hoff02]. It can be said, that micro end mills and micro drills are the cutting tools for softer materials that would clog the abrasive layer of MPGTs and that MPGTs are used on harder and more brittle materials that would break other micro tools.

Every process mentioned has its advantages and disadvantages. This dissertation will not focus on comparing these processes, but on manufacturing and using one of the most underutilized tools in micromachining: micro pencil grinding tools. Due to their small diameters, MPGTs have relatively low cutting speeds that limit their achievable feed rates and tool life, when compared to larger grinding tools such as dicing blades or conventional grinding wheels. PARK et

al. [Park10] conducted a parameter study for MPGTs with diameters of 100 µm by micro structuring silicon workpieces. They manufactured the abrasive layer using an electroless plating method. Channel lengths of up to 650 mm at a feed rate of 2.4 mm/min were achieved – results that looked promising for industrial use. This dissertation will combine the advanced machinery at the Institute for Manufacturing Technology and Production Systems Kaiserslautern (FBK), with the basics of PARK et al.'s tool manufacturing process to find ways to improve the process while decreasing the tool size to diameters below 50 µm. In his reference book "Fertigungstechnik," KÖNIG stated "The technological reserves of machining processes can only be exploited if the basics of the process are also known" [Köni80], which exactly what needed to be done here. This dissertation will as the title suggests not only focus on the more delicate points in tool manufacturing and the micro grinding process but also show the reader the conception method, allowing for alternative solutions to the problems discussed and solved in this dissertation.

2 State of the Art: Micro Grinding

2.1 Micro Machining via Micro Grinding

Micro-grinding is a manufacturing process used in micro-technology for single-unit production or prototype development to process hard and brittle materials [Carr16]. According to CHENG, the distinction between conventional grinding and micro grinding is made when the structures produced with the process have a dimension of less than 1000 µm in two directions in space [Chen13].

The most prominent micro grinding tools are MPGTs and thin grinding wheels. This section shows what each tool is, how it is used, and what it is used for. A comparison between both processes in terms of process kinematics and applications is presented, showing the strengths and weaknesses of each process.

2.1.1 Application fields

One of the first scientists to coin the term micro grinding was OKANO et al. in 1993 [Okan93]. The term describes micromachining processes that use miniaturized grinding methods. Micro grinding is generally used to machine planar surfaces, microchannels, and small micro components [Wend02] like cylindrical micro pins for micro tools [Schm06]. Micro grinding processes are mostly used to machine hard and brittle materials such as carbides, ceramics, glass, and semiconductor materials like silicon [Degn15] – the processes have a broader range of materials than most other micro manufacturing processes. Due to the high hardness of machined workpieces, only superabrasives such as diamond and cBN grits are used for micro grinding tools. Depending on the structure that is machined, micro grinding processes can be divided into processes that machine open and closed structures [Hess02]. Figure 2-1 shows the types of structures that can be manufactured via micro grinding with exemplary manufacturing methods according to WENDA [Wend02].

Thin grinding wheels like dicing blades can produce open and sometimes closed microstructures. Dicing blades are mainly used by the semiconductor industry to cut wafer products; however, these micro grinding tools can also be used to machine microchannels and arrays by peripheral grinding [Hoff02]. They are mostly used for open structures and rotationally symmetric structures such as micro molds for microlenses [Yama04]. SUZUKI et al. fabricated an individual variation of micro molds, that is suitable for glass mold micro-Fresnel lenses [Suzu01] – a particular type of compact and mass reducing lens, often used in the solar industry (see Figure 2-1) [Ma16]. Dicing blades usually have diameters of 50 – 60 mm and thicknesses that range between 10 µm [Lee05] – 1 mm [Brin10]. Dicing blades can have a rectangular, a round or a tapered grinding wheel profile.

Due to its significantly smaller diameter, MPGTs can machine any free form channel including everything dicing blades can manufacture [Hoff02]. HOFFMEISTER, GÄBLER, and WENDA coated MPGTs with a pure diamond layer via chemical vapor deposition (CVD) to machine different free forms in silicon and ceramics to demonstrate the potential of MPGTs [Hoff00] [Gäbl10]. Theoretically speaking, by using one of the tool manufacturing processes mentioned in section 3.2 combined with one of the coating methods discussed in section 3.3, MPGTs can achieve any form desired, producing channel cross-sections that cannot be provided by any other process.

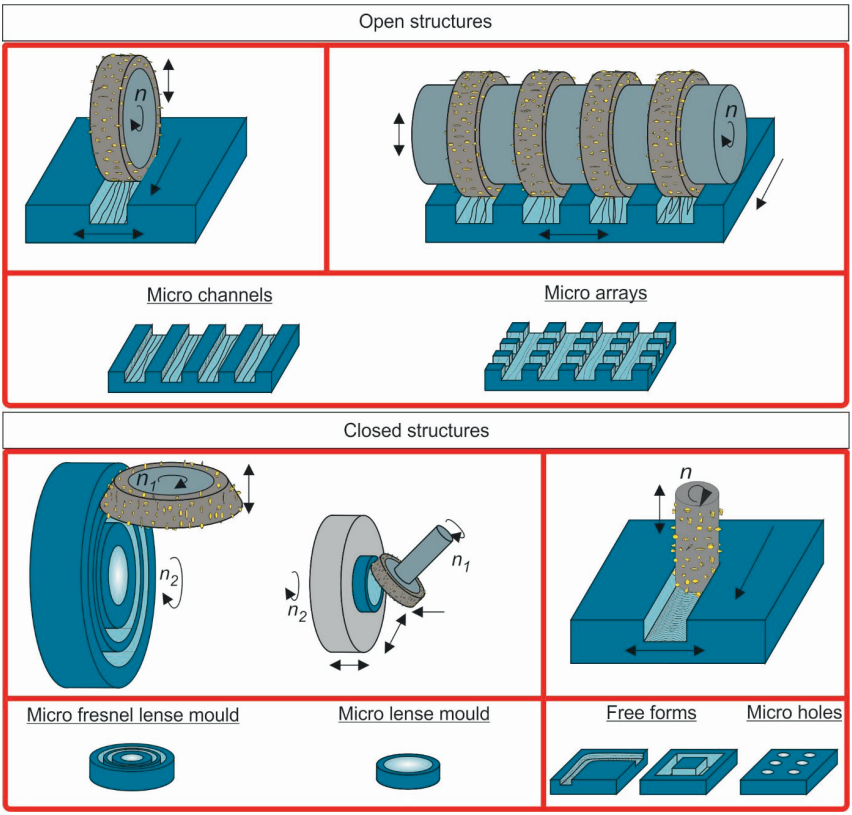

Figure 2-1: Applications for micro grinding according to [Wend02]

Desired cross-section shapes can be a hemisphere, a dovetail or a tapered cross-section with a defined angle and sharp edges [Arra19a]. MORGAN et al. used this unique tool attribute to manufacture D-shaped MPGTs (Figure 2-2 a). The recess is used as a coolant channel to ease the manufacturing of micro holes [Morg05]. Dröder et al. used thin grinding wheels to develop CVD coated MPGTs that have v-shaped microchannels that are machined in helix-form around the circumference of the tool [Dröd19] – Figure 2-2 b shows the MPGT-substrate. AZIZ et al. used a different approach, as he made a compound micro drilling tool that consists of a micro drill tip followed by an area on which an electroplated abrasive layer is coated [Aziz12a] (Figure 2-2 c). According to MASUZAWA, micro grinding tools can be used to manufacture micro holes in general. However, due to the considerable grinding forces that arise during the grinding process, the aspect ratio must be kept as low as possible. Therefore, the depth of the micro holes is not as deep as with competing processes like EDM [Masu00]. WALK [Walk16] and ENGMANN [Engm11] used an EDM process that incorporates a capacitive positioning method to produce cavities in the tool substrates of MPGTs accurately. These cavities took abrasive grits at the center area of the tool, out of the machining process, increasing the shape accuracy of produced microchannels. Figure 2-2 d shows an example of MPGTs with a cavity.

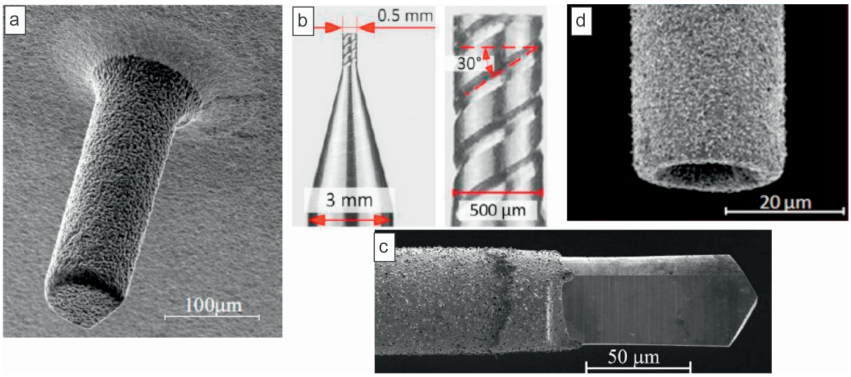

Figure 2-2: MPGTs with different geometries: a) D-shaped MPGT [Morg05], b) MPGT-substrate with a v-shaped microgroove that forms a helix around the cylinder [Dröd19], c) compound micro drilling tool [Aziz12b], and d) MPGT with a cavity [Auri10b]

2.1.2 Micro grinding process kinematics

In a machining process, MPGTs rotate around their axis using both the circumference and the face side of the tool to cut microchannels into workpiece surfaces. MPGTs engage the workpiece with simultaneous rotary movement in a circumferential direction and a translatory movement in the longitudinal direction (feed). The maximum width (a_e) a channel can reach in one pass, is determined by the diameter of the tool and machine tool influences like run-out. Process parameters like feed rate v_f, feed direction, rotational speed n, inclination angle a and depth of cut a_p are set using a computerized numerical control (CNC) system.

Processes that use pencil tools, in general, differ from other grinding processes in possible cutting speeds v_c and process kinematics. According to equation 1, the cutting speed v_c is defined by the tool diameter d_s and the rotational speed n [Denk11]. In comparison to a dicing process, MPGTs with a diameter of 50 µm need to rotate a thousand times faster than a 50 µm thick dicing blade with a diameter of 50 mm. To put this into perspective, to reach a cutting speed of 20 m/sec, a dicing blade with a diameter 50 mm requires a minimal rotational speed n_1 of 7,640 rpm. On the other hand, MPGTs with a diameter of 50 µm require a rotational speed n_2 of 7,640,000 rpm – all while maintaining an acceptable spindle run-out.

$$v_c = \pi \cdot n \cdot d_s \qquad 1$$

Another disadvantage MPGTs have over other grinding processes is that they use both the circumference and the face side of the tool. While the cutting speed reaches its maximum value at the circumference, on the face side, cutting speed drops from its maximum value at the circumference down to zero at the pivot point [Wend02]. With the cutting speed reaching the value of zero, only the feed rate participates in the machining process [Engm11], making the process similar to a scratch test, for grits at the pivot.

Figure 2-3 shows the process kinematics for both micro grinding tools. Another difference between both processes is the contact angle α_k. According to equations 2 and 3, the contact angle results from the tool diameter d_s and its width of cut a_e (depth of cut a_p for the dicing blade). The contact length l_g results from the arc on the circumference of the tool that comes in contact

with the workpiece [Schm08]. When machining microchannels, MPGTs have their entire diameter engaged in the process, resulting in a contact angle of 180° and a contact length of half the circumference [Engm11]. In comparison, when a dicing blade is used to manufacture microchannels, the contact angle is close to zero, making the contact length proportionally insignificant.

$$\alpha_{k,MPGT} = \arccos\left(\frac{0{,}5 \cdot d_s - a_e}{0{,}5 \cdot d_s}\right) \quad 2$$

$$\alpha_{k,Dicing} = \arccos\left(\frac{0{,}5 \cdot d_s - a_p}{0{,}5 \cdot d_s}\right) \quad 3$$

$$l_g = \frac{\pi \cdot d_s \cdot \alpha_k}{360°} \quad 4$$

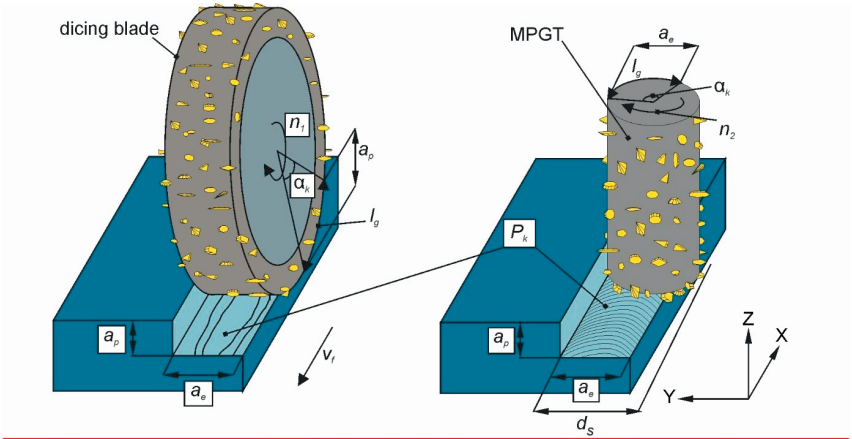

a_p	Depth of cut	n_1	Rotational speed of dicing blade	α_k	Contact angle
a_e	Width of cut	n_2	Rotational speed of MPGT	l_g	Contact length
d_s	Tool diameter	v_f	Feed rate (workpiece)	P_k	Working plane

Figure 2-3: Process kinematic for MPGTs and dicing blades

Cutting path

When considering the overall process, the cutting speed of the grinding wheel and the feed rate of the workpiece should always be considered intertwined. The path in which abrasive grits on a grinding wheel move is cycloidal. This cycloidal path is inverted between an up-grinding process in which feed rate and cutting speed move in the opposite direction, and a down-grinding process in which the motion of feed rate and cutting speed are in the same direction [Kloc09]. Since their entire diameter is constantly engaged when machining microchannels, both up- and down-grinding motions occur simultaneously for MPGTs.

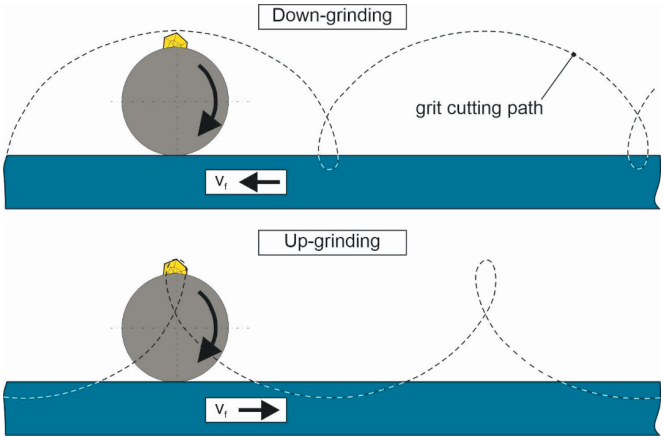

Figure 2-4: Cycloid cutting path of a single grit according to [Kloc09]

MALKIN analyzed the cutting geometry of a grinding wheel by likening it to that of a milling cutter. He idealized the grits on a grinding wheel by assuming that all grits on the wheel have the same protrusion and the same distance λ from one another – a schematic of such a case can be seen in Figure 2-5. Two simultaneous movements occur, the workpiece moves towards the grinding wheel with feed rate v_f and the grinding wheel moves a single grit with a cutting speed v_c. "s" represents the distance a single grit can travel each rotation and "a" represents the cutting depth of the grit [Malk08]. The process in Figure 2-5 depicts an up-grinding process.

Once a single grit passes the point F, the grit penetrates the workpiece following the curved path of FA´CB´. In this ideal scenario, the previous grit moved the same cutting path as the current grit but displaced with a distance s. The distance between cutting points is the product of feed rate and the time between successive cuts (Equation 5) [Malk08]:

$$s = \lambda\left(\frac{v_f}{v_c}\right) = \frac{\pi \cdot d_s}{j}\left(\frac{v_f}{v_c}\right) \qquad 5$$

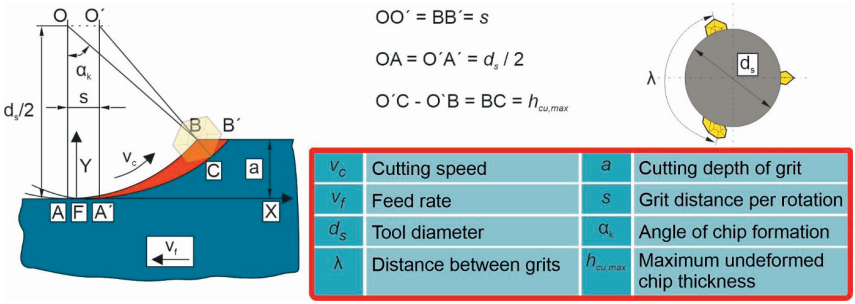

v_c	Cutting speed	a	Cutting depth of grit
v_f	Feed rate	s	Grit distance per rotation
d_s	Tool diameter	α_k	Angle of chip formation
λ	Distance between grits	$h_{cu,max}$	Maximum undeformed chip thickness

Figure 2-5: Cutting path of a single grit according to [Malk08]

In Equation 5, j is the number of grits. MALKIN described the cutting path FA´B´ as follows [Malk08]:

$$FA'B' = \text{Contact length} = l_k = \lambda \cdot \left(1 \pm \frac{v_f}{v_c}\right) \cdot (a \cdot d_s) + \frac{s}{2} \qquad 6$$

Maximum undeformed chip thickness

The maximum undeformed chip thickness $h_{cu,max}$ is a measure of the stress on the cutting edge [Kloc09]. For a single grit operation, i.e. a grinding wheel with only one grit, the chip thickness can be approximated as follows [Wern71]:

$$h_{cu,max} = 2 \cdot \pi \cdot d_s \frac{v_f}{v_c} \cdot \sqrt{\frac{a_e}{d_s}} \qquad 7$$

In the ideal grinding wheel case presented by MALKIN, the cutting length corresponds to the length BC in Figure 2-5. By calculating the geometrical relationships between length O´C (Which equals to $d_s/2$) and O´B, the maximum undeformed chip thickness can be calculated as follows [Malk08]:

$$h_{cu,max} = 2 \cdot \lambda \cdot \frac{v_f}{v_c} \cdot \left(\frac{\mathrm{a}}{\mathrm{d}_s}\right)^{\frac{1}{2}} - \lambda^2 \cdot \frac{1}{d_s} \cdot \left(\frac{v_f}{v_c}\right)^2 \qquad 8$$

As mentioned earlier, this model is based on the cross-section of an ideal grinding wheel using ideal grit distribution with an equal protrusion, grit size, and distance. However, in reality, an unknown number of abrasive grits occupy a random position on the grinding wheel, have an undefined grit protrusion from their abrasive layer, an undefined number of cutting edges that have an unknown orientation during the machining process. Nevertheless, it can be assumed that the rake angles are predominantly negative and that the cutting depth of each grit is only in the range of a few tenths of a micrometer [Frit08]. For MPGTs, a much lower number of grits participate in the process, increasing the workload on engaged grit. WERNER described the kinematics of the grinding process and derived a formula for calculating the mean maximum undeformed chip thickness $h_{cu,max}$ using data that can be obtained by characterizing actual grinding wheels (equation 6) [Wern71]:

$$h_{cu,max} = \frac{1}{A^p} \cdot \left(\frac{2}{\vartheta C_1}\right)^{\frac{1}{p+1}} \left(\frac{v_f}{v_c}\right)^{\frac{1}{p+1}} \left(\frac{a_p}{d_s}\right)^{\frac{1}{2(p+1)}} \qquad 9$$

$$A = \frac{1}{1 - \frac{p-m}{1+p}} \cdot 1{,}6^{\frac{p-m}{1+p}} \qquad 10$$

The static cutting-edge density C_1 indicates the number of cutting edges per grinding wheel surface unit, depending on the cutting-edge protrusion. Since most abrasive grits have several cutting edges, the static cutting-edge density does not describe the number of abrasive grits but the number of cutting edges. Grit density, grit size z, and the form ϑ of the grits used on the grinding wheel all influence that number. The static cutting edge density C_1 can be averaged by scanning the grinding wheel in the longitudinal and transverse direction [Spur89]. While scanning, the exponent of the static cutting-edge density p and the exponent m are determined simultaneously. m describes the average shape of the cutting-edge tips, a point-shaped cutting edge

has a value of 1 [Kass69], however, the average shape of a cutting edge tip has a rounded shape at a range of $0 < m \leq 1$ [Wern71]. Cutting edges may assume different wear-related changes during the grinding process that influence the parameters C_1, p, m, and ϑ [Spur89].

The significance of $h_{cu,max}$ is limited by the fact that it was derived under ideal kinematical conditions – a statement that can be made for all models based on WERNER's equation. Cutting edges will not only remove material but also displace it. The mechanisms of chip formation and material behavior are neglected; this is particularly noticeable with smaller cutting depths [Kloc09]. In addition, tool wear and machine tool errors are also neglected.

2.2 A Theoretical Study of Cutting Mechanisms

The quality of machined microchannels depends both on the kinematics of its process and the cutting mechanisms that occur during the process. These cutting mechanisms are categorized in ductile and brittle cutting mechanisms. Ductile material removal has breakout free surfaces that have a low roughness and sharp edges. Surfaces generated with brittle cutting mechanisms include edge breakages, microcracks, dislocations and thermally induced structural changes [Wend02] – a schematic illustrating these brittle cutting mechanisms is illustrated in Figure 2-6.

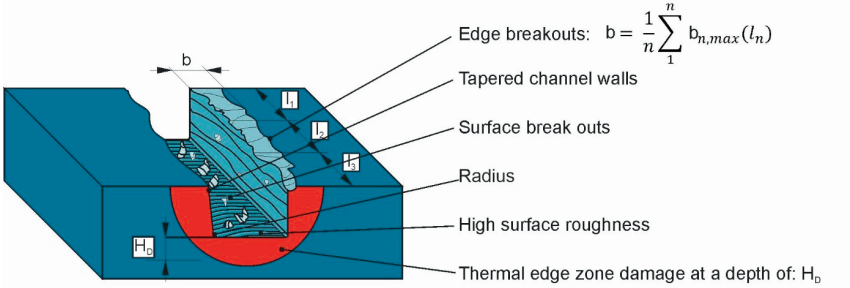

Figure 2-6: Brittle cutting mechanisms demonstrated in schematic of microchannel produced with MPGT according to WENDA [Wend02]

When cutting brittle materials, the chip thickness has a certain critical threshold under which the cutting mechanisms become ductile. Once this chip thickness is exceeded, the machining mechanisms become brittle [Bifa88]. In this section, both categories are discussed in detail, while showing research in micro grinding, that focused on these cutting mechanisms. In addition, the formation of step-like substructures is elaborated upon.

2.2.1 Grinding with ductile cutting mechanisms

KÖNIG described ductile machining mechanisms in a case in which the grit penetrates the workpiece in a straight, flat path with an effective cutting speed v_e and a cutting angle of η (Figure 2-7). Material removal occurs in three separate phases; each triggered at a different cutting depth. In the first phase of grit penetration, the workpiece only goes through elastic deformation – also called sliding in literature. No permanent displacements occur during this phase; however, friction between grit and workpiece is generated, producing heat. After surpassing a cutting depth threshold, elastic and plastic deformation occurs – a process called ploughing in literature. Friction between grit and workpiece and internal material friction are occurring mechanisms in this phase. Material is pushed to the sides of the scratched groove or pushed

under the cutting edge towards its clearance angle. Once the cutting edge reaches a cutting depth value at which the chip thickness h_{cu} surpasses the grit cutting depth T_μ, material is separated from the workpiece in the form of a chip. Due to the overlapping of material removal and displacement mechanisms, the chip thickness value h_{cu} does not equal the thickness of the actual chip removed. The actual chip thickness is called the effective chip thickness $h_{cu,eff}$ and depends on the effective cutting speed v_e and cutting angle of η [Köni80].

As one can imagine, not every grit on the outer topography of the grinding tool reaches phase III – as a matter of fact, most grits don't. Many grits do not participate in the process at all. Inactive grits reduce the chip space on the abrasive layer, decreasing the amount of metalworking fluid that reaches the abrasive layer, while also impeding the transport of removed chips. The cutting depth of many active grits does not surpass the grit cutting depth T_μ. Therefore, many grits only reach phase I or phase II, contributing immensely to the heat generated in the process [Kloc09].

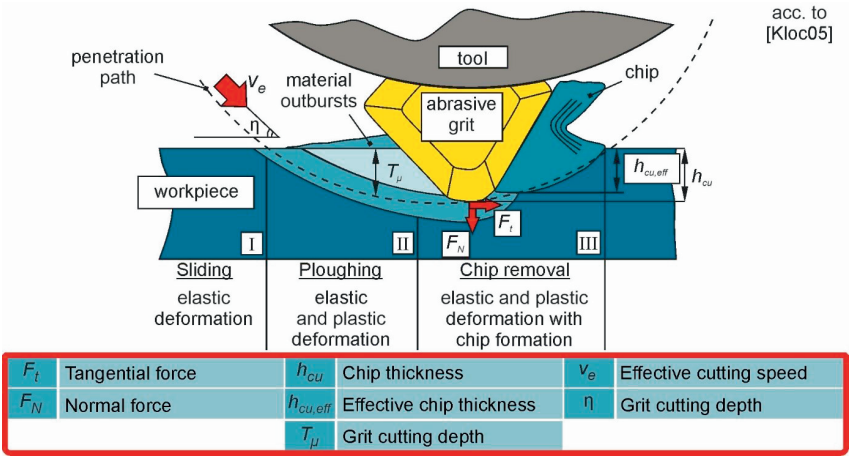

Figure 2-7: Ductile material mechanisms according to KLOCKE [KLOC09]

Ductile materials in micro grinding

Ductile materials are rarely investigated using MPGTs, as their abrasive layer would be clogged due to adhesions – a topic discussed in detail, during this dissertation. In one of the few cases documented in literature, ENGMANN machined 42CrMo4, in an attempt to achieve brittle cutting mechanisms in hardened steel workpieces. He used inclined MPGTs that have a diameter of 30 µm and an inclination angle of 6°. Tool failure prevented him from reaching brittle material removal mechanisms. It was noted, that a direct correlation between used feed rates and the size of formed burr as well as roughness values took place [Engm11].

2.2.2 Grinding with brittle cutting mechanisms

Based on wear mechanisms of abrasive layers, SALJE et al. describe material removal mechanisms that occur while grinding ceramic workpieces. Instead of chip removal mechanisms, material is scratched and crushed during grit penetration (Figure 2-8). Brittle material mechanisms are influenced less by plastic deformation and more through crack initiation and crack propagation. Similar to the ductile machining mechanisms model, brittle machining mechanisms can also be divided into three phases that are initiated by plastic deformation and depends on the depth of cut of the grit [Salj87] – all three phases are illustrated in Figure 2-8.

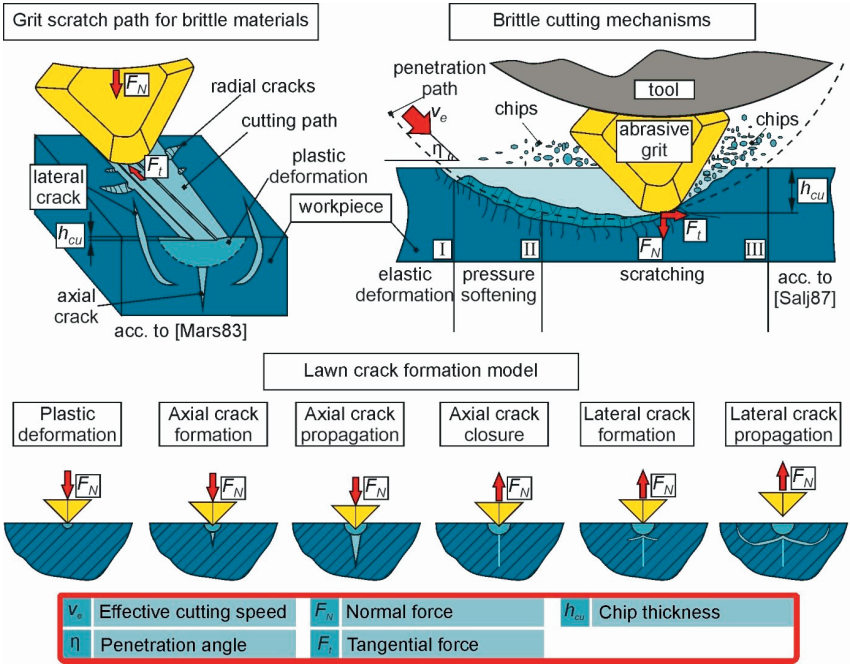

Figure 2-8: Crack formation model according to LAWN et al., brittle cutting mechanisms according to SALJE et al. [SALJ87] and scratch path model according to MARSHAL et al. [MARS83]

MARSHALL et al. [Mars83], and LAWN et al. [Lawn75] investigated material behavior for hard and brittle materials through indentation tests that employed VICKERS and KNOOP specimens. Initially, when specimen penetrated the workpiece surface, only plastic deformation was taking place. As the load on the specimen increased, the deformed area expanded, until eventually, a propagating axial crack initiated because of increasing axial and tensile stresses. During the subsequent relief of applied force, the axial crack closes, causing radial, tensile stresses which lead to the formation of lateral cracks. These can penetrate as far as the material surface and lead to the shell-shaped breakouts typical of hard and brittle materials. Immediate reloading of the specimen would reopen the axial crack and close the lateral cracks [Lawn75]. A crack formation model according to LAWN et al. is illustrated in Figure 2-8.

There are far more publications that treat brittle materials than ductile materials. In order to determine the process behavior of MPGTs, numerous machining experiments have been carried out at FBK, machining various materials. In machining experiments conducted in silicon workpieces using sintered MPGTs, the analysis of process forces showed that with increasing feed rate and the simultaneously increasing process forces, the size and number of edge and surface break-outs at the bottom surface of microchannels increases [Carr16]. A direct correlation between feed rate and the quality of the bottom surface of microchannels could, therefore, be demonstrated. Using electroplated MPGTs with a diameter of 30 µm, a similar cutting behavior could be observed in the machining of soda-lime glass, Zerodur (a special-glass ceramic from the company Schott) and quartz [Engm11].

2.2.3 Grinding brittle materials with ductile cutting mechanisms

While grinding hard and brittle materials, both brittle and ductile material removal mechanisms occur. When ductile material removal mechanisms occur during micro grinding, microchannels can achieve smooth, sharp and breakout free edges and surfaces. The transition between ductile and brittle cutting mechanisms is characterized by a critical chip thickness $h_{cu,crit}$. Once chip thicknesses below the critical chip thickness $h_{cu,crit}$ occur, brittle materials can be machined with ductile machining mechanisms. This leads to lower material removal rates as chip thickness is a value proportional to feed rate v_f [Joch16].

Scratch tests are usually performed to determine the critical chip thickness. During a scratch test, a single grit penetrates the workpiece surface at a defined cutting speed v_c and an increasing depth of cut a_p [Sing12]. The result is a scratch structure that transitions from ductile to brittle material removal mechanisms – Figure 2-9 demonstrates such a case. The chip thickness at the transition point between ductile and brittle machining is called the critical chip thickness $h_{cu,crit}$ [Bifa88]. Outbreaks, cracks, and high roughness characterize the edges and the bottom of the structure in brittle machining.

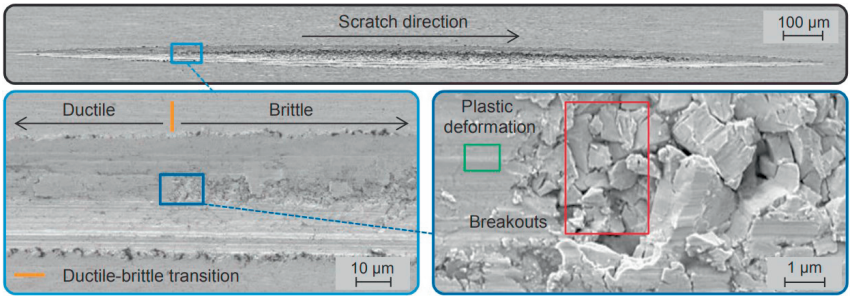

Figure 2-9: Ductile-brittle transition in scratch test on CTF12E cemented carbide [Kloc16]

MARSHALL et al. [Mars86] have determined from numerous scratch tests that the critical chip thickness value $h_{cu,crit}$ depends on the modulus of elasticity E, the hardness H, and the critical fracture toughness K_c of materials [Brin10]. This critical chip thickness value $h_{cu,crit}$ is a material-dependent constant that can be calculated as follows [Bifa88]:

$$h_{cu,krit} = \psi \cdot \frac{E}{H} \cdot \left(\frac{K_c}{H}\right)^2 \qquad 11$$

BIFANO [Bifa88] introduced a correction factor ψ to translate the critical chip thickness values determined by scratch tests into the more dynamic grinding process. The grinding experiments required for this analysis were carried out on a precision grinding machine developed by the author. Feed rate v_f, cutting speed v_c, the bond of the grinding wheels, and metalworking fluids were varied during the experiments. Based on these results, a proportionality factor of approximately $\psi = 0.15$ was determined. It can be said that with constant machine tool rigidity and process conditions, the material separation mechanism is determined by the chip thickness h_{cu}. The chip thickness is influenced by cutting speed v_c, feed rate v_f, grit density, grit size z, tool diameter d, grit form factor ϑ, and depth of cut a_p [Brin10]. According to CHENG et al., $h_{cu,max} \geq h_{cu,crit}$ can be assumed for brittle grinding [Chen14].

WENDA carried out micro grinding experiments using dicing blades that have thicknesses in a range of 40 to 100 µm to demonstrate the effect of critical chip thickness. He machined brittle materials such as monocrystalline silicon, glass, tungsten carbide, and aluminum oxide in peripheral grinding with dicing blades. The investigation tested the influence of abrasive grit size and chip thickness on surface roughness and edge breakout size. The process parameters were set so that the resulting chip thicknesses are smaller than the critical chip thicknesses of the individual workpieces to ensure a ductile machining process. Edge chippings smaller than 2 µm and arithmetic average surface roughness values down to S_a of 10 nm were achieved [Wend02]. WENDA successfully machined microchannels in all workpieces using ductile machining mechanisms.

2.2.4 Effect of up- and down-grinding on the process

The processes in sections 2.2.1 and 2.2.2 are both displayed in an up-grinding motion in which grits come in contact with the workpiece and gradually reach their maximum chip thickness. The process forces are directly proportional to the depth each grit cuts, reaching their maximum at the end of a grit's cutting path. Tool life is mainly limited by abrasive wear and the clogging of the abrasive layer with adhesions – especially for ductile materials. Tensile stresses and a lack of support of the workpiece material at the end of the cutting path, cause an increased number of edge breakouts for brittle materials [Pauc08] [Frit08].

In down-grinding, the maximum chip thickness and the highest process forces are at the start of the engagement. Impact-like maximum loads at the cutting-edge entry favor increased self-sharpening due to splintering or chipping; this is accompanied by increased form and radial wear, which is why dimensional deviations in machined structures can occur during long machining times. The motion of abrasive grits upon entry provokes compressive stress on the workpiece, which is favorable when machining hard and brittle materials as edge chippings are reduced [Pauc08] [Frit08].

Up- and down-grinding in micro grinding with MPGTs

Both up- and down grinding motions occur when machining microchannels with the full diameter; this means that micro grinding with MPGTs has all the tool wear mechanisms one has with either of the two grinding motions. These wear mechanisms are an increase in material adhesions when machining more ductile materials due to increased process forces, grit chipping because of high impacts, and radial and form wear. Higher maximum chip thickness is directly proportional to tool life.

Because of their low chip thickness MPGTs have at the start and the end of the engagement, burrs can form on either side of microchannels. The dimensional deviations due to tool wear are also a given. Tool wear is only one cause for geometrical deviations in micro grinding. These geometrical deviations are coined with the term “substructures” in this dissertation.

2.2.5 Effect of tool specifications on the shape of microchannels

During his research on MPGTs, ENGMANN noted that a large portion of the microchannels he produced had smaller channels at the bottom surface. These smaller channels formed a step-like structure that is deepest at the center [Engm11]. These substructures reduce the total channel depth and may compromise the function of microchannels Figure 2-10 shows an example of these smaller step-like substructures.

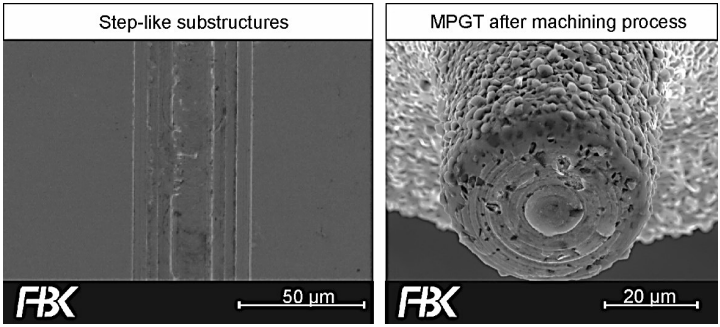

Figure 2-10: Step-like substructures and MPGT after machining

Step-like substructures originate from grits at the bottom of MPGTs having different protrusions. When grits at the pivot have a higher protrusion than the grits at the circumference, substructures are produced (as seen in Figure 2-10). A viable solution for this problem would be removing those grits at the pivot to prevent them from participating in the machining process. One method involves manufacturing a cavity at the pivot of the tool [Auri10a] – a practice quite common in commercial tool manufacturing [Haef17]. Another solution would be adding an inclination angle to the tool [Auri10b]. Aurich et. al. [Auri10b] conducted machining experiments that compared microchannels machined with regular MPGTs, MPGTs that have a cavity, and MPGTs with a 6° inclination. Both the inclined and the optimized MPGTs could machine microchannels without substructures.

SETTI et. al conducted kinematic simulations to prove a direct connection between abrasive layer specifications of MPGTs and substructures. They produced a number of different substructures based on varying grit positions and protrusions. The cutting paths of single grits on the circumference of MPGTs were determined based on their trajectories during the process [Sett18]. To compare the results from the simulation with experimental results, they developed a method to characterize the abrasive layers of MPGTs based on 3D-topography measurements of MPGTs. The topography measurements were used to determine the grit sizes, grit positions, grit protrusions, grit densities, and grit orientations for MPGTs with different diameters [Sett19]. With characterized tools, SETTI et. al conducted a parameter study with varying diameters, grit sizes, and planar grit densities to determine the effect of tool specifications on surface

generation in up-grinding and down-grinding modes machining 16MnCr5 hardened steel. Using the 3D-topography method mentioned earlier, the maximum radial grit height was determined for each tool – which the height of the most protruding grit. To inspect up- and down-grinding, a width of cut of 5 µm and depth of cut of 400 µm were used to machine the side surface of the workpiece. Material smearing occurred for experiments conducted in down grinding mode and especially those conducted with smaller tool diameters. Roughness values were mostly influenced by speed ratios (because of diameter) and maximum radial grit heights. Other than that, trajectories for the grits with the highest protrusions were visible, validating the kinematic simulations conducted [Sett20]. Basically, SETTI managed to develop a model to determine the topography of microchannels based on the characteristics of the abrasive layer.

Apart from the work done at FBK, topics related to the formation of substructures are rarely discussed. MORGAN et. al showed images that clearly illustrate substructures in some of the microchannels they machined [Morg07]. In a more recent publication, RÜGGEBERG discussed the tapered form, microchannels get due to tool wear [Rügg19]. This dissertation will make the relationship between tool specifications including wear and the formation of substructures, a central topic.

2.3 Tool Wear in Micro Grinding

Tool wear can be described as the gradual failure of a cutting tool that results from its regular operating conditions. MPGTs have two types of wear mechanisms that occur during the process: tool wear that affects the entire abrasive layer and tool wear that affects the abrasive grits.

2.3.1 Tool wear mechanisms

Thermal and physical loads cause tool wear. Workpiece material, cutting-edge material, and cutting conditions during machining, influence tool wear. The wear process itself results from chemical and physical processes that are referred to as wear mechanisms and often occur in the form of material adhesions [Frit08]. FRITZ et al. describe five types of tool wear that can occur during machining; diffusion wear, oxidation, adhesive wear, abrasion, and plastic deformation with crack-formation.

Diffusion wear

Diffusion wear describes the carbonization, which typically occurs for cemented carbide tool surfaces at temperatures of over 800 °C. The cobalt matrix dissolves into steel workpieces, and the tungsten carbide particles break out of the tool surface, due to a lack of bonding matrix. This wear type is less relevant for tooling steels and coated tools [Frit08].

Oxidation

Oxidation wear is damage caused by scaling the tool surface, which is indicated by annealing colors in the machining zone. This effect occurs for cemented carbide tools at temperatures of 700 – 800 °C [Frit08].

Adhesive wear

Adhesive wear describes the adhesion and welding of material to oxide-free surfaces on tools and workpieces [Frit08]. The process of adhesion can result from an atomic bond in the form of thermally induced diffusion, electron exchanges or electric polarization [Töns93]. The higher the normal forces that press chips into the bores of the abrasive layer, the higher their adhesive

strength [Kloc09]. These adhesions can have a higher mechanical strength than the actual material partners and may lead to micro-chipping when detached [Frit08]. Adhesions can be reduced by forming a separating lubrication film or by forming reaction layers from lubricant additives. Adhesions can also be minimized by combining materials with different structures such as metal/plastic, plastic/plastic, ceramic/plastic, and ceramic/ceramic. Figure 2-11 shows an example of this wear mechanism. The image shows adhesions that gathered on the hardened chisel of a jackhammer due to a lack of lubrication [Somm14]. Rowe describes the effect of adhesions as following [Rowe09]: "This has a disastrous effect on the grinding process. Forces are increased, temperatures are increased, and the process is out of control. "

Abrasion

Abrasive wear occurs when cutting material particles are removed under the influence of external forces. This wear mechanism usually develops in combination with other wear mechanisms [Frit08]. Figure 2-11 demonstrates abrasive wear on a press mold made of X155CrVMo12-1 (665 HV10), caused by the Silicon carbide molding compound (2700 HV10) at a forming pressure of 90 N/mm² [Somm14].

Plastic deformation with crack formation

Excessive strain on the cutting edge due to mechanical and thermal conditions can lead to plastic deformation and cracks. Plastic deformation happens when the toughness of the cutting edge is not able to counter ensuing cutting forces – high temperatures favor plastic deformation. Processes that have multiple cutting edges that participate in the machining process in an interrupted cut, usually suffer from thermal and mechanical alternating loads that lead to cracks [Frit08].

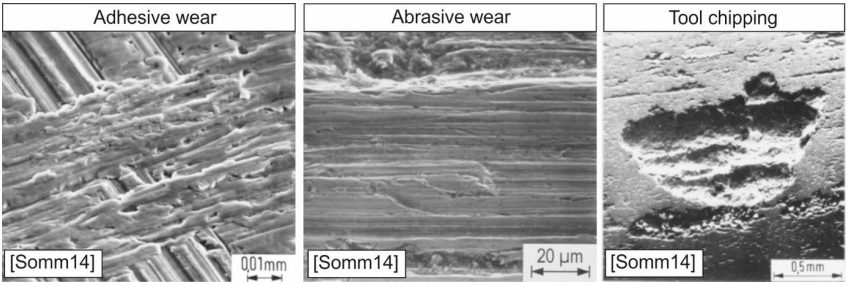

Figure 2-11: Tool wear mechanisms for abrasive and adhesive too wear and tool chipping [Somm14]

2.3.2 Abrasive layer wear mechanisms

The wear mechanisms described by FRITZ also apply to abrasive grits and their bond. Figure 2-12 describes the wear mechanisms that grits and their bond have during a grinding process. Grit wear mechanisms start in the crystal layers closest to the surface of the cutting edges. High pressures and temperatures cause oxidation and diffusion processes that decrease the abrasion resistance of abrasive grit materials. The softened layer is worn down by mechanical stress, causing abrasion. This means that new crystal layers are always subject to being worn down and to crack formation. In addition, alternating mechanical and thermal loads, cause crystal

bond fatigue, which in turn causes cracks that lead to surfaces breaking down, chipping individual grit particles or initiate the formation of cracks that cause entire grit populations to break off [Kloc09].

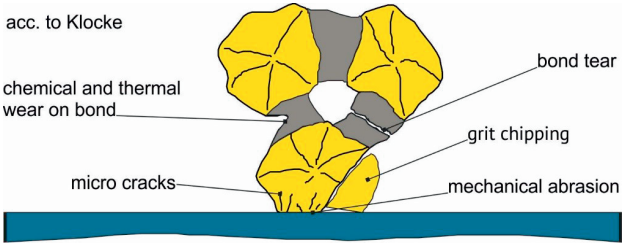

Figure 2-12: Grit wear mechanisms according to KLOCKE [Kloc09]

In many cases, grits wear down as an indirect cause of bond wear. The flattening of the cutting edges or attrition of abrasive grits leads to an increase in cutting forces; this increases surface friction and mechanically overstresses the bond. Whole grits or grit populations can then break out of the bond. The bond can also wear down directly due to chemical, mechanical or thermal influences [Kloc09].

FENG investigated the wear on individual abrasive grits on the face of MPGTs in micro grinding experiments in zirconium oxide workpieces. The micro grinding process was interrupted after machining a defined number of microchannels. MPGTs were examined under a scanning electron microscope (SEM) before being reused to machine an additional number of microchannels. Each grit was examined and tracked individually to quantify the different wear mechanisms. The investigations showed that the abrasive grits are subject to different wear mechanisms. While grinding the first channels, some abrasive grits break out directly from the bond as they lack sufficient grit embedding while other grits have various fractures occurring. Since some of the abrasive grits are inactive, they remain unaffected at first. After machining further microchannels, active grits flatten out due to mechanical abrasive wear; both wear mechanisms can occur simultaneously. Grit breakage occurs and the grits continue to flatten until they finally break out. The number of grits decreases initially due to the breaking out and fracturing of grits but increases again because of embedded grits being exposed as the bond is worn down [Feng10].

In terms of grit positions at the bottom of MPGTs, FENG discovered that grits at the pivot of the tool have lower cutting speeds, causing them to do more scratching than cutting operations, therefore, making them more vulnerable to abrasive wear. The grits closer to the circumference of the tool are more prone to grit fractures, as they are more exposed to mechanical impact [Feng10].

2.4 Metalworking Fluids in Micro Machining

In micro grinding, material removal takes place by stochastically distributed grits [Sett15]. These grits have different positions and different protrusions, resulting in material removal at different chip thicknesses. As stated in section 2.2, the value of chip thickness needs to surpass a minimum to start material removal; otherwise, only elastic and plastic deformation occurs during the machining process. Most grits do not surpass this threshold, resulting in very high

local temperatures because of friction [Kloc09].Increased process temperatures result in a number of different wear symptoms that were discussed in the previous section (2.3) [Arra17a].

During a grinding process, shearing, cutting, and friction processes generate large amounts of heat, which are only dissipated to a small extent with the chips and can, therefore, lead to considerable thermal stress on the workpiece and tool [Kloc09]. Metalworking fluids (MWFs) have the task of preventing or inhibiting the formation of the aforementioned wear mechanisms by optimizing the cutting process as a whole. The primary tasks for MWFs are reducing friction between abrasive grits and workpiece surfaces as well as friction between binder and workpiece surface while simultaneously cooling the contact zone by absorbing and transporting resulting heat [Kloc09]. The correct use of MWF can reduce friction and shear forces while simultaneously dissipating heat, reducing thermal and mechanical forces. MWF also helps chip removal from the machining zone [Frit08].

The supply of MWF that is dragged into the machining zone is impeded by a boundary layer that surrounds the grinding tool [Ebbr00]. This air barrier can be overcome by matching the fluid jet velocity with the grinding tool cutting speed and by supplying enough MWFs [Gvin05]. If an adequate supply of MWF is provided, the amount of MWF that enters the machining zone increases with increasing rotational speed. However, as the rotational speed of micro tools increases too much, the amount of MWF that enters the machining zone decreases [Roul17]. Larger abrasive grits allow for more MWF to circulate in the machining zone, increasing the cutting efficiency of the grinding tool [Engi92] [Rowe18].

2.4.1 Types of metalworking fluid supplying methods

There are generally three methods to supply MWF to the machining zone: dry machining, flooding, and minimum quantity lubrication (MQL) and through-tool coolant. Both flooding and minimum quantity lubrication have been used in micromachining [Rowe09]. In micro machining processes with diameters of less than 100 µm, conventional MQL systems, supply a flood amount of MWF, making the flooding supplying method unnecessary. An additional method is also introduced for the micro grinding process: submerged cutting – a method in which machining takes place inside a small pool of MWF. BRUDEK et al. introduced this method and tested the effect of different MWF on a micro-milling process, while also comparing a MQL system with a submerged cutting system. Figure 2-13 shows both of these processes, as published by BRUDEK et al. [Brud06]. MWF supplying methods are important for any grinding process, yet they are rarely discussed in literature about micro grinding. In this dissertation, both of these processes are implemented for the micro-grinding process.

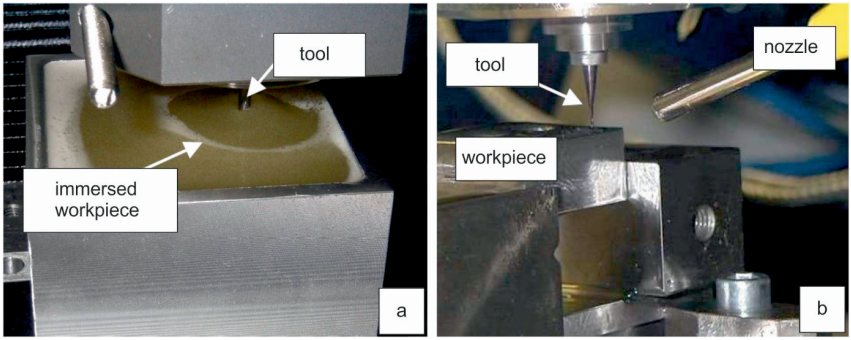

Figure 2-13: a) submerged cutting [Brud06] b) MQL system [Brud06]

2.4.2 Types of metalworking fluids

DIN 51385 [DIN13] classifies MWFs into water- and oil-based MWFs. Oil-based MWFs can be further divided into mineral oils and synthetic oils. Within the water-based and oil-based groups, a very diverse set of oils and chemicals are used according to the type of abrasives used and the properties of the workpiece material [Rowe18]. Oil-based MWFs are usually made of mineral or synthetic oils and additives that influence MWF properties such as foaming behavior, aging resistance, and lubricity [Frit08]. Water-based MWFs can also be of synthetic or natural origin and often contain additives. Water-based mediums are grouped into homogeneous mixtures called solutions or emulsions. Emulsions are heterogenic mixtures made of oil, water, and additives that form a dispersion. The high water content in water-based MWFs ensures an excellent cooling effect, while oil-based MWFs offer a better lubricating effect and less corrosion [Wein99].

A well-designed mineral oil system may outperform water-based emulsions because of the long life of the fluid, better lubrication, low corrosion, and absence of bacterial and fungal growth. On the other hand, water-based MWFs have a much higher heat capacity than oil and a much higher thermal conductivity value. In simpler terms, water can absorb much more heat. In addition, water-based MWFs are preferred if the machine tool is not capsuled – which is often the case with experimental machine tools in micro engineering labs. A negative aspect water-based MWFs have when used with cBN abrasives is that water accelerates wear due to chemical affinity. However, it has also been shown that benefits from improved lubrication and cleaning of the grinding tool surface offset the disadvantages of increased wear [Rowe09].

BRUDEK et al. conducted an experimental series in which he compared the surface quality of micro milled workpieces using different MWFs. In this experimental series, several commercially available MWFs, as well as a variety of vegetable oils, were used in experiments conducted with a MQL and a submerged cutting system. To evaluate the surface quality, BRUDEK et al. measured and compared the roughness values R_a and R_z of the different specimens. Both MWF supplying methods showed similar results with the commercial MWFs being slightly better than the vegetable oils. Canola oil and a commercially available MWF called *Lubrimax Edel C* provided the best results [Brud06].

NAM et al. used nanofluids for micro-drilling alternatively to conventional MWFs. Nanofluids comprise water- or oil-based fluids and nanoparticles like graphite, Al_2O_3, C60 or diamond to increase thermal conductivity and decrease friction in the contact area using the ball bearing effect [Arra17a]; NAM conducted the experiments using nanoparticles with base fluids made of paraffin oil and vegetable oil. Drilling torques and thrust forces were reduced and the metal removal rate was improved [Nam15].

PHAM et al. used ionic liquids for micro-milling operations in aluminum workpieces. Ionic liquids are liquid salts that comprise an organic cation and an inorganic anion that are non-flammable, have a low vapor pressure, and a high thermal stability. The experiments showed that workpieces machined with ionic fluids reached similar cutting forces and roughness values to workpieces that were machined with commercially available MWFs [Pham14] [Arra17a].

KIEREN-EHSES et al. conducted a MWF study with micro end mills that have a diameter of 50 µm using an MQL system. In this study, the influence of the MWF on the formation of build-up edges while machining cp-titanium is explored using the MWFs: sodium dodecyl sulfate (SDS), Isopropanol (C_3H_8O) and the commercially available, synthetic oil *Diamond 80*. Isopropanol was used because of its ability to absorb heat and vaporize at low temperatures; due to this ability, the least amount of tool wear occurred when using isopropanol. Due to its lubricating effect, the tools used with *Diamond 80* achieved the least amount of adhesions on the cutting edges and the best surface quality in machined microchannels [Kier18].

2.5 Summary

Generally, there are two types of micro grinding tools: thin grinding wheels, called dicing blades and micro pencil grinding tools (MPGTs). Dicing blades are used in a peripheral grinding process that can manufacture open structures and rotationally symmetric structures such as micro molds for microlenses. MPGTs use their peripheral area as well as their face area during the machining process; they can machine the same structures as dicing blades, and additionally closed structures as well as micro holes. The shape of MPGTs can be altered to produce a variety of different cross-section geometries. MPGTs have the advantage when it comes to adaptability, but have far less process stability and tool life because of their small cutting speeds and grit sizes. Another problem MPGTs have, is the formation of step-like structures (later introduced as substructures) at the bottom of microchannels, because of different protrusions and different grit positions at the bottom surface of MPGTs, including wear induced tool form deviations. This problem was solved in the past by adding an inclination angle during machining or by manufacturing a cavity at the bottom surface of MPGTs. While both process optimizations produced microchannels with improved surface quality, their effect on tool life was never tested.

Micro grinding is used to manufacture microchannels in hard and brittle materials and in hardened steel workpieces. In literature, hard and brittle materials like silicon, tungsten carbide or glass have been machined using both brittle and ductile machining mechanisms. A more ductile material like hardened steel has been only briefly investigated before in the dissertation of ENGMANN [Engm11]. When machining hard and brittle material the abrasive layer, the main wear mechanisms are abrasive wear, grit chipping, and damage to the binding matrix. Ductile materials can also cause material adhesions that clog the abrasive layer when a lack of lubrication

occurs – which is why selecting a suitable metalworking fluid (MWFs) becomes more important when machining steel than with harder and more brittle materials. A number of MWFs have been introduced, a selection of these MWFs will be applied to the process.

Two MWF supplying methods have been introduced. The first being a spraying method that uses an MQL system to spray an aerosol of pressured air and MWF on the machining zone. The second method is submerged cutting. Variations of an MQL system have been used before in micro grinding, submerged cutting has only been used in micro-milling. Both methods come with their advantages and disadvantages. To be considered is that the machine tools are not capsuled, which means that when MQL systems are used, only safe water-based MWF can be used; water-based MWFs increase wear on abrasive grits made of cBN due to chemical affinity. On the other hand, MQL-systems provide the process with a stronger flow of MWF that transfers chips better and transfers heat faster. Ultimately, an MQL system with a suitable water-based MWF needs to be compared to a submerged cutting process with different MWFs.

In general, a lot of research has been done in micro grinding. However, for MPGTs with diameters of less than 100 µm, no significant material removal rates could be achieved apart from the work of Park et. al [Park10]. In addition, no publication dives into comprehending the basics, the advantages, and the disadvantages of the process to give the readers guidelines that can be used to improve the process. Another key point missing is the lack of research on the manufacturing of abrasive layers, which will be discussed in the next chapter.

3 State of the Art: Conception of MPGT Manufacturing

In this separate state of the art chapter, the conception process for MPGT manufacturing is presented. This encompasses potential manufacturing processes for the MPGT geometry, an EDM process to manufacture cavities at the bottom of MPGTs, as well as coating, and surface treatment processes for the abrasive layer.

MPGTs comprise a base body, abrasive grits, and a bond [Engm11]. Superabrasives made of monocrystalline diamonds are used to grind non-ferrous, hard and brittle materials like silicon, cemented carbide, or ceramics [Hoff02]. For ferrous components like 16MnCr5, hardened steel workpieces and other materials that react with diamond, cubic boron nitride (cBN) grits are used instead [Brin10].

The cylindrical geometry of MPGTs can be manufactured with EDM [Egas11b], Focused Ion Beam (FIB), or via various grinding processes [Auri09]. The abrasive layer can be applied using CVD (Chemical Vapor Deposition) [Gäbl10], sintering [Haef17], and electroplating processes [Engm11] or as recently introduced by PARK et al. [Park10], electroless plating.

3.1 Substrate Material

The substrate material for MPGTs and micro tools has high requirements regarding manufacturing tolerances and surface quality. Because of the small size of MPGTs, it is difficult to add a dressing process to decrease the effect of run-out. Deviations in concentricity between the tooltip and tool shaft result in uneven process forces that cause vibrations that might ultimately break the tooltip off. In addition, machined microchannels exhibit form and dimensional deviations [Walk16].

The base bodies of these tools are made of tooling steels, cemented carbides or heavy metals [Hoff02]. Most micro tools are made of ultra-fine grained cemented carbide tool substrates because the material has a high hardness and a high bending strength [Chen13]. A high bending strength makes it possible to machine micro tools with high aspect ratios – micro tools that have diameters below 5 µm with an adequate aspect ratio are possible [Arra18]. Because of their high stiffness, micro tools manufactured with cemented carbide have a lower run-out and a better form accuracy than tooling steel. The brittle nature of cemented carbide, combined with its fine-grained matrix, make sharp cutting edges possible. When tooling steel is machined, burrs are formed around the edges.

Nevertheless, cemented carbide is only moderately suitable for metallic coatings [Bobz13]. In cemented carbide, only the metallic matrix can be coated with a nickel layer. In this dissertation, substrates with a cobalt matrix are used – the adhesive qualities of nickel on a cobalt surface are worse than those of steel or copper substrates. The hard particles of cemented carbide comprise tungsten with embedded carbon on the interstitials (making it tungsten carbide). Regularly arranged carbon atoms give these tungsten carbide particles a more ceramic structure. In combination with binder materials such as cobalt or nickel, cemented carbide has small but limited metallic characteristics like better heat transfer or better electrical conductivity.

In addition, it is also assumed that during machining, high temperatures occur on the bottom of MPGTs due to friction. Tungsten carbide with an 8% cobalt content has a linear thermal expansion coefficient of $5 \times 10^{-6}\ K^{-1} – 5.2 \times 10^{-6}\ K^{-1}$ which is much lower than that of nickel which lies in a range of $12 \times 10^{-6}\ K^{-1} – 13.5 \times 10^{-6}\ K^{-1}$ [Gran17]. Thus, the abrasive layer has a much

higher thermal expansion coefficient, causing it to loosen until the process forces eventually result in the abrasive layer's failure [Arra17a]. Tooling steels, on the other hand, have thermal expansion coefficients similar to that of nickel and will, therefore, to a certain extent, expand with the abrasive layer.

During this dissertation, it has to be determined which substrate material performs better. The tooling steel based on its better adhesive qualities or the cemented carbide substrates based on its superior mechanical qualities.

3.2 Manufacturing Processes for Micro Tools

Three manufacturing processes are used in literature; FIB, EDM methods, and grinding methods. Although no case for a Laser beam machining (LBM) method being used for such an application has been documented to this date, it can be used in the same manner as the FIB method.

The oldest and most common methods to manufacture small cylindrical micro pins are conventional and micro grinding methods. VAN OSENBRUGGEN et al. manufactured µelectrodes (cathodes for EDM process) with a diameter of 2.5 µm for EDM processes using conventional grinding wheels in as early as 1965 [Osen65]. Grinding of micro pins is by no means a new technology. CHENG et al. state that using larger grinding wheels (usually with a side grinding method) is not precise enough to manufacture small diameters with more complex geometries like micro end mills. One of the main reasons for this is the large cutting forces during the manufacturing process, which results in tool deflection as well as heat-affected zones [Chen13].

Figure 3-1 depicts an example of such a conventional grinding method. The side surface of a large grinding wheel is used to machine a cylindrical tooltip. The peripheral surface of the grinding wheel can manufacture the end face of the cylinder. The face side of the grinding wheel then removes material, while the substrate rotates around its axis, slowly achieving the end diameter of the cylinder. The form of the grinding wheel is translated to the bottleneck of the substrate.

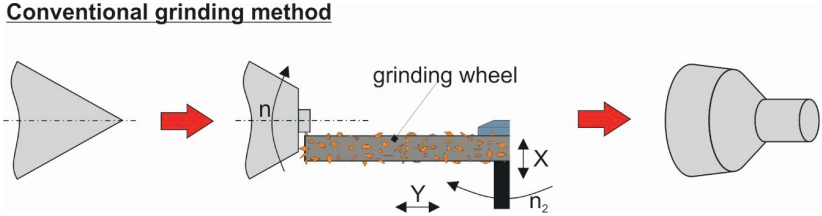

Figure 3-1: Substrate machining with conventional grinding method

FIB successively removes small portions of hard materials like tungsten carbide or ceramics to fabricate micro tools. It offers precise control over size, complex geometries, and especially sharp cutting edges. In addition, almost no process forces act on the tool surface during manufacturing. In 1996 VASILE et al. and FRIEDRICH et al. used a FIB process to show its capabilities in micro tool manufacturing. They produced micro mills with a diameter of 22 µm that have various geometries. Produced micro mills were used in micro milling experiments on polymethylmethacrylate (PMMA) workpieces. They produced microchannels that were 24 µm wide, 26 µm deep and 2.3 mm long [Vasi96]. The FIB process they used had a material removal

rate of 0.5 µm^3 [Frie96]. As CHENG et al. stated, FIB is one of the slower tool manufacturing processes and on the more expensive end in equipment costs [Chen13].

Figure 3-2 demonstrates the method for substrate manufacturing with a FIB process. The end face of the cylinder is manufactured first. The beam is then used to remove substrate material while the substrate moves around its axis. Translatory movement of the beam in the X-axis defines the diameter of the cylindrical tip and movement in the Y-axis, defines the length of the tooltip.

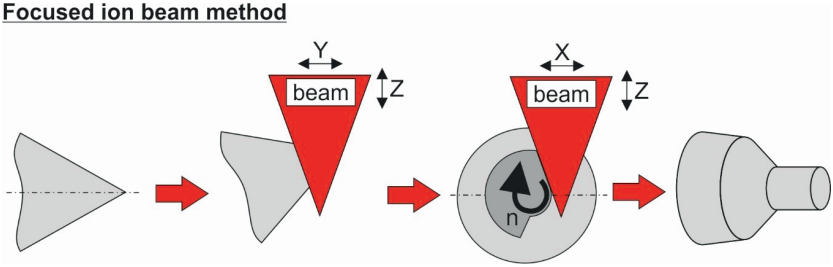

Figure 3-2: Substrate machining with focused ion beam method

The most commonly used EDM method to manufacture micro tools is the wire electro-discharge grinding (WEDG) process – depicted in Figure 3-3. As mentioned in the introduction chapter, EDM uses spark impulses on a workpiece, evaporating selected areas with temperatures of up to 40000 K [DiBi89]. This, of course, removes material from both the substrate and the electrode, which is why most users of this process use a whole coil made of the wire electrode material. This electrode is then moved close to the rotating substrate, successively removing material until the tooltip reaches its end diameter and end length – more on how this process works in section 3.5.

MASUZAWA first proposed WEDG in his CIRP annals article in 1985 [Masu85]. In his paper, the then newly developed WEDG method was used to manufacture thin rods with diameters of less than 15 µm, with high repeatability and an accuracy of less than 1 µm. Using this technology EGASHIRA et al. produced single flute micro end mills with a diameter of 20 µm and a cutting edge radius of 0.5 µm in 2002 [Egas02] – proving that some of the more complex tool shapes can be manufactured with the WEDG technology. As of today, the smallest micro end mills manufactured with WEDG have a diameter of 3 µm and are produced by the same author (EGASHIRA et al.) [Egas11b].

At the Institute for Manufacturing Technology and Production Systems Kaiserslautern (FBK), AURICH et al. developed a process in which thin grinding wheels or dicing blades, as they are called, are combined with high-end machinery to manufacture micro tools. In 2008, micro end mills made of cemented carbide were manufactured with this process to diameters of down to 7 µm with a cutting edge radius of less than 0.3 µm [Auri08]. MPGTs with substrate diameters of less than 2 µm were manufactured with this process in 2018 [Arra18]. A simple cylindrical tooltip can be machined in under two minutes; this makes it the most suitable process for a grand scale substrate manufacturing operation. It is assumed that over 5000 substrates have been machined for all the studies conducted in this dissertation. For the given timeframe, both WEDG and FIB processes cannot handle this kind of capacity.

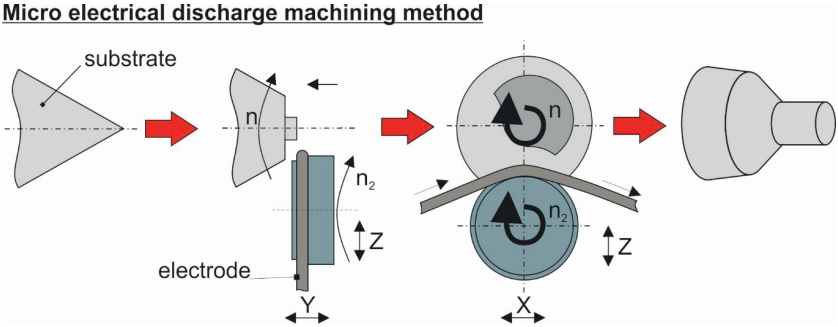

Figure 3-3: Substrate manufacturing with wire electrical discharge machining

As Figure 3-4 depicts, the process is a peripheral/plunge grinding method. The end face is first manufactured, then the cylindrical tooltip is machined in a number of machining steps. The machining steps include a few rough-cutting steps and a fine grinding step. For this, two grinding wheels can be used, a coarser one for the rough grinding operations and one with finer grits for fine grinding [Auri12]. More on this process in section 6.1.

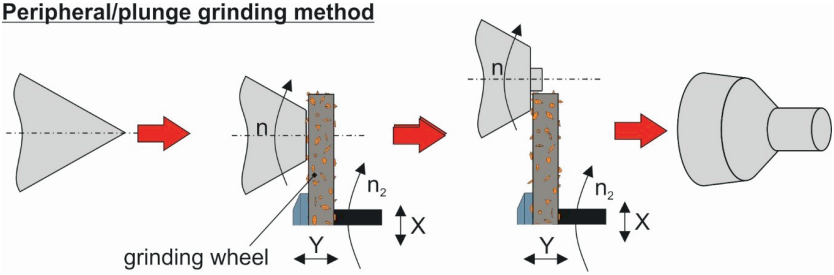

Figure 3-4: Substrate machining with peripheral/plunge grinding method

3.3 Abrasive Layers for MPGTs

Four methods are discussed in this section: sintering, CVD, electroplating, and electroless plating. In sintering, electroplating, and electroless plating, the abrasive body is made of a metallic matrix, and abrasive grits, CVD produces a layer made of pure diamond. All methods are presented with their advantages and their known disadvantages.

A larger focus is placed on electroplating and electroless plating as they are more relevant to this work than the other two processes.

3.3.1 Sintering

One of the most common ways to produce an abrasive layer for MPGTs is sintering. In a sintering process, products and semi-finished products are produced by pressing powder mixtures made of a hard granulate and granulate made of a binder into molds that are shaped like the final product. This pre-compressed powder masses or pellets as they are called, are put in a sintering oven and are heated to temperatures below the melting point of one of the components – in this case, the abrasive grits [Frit08], whilst under pressures of up to 20 MPa [Engm11]. In powder mixtures that form a di- or multi-component system, e.g., diamond and bronze; the

sintering temperature can be such that one of the substances melts filling the remaining pore volume [Frit08]. Figure 3-5 shows an exemplary schematic of how a sintering process works.

Sintered MPGTs, have a tool head that consists of a bronze matrix (bond) that embeds abrasive grits (hard material) almost wholly [Wein07]. The advantage is that almost the entire tool head can be used for grinding. Sintered MPGTs need to be dressed before initial use to ensure grit protrusion, adding preparation steps before use. The smallest commercially available sintered MPGTs have a diameter of 180 µm and are used in the watch industry [Haef17].

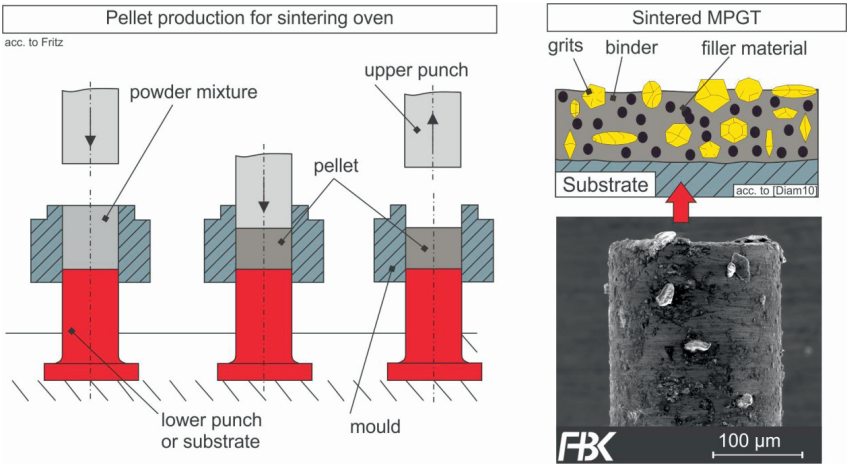

Figure 3-5: Principle of pellet production for sintering oven acc. to FRITZ [Frit08] and abrasive layer on sintered MPGT acc. to [Diam10]

3.3.2 Chemical vapor deposition

Chemical vapor deposition (CVD) as the name implies, is a process that involves a gas-phase chemical reaction on top of a solid substrate. The gas reaction causes a coating to grow on these surfaces [May00]. The Institute of Machine Tools and Production Technology (IWF) in Braunschweig, used a hot filament CVD technology to produce thin diamond layers for MPGTs [Gäbl99]. All CVD deposition methods that produce diamond layers require an activation gas that contains carbon molecules. The activation method involves thermal methods that heat the substrate to temperatures of over 700 °C. The gas used to produce diamond layers is usually made of hydrogen and 1 vol.% methane (CH_4) [May00].

A hot filament method according to MAY [MAY00] and an MPGT produced by GÄBLER et al. [Gäbl10], are depicted in Figure 3-6. The gas flows into a vacuum chamber that maintains a constant pressure of 20 – 30 Torr (0.0266 – 0.04 bar). A substrate heater heats the substrate to 700–900 °C. The substrates to be coated are activated by being placed a few millimeters below a filament that is inductively heated to temperatures of about 2200 °C. The filament itself is usually made of tantalum or tungsten and do not react significantly to the gas used in the process [May00]. Since diamond grows slowly on other surfaces, the substrates are immersed in a sus-

pension of diamond particles (<1 µm) and water. The diamond nanoparticles adhere to the substrate surface. During the coating process, this increases the nucleus density of diamond crystals [Gäbl03].

The hot filament CVD process produces diamond layers at a rate of 1–10 µm h^{-1} [May00]. Due to low pressures, the process makes it possible to coat much smaller diameters than with a sintering process. The chip space and grit protrusion (crystalline height), however, remains rather small, causing frequent clogging [Hoff02]. Moreover, this manufacturing process is only economical with a higher number of MPGTs.

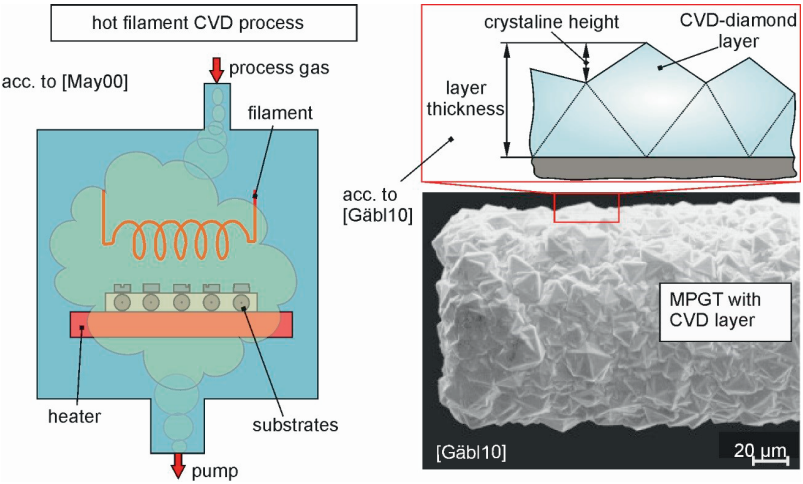

Figure 3-6: Hot filament chemical Vapor deposition process [May00] for MPGT manufacturing and CVD layer [Gäbl10]

3.3.3 Electroplating

The earliest reference to a nickel-plating solution is dated back to 1837 when BIRD deposited nickel on to a platinum electrode from a nickel chloride/sulfate solution. SHORE was the first to patent a nickel nitrate solution in 1840 and BOTTGER developed the first practical formulation for a nickel-plating solution in 1843. BOTTGER's solution remained in commercial use for 70 years. The most common solution that is still dominant to this day was developed by Professor Oliver P. Watts at the University of Wisconsin in 1916 [Watt16]. He developed a high-speed coating solution made out of nickel sulfate, nickel chloride and boric acid [DiBa10] – a composition still in use today.

The electrolytic principle, in which chemical energy is turned into electrical energy [Stra90] is used. The principle states that ionic compounds are broken down to their basic components by applying an external voltage – a process that can take place in an aqueous solution or molten mass [Brie14]. Two simultaneous reactions need to occur here: an oxidation process in which nickel atoms lose electrons and a reduction process in which nickel ions gain electrons.

We make use of the electrolytic principle by immersing two electrodes in a conductive aqueous solution that contains nickel ions (Ni^{2+}) – Figure 3-7 illustrates a schematic of the process. The

metal salt – here nickel sulfate – disassociates to its ionic compounds Ni^{2+} and SO_4^{2-} after being added to the solution. The substrate acts as the cathode and an electrode made of the desired material (nickel), serves as an anode. The flow of electric current causes the anode to dissolve into the solution and the cathode to gain a layer made out of the anode's material [Schl10a]. The current flow creates an electric field that transports nickel ions to the substrate, and an electron transport takes place via the electrical circuit to supply the nickel ions with the required electrons [Lou06] – allowing the oxidation and reduction processes to take place. The nickel atoms from whom the electrons were separated, become nickel ions and separate from the anode to replenish the plating solution with new nickel ions [Gaid12]. The plating solution is usually called an electrolyte, which is an electrically conductive solution that contains both cations (positively charged ions) and anions (negatively charged ions).

The most significant advantage of the process when coating grinding tools, is that tool specifications such as grit size, grit concentration, layer thickness and/or grit protrusion, can easily be adjusted by changing component concentrations, pH-value, solution temperature, current density and/or coating time.

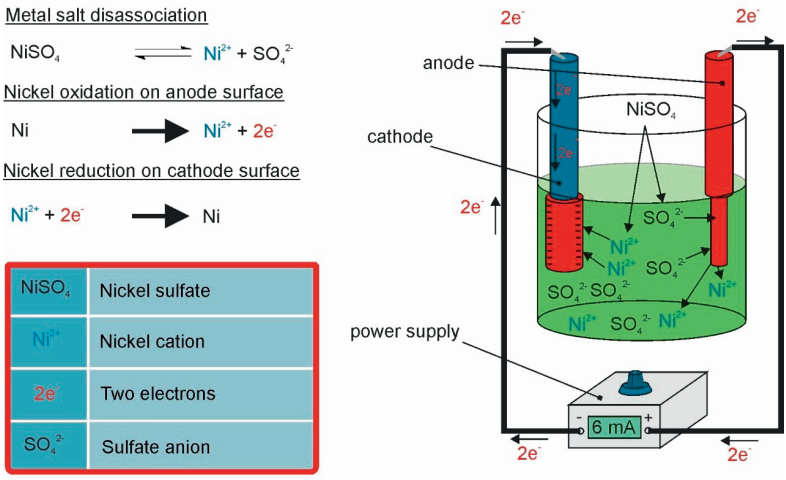

Figure 3-7: Electroplating process

Automated electroplating

One of the greatest advantages of electroplating is that it is one of the easier processes to automated. In his dissertation in 2011, ENGMANN [Engm11] explored manufacturing methods for MPGTs. He developed a machine tool that automated the tool grinding and the electroplating process (see Figure 3-8). The machine tool contained a spindle that is maneuvered in the Z-axis with a linear stage and a table that is maneuvered with two additional linear stages in the X- and Y-axes. A grinding unit to manufacture the geometry of the substrates was attached to the machine table. An additional rotational stage with small plastic beakers was also attached to the table. These beakers contained electrolyte and surface treatment substances. The substrate would be moved with the stages from one beaker to the next. An electric circuit was used to

determine the contact point between the substrate and the electrolyte surface. A microscope was used to monitor the whole manufacturing process.

The electroplating process would be performed in three steps: precoating, coating with grits, and grit embedment – all three steps performed with a commercially available electrolyte. The precoating step was conducted to add a small thin nickel layer on the substrate surface. In the next step, the substrate is immersed in a beaker that contains a mixture of abrasive grits and electrolyte – the substrate is coated with nickel and is embedded with any grit in contact with the substrate surface. Excessive grits are then removed with pressured air. In the last step, an additional thin nickel layer is added to increase grit embedment.

WALK [Walk16] expanded the system developed by ENGMANN by developing a machine tool that contained a tool grinding unit, an electroplating unit, an EDM unit, and an application unit. A high-speed spindle was used to allow the user to completely manufacture MPGTs and use them on a workpiece that is mounted on the application unit, all in one tool clamping.

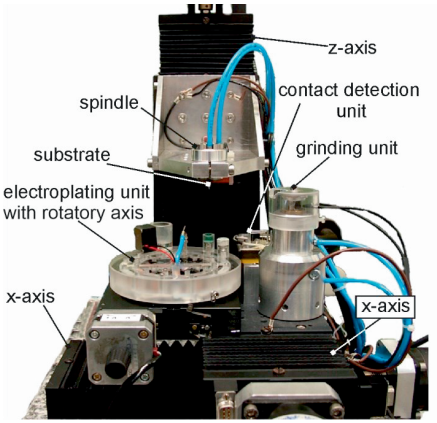

Figure 3-8: Electroplating unit by ENGMANN [Engm11]

3.3.4 Electroless plating

The electroless nickel plating process was accidentally discovered by BRENNER and RIDDELL in 1946 [Bren47] when they observed that the presence of sodium hypophosphite in a conventional nickel electrolyte led to an apparent current yield of more than 100%. The conclusion that was drawn was that there must be an additional chemical reaction providing additional growth in nickel. Further research resulted in the development of the then-novel electroless plating process. Electroless plating – or electrodeless plating as it was initially called – is an autocatalytic reduction process that is quite similar to the electroplating process. Instead of using an external electric cycle to provide the substrate with electrons, a reducing agent is added to the plating solution. The abbreviated name itself is quite misleading; there are no external electrodes present during the process, however, there is an electric current involved [Schl10b].

Once dissolved in water, this reducing agent releases free electrons. These electrons adhere to the substrate surface and react to metallic ions in the solution. The term “autocatalytic” means

that the nickel forming on top of the substrate functions as a catalysator to the process [Kana07]. Most electroless plating solutions used today are sour and use either nickel sulfate ($NiSO_4$) or nickel chloride ($NiCl_2$) as metal salt with sodium hypophosphite (NaH_2PO_2) as reducing agent [Kana07]. Figure 3-9 shows a schematic of the process including the main reactions and side reactions that produce a phosphorus nickel composition (Ni-P). Additional side reactions occurring in the solution produce hydrogen (H_2), sulfuric acid (H_2SO_4), and orthophosphite (H_2PO_3) [Cheo04].

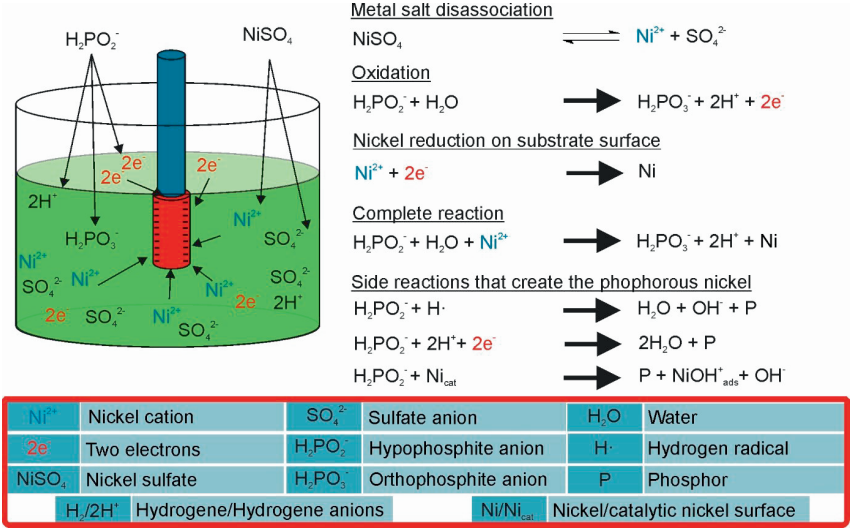

Figure 3-9: Electroless plating process

According to CHOENG et al., the phosphor in the phosphorous nickel layer, develops during side reactions that occur parallel to the main reaction (the reactions are listed in Figure 3-9) [Cheo04]. These simultaneous side reactions and others, reduce the lifespan of the solution [Kana07]. In the first reaction, hypophosphite anions react to hydrogen radicals H· to produce water, hydroxide ions, and phosphor. In the second reaction, an electrochemical mechanism occurs directly on the cathode. A hypophosphite anion, two hydrogen cations, and two electrons produce two water molecules and phosphor. The third option is the CAVALOTTI-SALVAGO [SALV72] mechanism. Here, direct contact with a nickel surface leads to a catalytic reaction, which results in phosphorus deposition [Cheo04]. The amount of sodium hypophosphite (NaH_2PO_2) added to the solution directly influences the phosphorous content in the Ni-P layer [Kana07].

The phosphorous content of Ni-P layers has a direct impact on its lattice structure. Phosphorus-nickel layers with a phosphorus content of less than 7 wt%, predominantly show a microcrystalline structure [Lin02]. According to CHEONG et al., layers with a phosphorous content above ~8.5 wt%, start to develop more amorphous structures [Cheo04]. The phosphorus content in a nickel coating determines the coating's physical, mechanical and chemical properties [Park97]; Table 3-1 lists some of these properties.

The effect of the phosphorous content on the performance of MPGTs is not investigated in this dissertation; this, however, is a rather interesting study for future works.

Table 3-1: Influence of phosphorous content on Ni-P layer properties according to [Kana07]

Phosphorous content in %	1 – 4	7 – 9	10 – 12
Structure	crystlline		amorphous
Physical properties			
Density in g/cm^3	8.5	8.1	7.9
Specific electrical resistance in µΩ·cm	20-30	50-60	100
Thermal expansion coefficient in µm/(m·K)	13	12	11
Magnetic susceptibility in %	–	4	–
Coercivity in O_e	~10	1-2	0
Mechanical properties			
Tensile strength in N/mm^2	200	800-900	750-900
Elongation at break in %	0.5	0.7	~1.5
Hardness in HV	650-700	550-600	500-550
Taber-Abraser-Index	10-12	15-20	20-25
Residual stress (on substrate surface) in N/mm^2	-10	±5	+5
Chemical properties			
Salt spray test in h	24	200	1000
Acid resistance	low	moderate	high

Additional solution components

The main components used in a nickel plating solution are metal salts like nickel sulfate, a reducing agent like sodium hypophosphite, and additives [Arra17b]. Theoretically speaking, a metal salt and a reducing agent are enough to complete the coating process. In practice, however, an additive-free plating solution is unstable, can spontaneously decompose, or produce defective Ni-P layers [Kana07]. Two of the substances used as additives are complexing agents and stabilizers. Complexing agents like sodium acetate are substances that form compounds with other substances. They consist of ions or molecules and can be used to prevent side reactions that are characteristic of certain ions – a process called masking [Jand03]. The complexing agent forms a bond with free nickel ions in the solution, creating a complex [Mall90]. This way, undesirable reactions with Ni^{2+} ions are prevented during electroless nickel plating [Jand03]; this helps maintain a constant pH value, it helps prevent precipitation of metal salts, and reduces the concentration of free metal ions in the solution [Schl10b].

Another important additive is the stabilizer agent. Electroless plating solutions can be used for long periods of time but may decompose spontaneously during the metal deposition process [Schl10b]. Spontaneous decomposition is usually triggered by catalytic, foreign particles that float in the solution [Kana07]. Bath decomposition is usually marked by an increase in the

volume of hydrogen gas formation and the appearance of black precipitate through the container and its content – for example, gray abrasive grits that are added to the solution, would turn black. This precipitate consists of nickel particles and nickel phosphide (Ni_3P) [Mall90]. Stabilizers like thiourea (CH_4N_2S) are used to prevent the solution from spontaneously decomposing [Cheo04]. These stabilizers usually contain metals that have a higher electrochemical potential than the metal in the solution – in the case of thiourea, it contains sulfur, which has a much higher electrochemical potential than nickel. Stabilizers adhere to the surfaces of catalytic, foreign particles and prevent nickel crystallization nuclei from forming; of course, this same effect can also occur on the substrate surface [Kana07]. Diligent handling is required when using these additives, as too high concentrations, can inhibit metal deposition completely [Japp05] – this concentration is also called the critical concentration. Generally, nickel deposition decreases the higher the stabilizer concentration is; however, some stabilizers increase deposition rate until a maximum deposition rate is reached, after which the deposition rate decreases. Thiourea is chosen as the stabilizer for this work, following the works of PARK et al. [Park10] and CHEONG et al. [Cheo04].

Influence of parameters on deposition rate and phosphorous content

It is, of course, essential to understand what components influence the nickel deposition rate and which components influence the phosphorous content. Table 3-2 lists the influence of different parameters with arrows indicating an increase or decrease in value. The list does not include stabilizer concentration as this depends on the type used.

Table 3-2: Influence of parameters on deposition rate and phosphorous content

Parameter	Nickel deposition rate	Phosphorous content
Solution temperature ▲ [Wats89]	▲	▲
pH-Value ▲ [Wats89]	▲	▼
Complexing agent concentration ▲ [Schl10b]	▼	▼
Reducing agent concentration ▲[Bren47]	▲	▲

3.4 Surface Treatment

There are a number of processes that qualify as surface treatment for coating processes. In this section, methods in degreasing, electrochemical machining, and pickling are discussed.

3.4.1 Degreasing

Degreasing is a process that is used to remove fat, grease, oil, manufacturing residues and other contaminations from the surface of the substrate. An alkaline solution that is usually composed of a cleaning agent like sodium hydroxide water and additives like surfactants. The solution soaks into the contamination layers on the substrate, weakening their adhesive strength. According to SINGER and STRAUß, to guarantee a great cleaning effect, a relative movement between the substrate and the degreasing solution needs to occur. This relative movement is added to the solution by vibration, rotation, boiling (or near boiling) and electrolysis. Two methods have been used in this dissertation: boil degreasing and cathodic degreasing. The boil degreasing method accomplishes this relative movement using a wavering motion the solution achieves

when nearing boiling temperatures [Sing78]. In addition, substrate rotation and a whirling solution via magnetic stirrer add to the desired wavering motion.

The second method used is an electrochemical method. According to SINGER and STRAUß, the main cleaning effect here is the gathering and combination of gas ions below the grease layer on the substrate surface. When combined, the gas increases in volume, blasting parts of the grease layers off [Sing78] – Figure 3-10 depicts a schematic of the process. There are two ways to conduct this process; cathodic degreasing, which combines hydrogen ions into hydrogen molecules (H_2) and anodic degreasing, which combines hydroxide ions. It is generally agreed upon, that a cathodic degreasing process is more effective because the combined volume of developing hydrogen molecules is much larger than that of oxygen in an anodic process. Besides, oxygen promotes corrosion. In contrast, the diffusion of hydrogen has a negative effect on the material properties of steel parts and is partially responsible for bubble formation under the subsequently deposited metallic layer [Stra87]. It is therefore advised to complete the degreasing cycle below two minutes or to alternate between the two processes in cycles [Sing78].

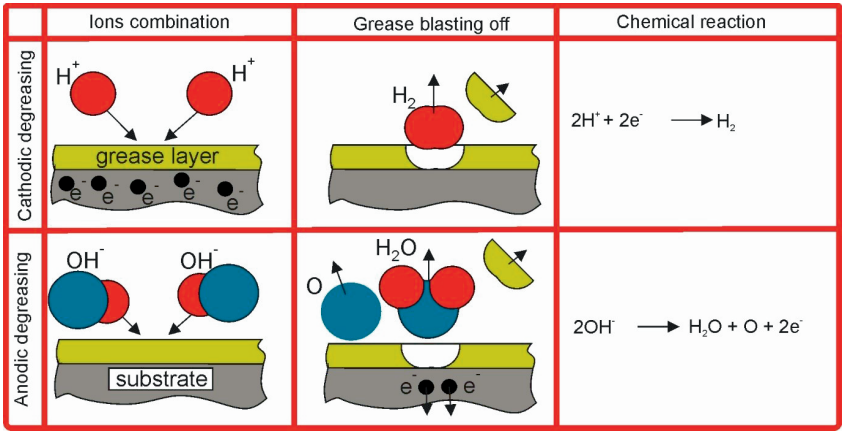

Figure 3-10: Electrochemical degreasing: cathodic and anodic

3.4.2 Electrochemical machining

ECM functions on the same principle as the electroplating process introduced in section 3.3.3, except here the substrate functions as an anode – quite similar to the anodic degreasing actually. As an anode in an electrolysis process, the substrate loses ions to a cathode, removing a layer of material in the process. According to GAIDA, ECM is used to round off sharp edges, improve surface quality and remove burr [Gaid12], as the highest concentration of the electrical field is on the edges, causing a sort of disproportionate material removal between the edges and the rest of the substrate [Sing78].

According to BUHLERT, carbides inside tooling steel are electrically inert and cannot be dissolved by electrochemical means. Therefore, carbides remain while carbide-free material is removed, resulting in small cavities [Buhl17]. In other words, this process can also be used to roughen steels surfaces.

3.4.3 Pickling/etching

Corrosion is an undesired chemical or electrochemical reaction between the surface of a substrate and its environment [Stra87]. A pickling process removes corrosion and scale residues from metallic surfaces with acids and sometimes alkalis. Sulfuric acid and hydrochloric acid are mostly used for pickling processes on steel substrates, with hydrochloric acid being the more suitable one [Bill57]. Figure 3-11 shows a schematic of the reaction occurring on the surface of substrates. Iron (III) oxide on the substrate reacts with six hydrochloric acid molecules. The product of this reaction consists of three water molecules and two iron (III) chloride molecules.

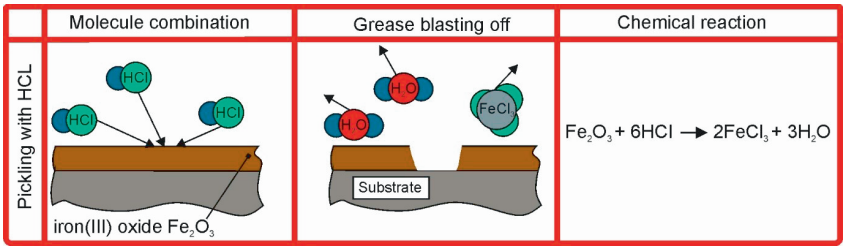

Figure 3-11: Pickling process schematic

3.5 Manufacturing Cavities via Electrical Discharge Machining

Electrical discharge machining (EDM) is a process that removes material from substrates utilizing a succession of electrical discharges [Zhan04]. EDM is a contactless process that is almost unaffected by the mechanical properties of its substrates. Thermal and electrical properties, on the other hand, determine how well a substrate can be processed and how well it can be heated up, vaporized, and cooled down [Fond08]. Despite the poor thermal and electrical conductivity of hard and brittle materials, the process proved to be suitable to manufacture microchannels with high aspect ratios.

In EDM, an electric cycle that uses pulse voltage is closed between the substrate and an µ-electrode. To prevent the ionic transfer of material between the electrodes and effectively coating the µ-electrode, a dielectric working medium like distilled water or synthetic oil is used. Figure 3-12 presents a schematic of the process and the gap between the electrodes.

Since the working medium is dielectric, a minimal voltage is needed to surpass its dielectric strength. The distance between electrodes directly influences the dielectric strength; the closer the electrodes are, the lower the dielectric strength [Mahe10]. The location a spark discharge occurs in is directly influenced by the microstructure of the electrodes and the number of ionic particles found in the gap that may divert the spark. The spark is more likely to occur in areas in which electrodes have the smallest distance due to their microstructures. This discharge spark is a radiating light that results from the discharge of ionic gas in a plasma channel that occurs between both electrodes. Inside this plasma channel, the workpiece is locally heated to temperatures of up to 40,000 K. This temperature is higher than the melting temperatures of most substrates, causing material to be removed via evaporation [DiBi89].

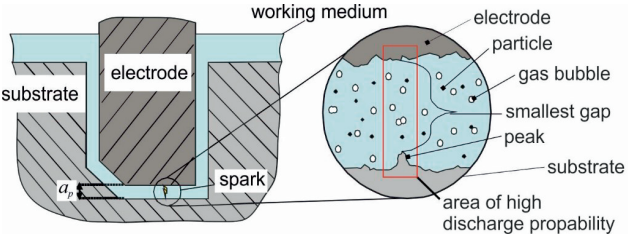

Figure 3-12: Spark discharge area according to ZIEDLER [Zeid12]

Figure 3-13 shows the three phases that occur during the EDM process that is presented in Figure 3-12. In principle, two electrodes that have an open circuit are charged with a pulsating supply voltage u_0 and are separated by an initially non-conductive, dielectric working medium. The substrate electrode moves towards the µ-electrode with a feed rate v_E. No discharge occurs until a minimal gap distance or spark gap of S_G is reached. An ionization path is created between the electrodes and sparks are generated between both electrodes, [Mahe10] one spark for each pulse generated [Pate89]; this is called the ignition and plasma formation phase. When the peak current i_e starts flowing between the electrodes causing the voltage to drop to a discharge voltage of u_e and to stabilize at given spark gap S_G [Ferr07]; this marks the beginning of the discharge phase. In the discharge phase, a plasma channel that contains ionized electrically conductive gas is formed. This conductive gas heats melts and evaporates portions of the substrate as well as the µ-electrode, forming a growing crater. Less material is removed from the µ-electrode since the plasma radius is much smaller than on the substrate side [Mahe10]. Material removal on the µ-electrode is reduced by one to two orders of magnitude due to the lower mobility of the positively charged ions [DiBi89]. A thermal influence occurs due to the melting and solidification of material in the plasma channel. This thermal effect depends on the substrate material. The intensity of the thermal effect influences the quality of manufactured EDM products in terms of its surface integrity, which is characterized by surface roughness, the existence of surface cracks, and residual stresses [Ekme07].

The gas pocket expands until the pulse duration t_i is over. The gas pocket then implodes, and a rapid drop in pressure that flushes the molten material out of the processing zone occurs [Mahe10]. After a discharge duration t_e, the next cycle begins. The material removed from the electrodes is re-solidified in the working medium forming hundreds of residual particles. Inadequate flushing in the EDM system can cause these particles to become a conductive bridge between both electrodes [Luo98].

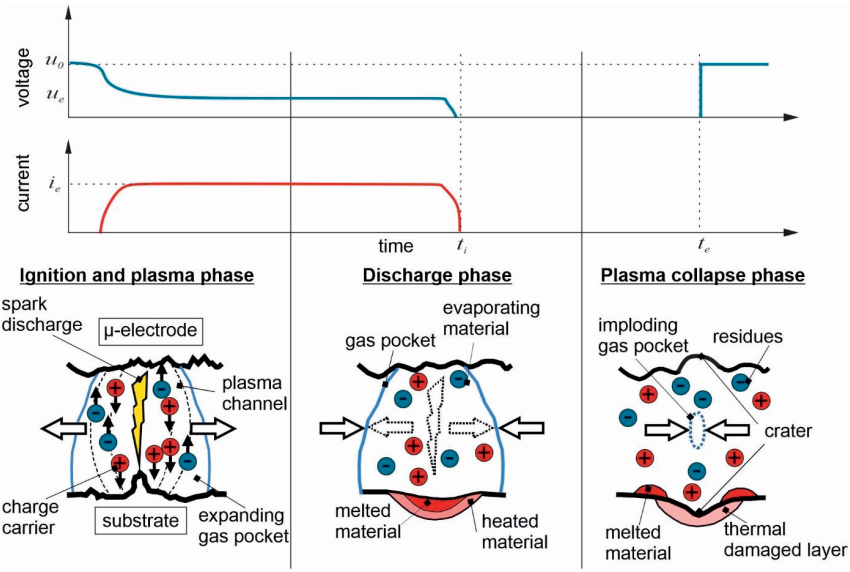

Figure 3-13: EDM principle according to ZIEDLER [Zeid12]

3.6 Summary – Tool Conception

When it comes to tool conception four topics need to be discussed:

- How to manufacture the tool geometry?
- What processes are used for surface treatment?
- Which coating process is chosen to manufacture the abrasive layer?
- How to manufacture a cavity (if desired)?

In literature, focused ion beam (FIB), wire electro discharge grinding (WEDG), and a number of grinding processes have been used to manufacture the geometry. At our institute, dicing blades combined with high-end precision machine tools are used to manufacture micro tools. The technology can manufacture the cylindrical shape of MPGTs in under two minutes with high precision, which is why it will be used in this project.

After preparing the substrate geometry, surface treatment is required to prepare for the coating process. A degreasing process that employs an alkaline solution to removed grease, fat, oil, and manufacturing residues is the first surface treatment step. Degreasing is either performed under boiling temperatures or using electrolytic methods that add an electrode to the solution. In this electrolytic cycle, the electrode is either anodic or cathodic – a combination of both is suggested in literature. Both boiling degreasing and cathodic degreasing is investigated in this work, anodic degreasing is substituted by another process: electrochemical machining (ECM). ECM is basically anodic degreasing with a much higher current. The current is high enough to remove material from the substrate, polishing the surface in-process. Following ECM, a pickling process is used to neutralize previous solutions and to remove passive layers from the substrate.

Following surface treatment, a suitable coating process is required. Four coating methods have been introduced in literature: sintering, chemical vapor deposition (CVD), electroplating, and electroless plating. Sintering is not selected because it is a process that is restricted by its high process temperatures, and pressure as well as our limited control in forming the abrasive layer according to our wishes – high temperatures and limited control over the abrasive layer, are also problems when manufacturing CVD-layers. When comparing electroplating and electroless plating, both function similarly, a substrate is immersed in an electrolyte and a metallic layer grows at a constant rate on the substrate. The difference is, electroplating is electrolytic and requires an electrode with a closed electrical cycle, while electroless plating is an autocatalytic process in which the substrate functions as the catalyst that initiates a chemical reaction. Another difference would be that electroplating can produce pure nickel layers while electroless plating produces a nickel phosphorous alloy that can be manipulated with different phosphorous contents and heat treatment. When compared for their advantages and disadvantages, both processes are excellent choices as they do not have the same disadvantages as sintering or CVD, giving the manufacturer complete control over the tool specifications. Electroplating offers a longer electrolyte service life as the solution is constantly replenished with new metallic ions; this attribute and the low operation temperatures make this process much easier to automate. Another disadvantage electroless plating has is that it requires an active surface the is receptive to electroless plating, often requiring an electroplated precoating. The advantages of electroless plating are that it produces harder, more uniform coatings, because of its isotropic nickel growth on the substrate; distance from the electrode is an issue with electroplating. Isotropic nickel growth means that any surface the electrolyte touches is coated, meaning that undercuts in geometry do not require additional assisting electrodes.

In general, almost all investigations performed in this dissertation can be performed with either of the two coating processes as their abrasive layers have similar attributes. Electroless plating is chosen in this work because the experimental setup used in this thesis produced better results when using electroless plating. The most noticeable difference is that grit adhesion to the substrate surface proved to be much better than with electroplating.

Optionally, a cavity can be manufactured at the pivot of MPGTs to prevent step-like structures – also called substructures – to occur at the bottom of microchannels. Substructures occur when grits closer to the pivot have a higher grit protrusion than the grits around the circumference area – an effect that is likely to happen because grits around the circumference are more prone to abrasive wear. At our institute, two methods have been developed to prevent substructures: adding an inclination angle to the tool and manufacturing a cavity via electrical discharge machining (EDM). In principle, in EDM, a µelectrode is positioned at the pivot of the substrate and material is melted/evaporated from the substrate, creating a cavity.

The goal of this work is to show the reader what micro pencil grinding tools (MPGTs) are, how to manufacture them, and how to use them. While ENGMANN focused more on the machine tool and machining aspects, this dissertation will dive into the chemistry behind the abrasive layer that coats these micro tools, showing you the reader exactly why this layer is the backbone of the process. This dissertation will also take a different approach to the machining process. While ENGMANN demonstrated some of the accomplishments he achieved with his then-newly developed tools, this dissertation will show the reader a conception of the machining process. A study

that shows what needs to be done to maximize tool life to achieve the most complex of structures is demonstrated.

4 Research Framework and Objectives

4.1 Preface and Framework

The framework of this dissertation is divided into three major categories: tool manufacturing, experimental setups, and tool application studies. Each category will be heavily influenced by the conception process that led to the solutions presented.

Machining experiments are conducted with MPGTs that have a diameter of 50 µm. The workpiece material was made of 16MnCr5 hardened steel (665 HV30). This workpiece material was chosen because it was used in the Collaborative Research Center 926 (CRC 926) "Microscale Morphology of Component Surfaces" through the subproject B09 "Geometrical Structuring of Component Surfaces by Micro grinding". A cooperation with the two subprojects C01 "Influence of Morphology on Radial Shaft Sealing Systems" and C02 "Interaction between Surface Morphology and Wear Chain Drives", required the mikrostructuring of tribological surfaces. 16MnCr5 was, therefore, chosen as the primary workpiece material to gain a better understanding of the material removal mechanisms in micro grinding.

All major experiments conducted in this dissertation will be conducted in this hard yet ductile material. Machining ductile materials bring along challenges that will be elaborated further in chapter 8.

In the following the cornerstones of each category are presented:

4.2 Course of Action

Based on the framework of the dissertation, the course of action is illustrated in Figure 4-1. In chapter 5, experimental setups for machining processes, as well as evaluation technologies, are presented and discussed – the experimental setup for electroless plating is presented in chapter 6. The most relevant modules, the influence of spindle errors on the machining process as well as used substrate materials are also discussed.

In chapter 6, concepts introduced in chapter 3 are implemented to manufacture the tool geometry, the cavity, and the abrasive layer of MPGTs. In section 6.1, a tool grinding process is introduced. Following that, a small parameter study for the EDM setup is presented, detailing the parameters configured to achieve cavity diameters of 20 µm or less. Section 6.3 introduces the experimental setup used for electroless plating. The setup includes surface treatment, electroplating, and electroless plating. A parameter study is conducted to determine a suitable concentration for components used for the electroless plating solution. In addition, a grit study is conducted to determine the required grit concentration as well as grit embedment time for a variety of grit sizes and substrate diameters. The influence of substrate rotational speed on grit density and distribution is also explored.

Chapter 7 contains the process kinematics, process conditions, and evaluation methodology used in chapter 8. This evaluation methodology includes microchannel analysis via confocal microscopy, material analysis to determine the concentration of iron adhesions on the abrasive layer, and a statistical analysis method.

Chapter 8 contains application studies by which the process is analyzed and constantly improved. In section 8.1, the effect of a water-based sodium dodecyl sulfate solution on the micro grinding process is determined. Based on this study, a larger parameter study was conducted

with a minimum quantity lubrication (MQL) system. The parameter study included three case studies with the first being a full factorial study that tests the influence of grit size, rotational speed, feed rate, and tool inclination on the process. The two cases with the best surface quality were then compared in a second study with MPGTs that have a cavity, testing its effect on substructures and surface quality. In a third study, the best parameters from the first parameter study were used with larger feed rates to determine the limits of the now optimized process.

Two major problems were discovered from the results of the MQL study. The first problem was the formation of adhesions at the tool bottom – discussed in section 8.4. The second issue was the formation of step-like substructures at the bottom of machined microchannels, which is discussed in section 8.2.

In section 8.5, the submerged cutting process that was introduced in section 2.4 is applied to micro grinding. The supplying method is used in a MWF application study to find a MWF that reduces adhesions at the tool bottom during machining experiments.

In section 8.6, a pendulum grinding process is introduced, that increases feed rate, makes deeper microchannels possible and generally increases tool life while maintaining process accuracy. Using submerged micro grinding and pendulum grinding, an additional parameter study is conducted to test tool life based on the parameters: grit size, rotational speed, MWF, and cavity.

In section 8.7, the processes capabilities to manufacture complex structures is demonstrated.

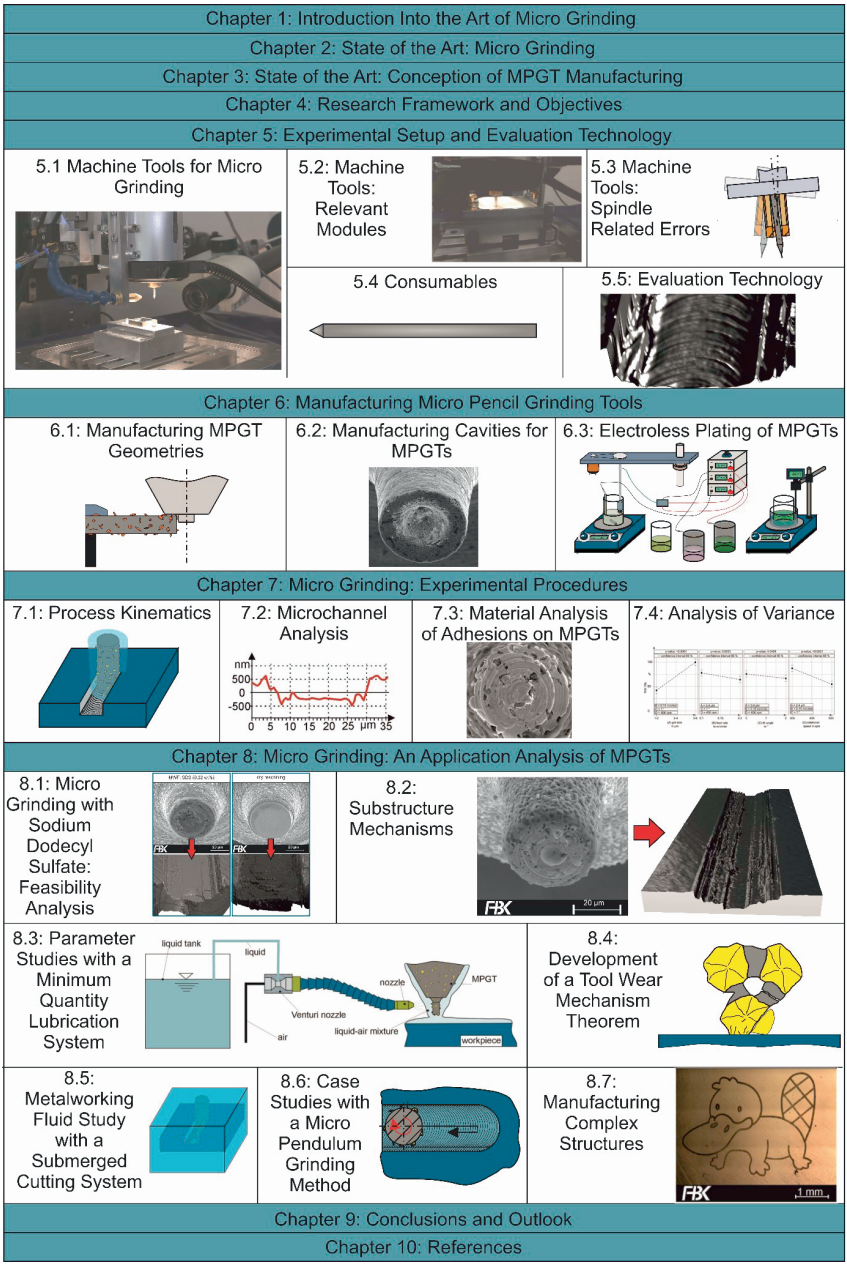

Figure 4-1: Research Framework of Dissertation

5 Experimental Setup and Evaluation Technology

In this chapter, the machine tools, and their most relevant modules are introduced; these modules are a µEDM-module, an MQL system, and a submerged cutting system. Following that, the run-out of spindles is elaborated upon to clarify its effect on the process. Finally, the evaluation technology is presented.

5.1 Machine Tools for Micro Grinding

Three machine tools have been used in this work: A cylindrical grinding machine to manufacture MPGT geometries and two machine tools for machining experiments.

5.1.1 Cylindrical tool grinding unit

Both this cylindrical grinding unit and the ultra-precision four axes machine tool (the fourth axis was added in [Auri17], [Reic17]) that is introduced in the next section were manufactured as part of the dissertation of SCHMIDT [Schm06]. Figure 5-1 shows a schematic of the cylindrical tool grinding unit. The grinding unit is built on top of a granite plate which is mounted on top of air springs, decoupling the system from vibrations. It has two grinding wheels, a coarser one and a finer one, each with their separate drive unit. The main spindle is mounted on top of an X-Y table and can be connected to one of two different drive systems: an electric motor for high rotational speeds for better surface quality and a much slower stepper motor that can only do a few rotations per minute but allows the user to manufacture more complex geometries, like that of a micro end mill. The stepper motor can do up to 25400 steps per rotation. The smallest axis movement of the X and Y axes is 100 nm [Schm06].

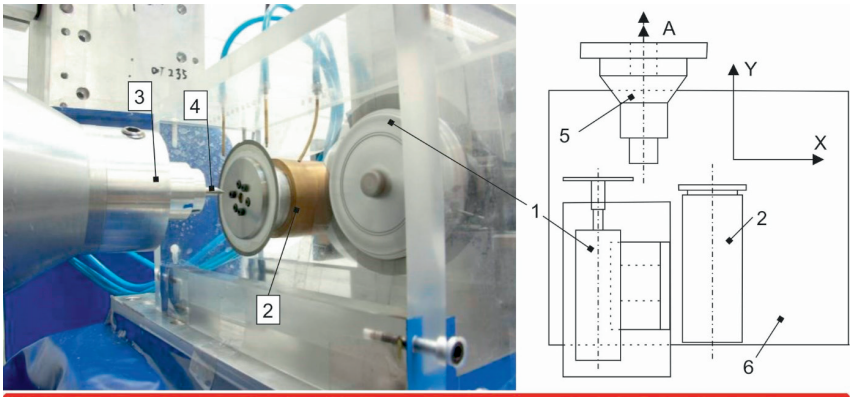

1	Coarse grinding spindle	3	Clamping device	5	Substrate spindle
2	Fine grinding spindle	4	Substrate	6	X-Y table
A	Rotational axis				

Figure 5-1: Cylindrical tool grinding unit by SCHMIDT [Auri12]

Dicing blades

The company Disco manufactured the grinding wheels used for this thesis. Like with MPGTs, diamond grits were used for non-ferrous materials like the cemented carbide substrates and cBN for HSS substrates. Since almost all MPGTs, produced for this thesis had diameters of ≥ 50 µm,

coarse dicing blades have been used almost exclusively. Table 5-1 shows the dicing blades used in this thesis [Disc18]:

Table 5-1: Dicing blades used to manufacture the tool tips

Substrates	Type	Grit size in µm	Diameter in mm	Thickness in µm
Cemented carbide	P1A851 SD800R10MB01	10 – 20	58	250
HSS	P1A851 B800R10MB01	10 – 20	58	250
HSS	PA851S B4000R10MB01	2 – 4	58	150

5.1.2 Ultra-precision four axes machine tool

The ultra-precision four axes machine tool is a moving table design machine tool that was used for almost all micro grinding experiments – presented in Figure 5-2. The machine tool is built on top of a granite platform that dampens vibrations and thermal influences. The machine tool comprises three axes units, a spindle, and a camera system connected to a control system. The spindle and the rotational axis (A-axis) are mounted on top of the Z-axis. A stepper motor with a resolution of 2.54 nm powers the Z-axis and a cross-rollers system guides it. The Z-axis has a travel of 101.6 mm and a positioning accuracy of <1 µm. The rotational axis A is a harmonic drive servo system that can tilt the spindle at angles of ± 30° around the Y-axis with a resolution of 0.00045°. The third axes unit is composed of X-Y tables that are guided by an air bearing system, have a maximal travel range of 100 mm at a positioning accuracy of < 1 µm, and are powered by a stepper motor at a resolution of 2.54 nm [Kirs17].

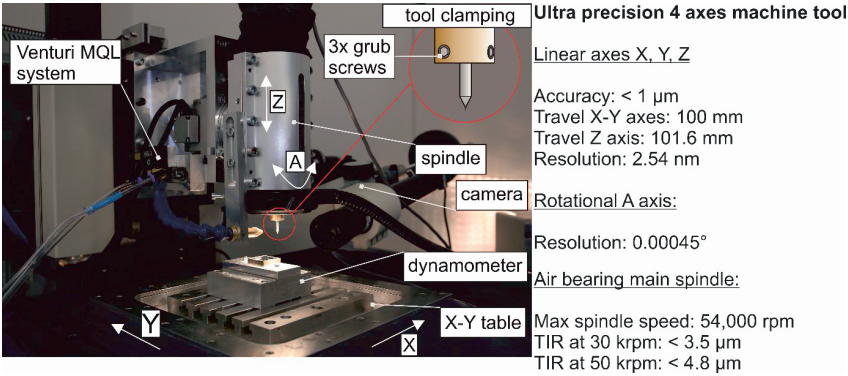

Figure 5-2: Ultra precision four axes machine tool [Arra17a]

The air bearing spindle rotates at a maximum rotational speed of 54,000 rpm with a run-out error of 6 µm. In this dissertation, the rotational speeds of 30,000 rpm and 50,000 rpm were used for the experiments, which have a run-out of 3.5 µm and <4.8 µm respectively. A manually adjustable clamping system was used to reduce reclamping errors of the tools to a minimum; this feature corrects reclamping errors from the tool machining process [Arra19c].

The machine tool is equipped with two different MWF supplying systems. The first system is a minimum quantity lubrication (MQL) system that provides the micro grinding process with

metalworking fluid (MWF). This system sprays the machining zone with an aerosol mixture, using an adjustable nozzle [Arra17a]. The second system is a submerged cutting system that consists of a pool filled with MWF – machining takes place in the MWF.

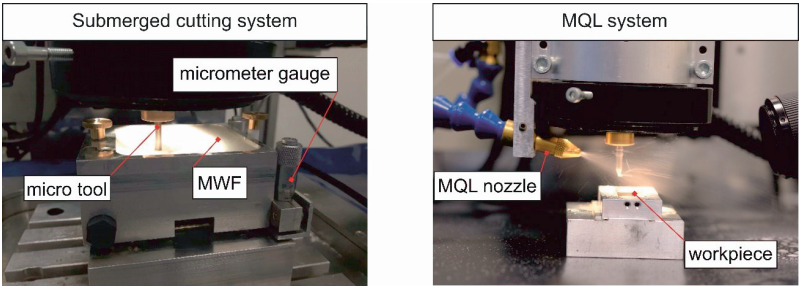

Figure 5-3: Lubrication systems for ultra-precision four axes machine tool: a submerged cutting system and a MQL system

5.1.3 The Nano Grinding Center

Developed and built during the dissertation of WALK [Walk16], the Nano Grinding Center (NGC) is an in-house developed, gantry type machine tool, that can manufacture the geometry, the cavity, and the abrasive layer of MPGTs and directly use them in a machining experiment, all in one clamping. Figure 5-4 displays a 3D-model of the machine tool. The machine tool is built on top of a granite platform that dampens vibrations and thermal influences. Up to six different modules have been built into the machine tool: a grinding unit similar to the one introduced in section 5.1.1, a µEDM unit that will be introduced in section 5.2.1, an electroplating unit, a spindle unit, a camera unit and an application unit on which workpieces are mounted.

The application unit contains a cross-table that moves in X and Y direction. The linear axes can adapt both MWF supplying units, introduced in Figure 5-3 and can move at an accuracy of 0,5 µm at a resolution of 1 nm – the travel is 60 mm.

An air bearing spindle with a maximum rotational speed of 160,000 rpm and a collet chuck system is used. Only a rotational speed of 120,000 rpm is used in experiments, which has a TIR of approx. 3.5 µm. The spindle is attached to a linear motor that moves in the Z-Axis at an accuracy of 0.5 µm at a resolution of 5.12 nm – the travel is 125 mm. The Z-axis is attached to a traverse that moves the spindle via a ball screw axis from one module to the next at an accuracy of 0.1 mm – also described as the U-axis.

The NGC is only used in a study in section 8.6. Electroless plating was performed in a laboratory fume hood, a manually adjustable clamping unit was preferred, which is why the machine tool in section 5.1.2 was ultimately chosen as the primary machine tool for the application study.

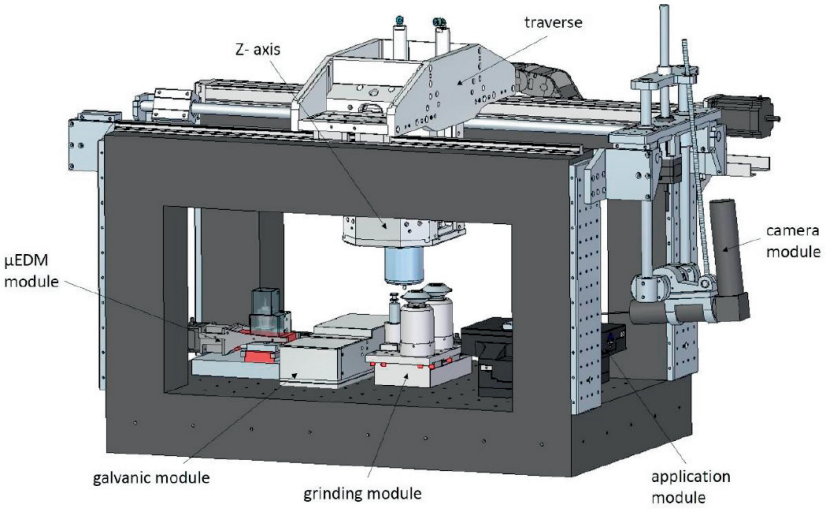

Figure 5-4: The nano grinding center [Walk14]

5.2 Machine Tools: Relevant Modules

5.2.1 µEDM module[1]

The µEDM unit was developed by WALK and ENGMANN [Engm11]. The system used a capacitive measuring method to determine the position between the center of the electrodes [Walk16]. An alternating voltage of 10 V with a frequency of 2 kHz was set between the electrodes. The electrodes are maneuvered to have a small distance between them, to empower the signal. The positioning was possible with the CCD-camera built in the system. The working medium used was deionized water. Since the working medium is an insulator, a capacitor is created between the electrodes. The X- and the Y-axes were used to move the µ-electrode around the substrate to determine the position in which the capacity is the highest and the voltage is the lowest; once determined, the center of the electrodes are aligned [Walk16].

It was determined during this dissertation that this system works well in theory but lacks the accuracy in aligning both electrodes. In present dimensions, it is difficult to accurately determine voltage discrepancies that result from positioning errors. In addition, the working medium might contain rogue particles from previous EDM cycles that disrupt the measurement by changing the electrical resistance. Another problem is caused by turbulence, caused by the flow of the working medium cycle; this flow has a positive effect on the EDM process, as it flushes removed material particles out of the cavity but is detrimental for a capacitive measuring method.

It was possible to calibrate the µEDM system by try and error until the exact coordinates were determined. The axes could then be locked with only the substrate changing. A µ-electrode with a diameter of 10 µm and a length of 300 µm was used to manufacture MPGTs with a diameter of 30 µm [Engm11].

[1] This module was optimized in [Arra19c] .

Figure 5-5 shows the new µEDM system. The positioning accuracy of the system was improved by adding two measurement probes, each with a positioning accuracy of 1 µm (depicted in Figure 5-5 as No. 3. The measurement probes were fixed on the X- and the Y-linear axes. Both axes are driven by a stepper motor that can do up to 125,000 steps per rotation. The measurement probes do not interact with the spindle or the working medium, they eliminate all inaccuracies except for the run-out error and the backlash of the linear axes.

The use of an inert liquid is indispensable for the stability and efficiency of this process when manufacturing cavities for micro tools. While gas mediums might also be able to flush machining debris from the machining zone, they are far worse cooling mediums [Zhan04]. Distilled water is used in this dissertation. When Compared to oil-based mediums, distilled water can cause rust, increase µ-electrode wear, and provide a less stable process. During discharge, a more viscous dielectric has better energy density as it limits the dilatation of the plasma channel. Oil-based mediums are far more suitable for a stable process. However, due to the easier filtration, its colorlessness, and it being less hazardous for a clean room, distilled water was ultimately chosen.

As in the previous setup, a container made out of polymethylmethacrylate (PMMA) is manufactured and deionized water (distilled water) is used. The working medium is circulated through a filtration/deionization unit to filter material removed from the process, keeping the conductivity below 5 $\mu S \cdot cm^3$, which translates to roughly 200kΩ. Using PMMA and distilled water makes the process visually accessible for the camera.

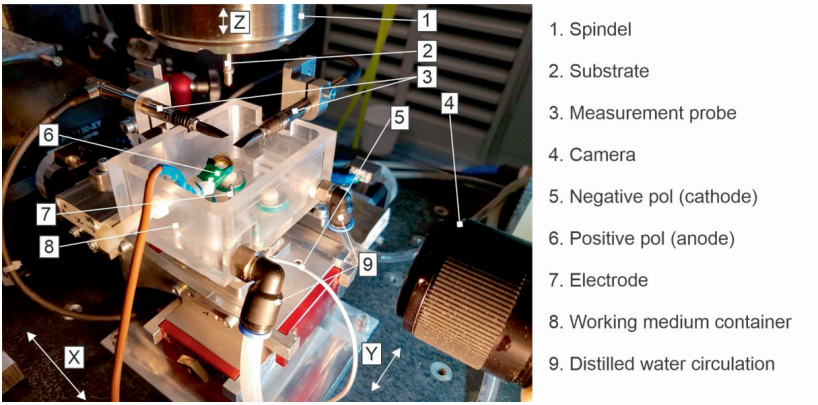

Figure 5-5: µEDM system [Arra19c]

A pulse generator that can generate pulses with a voltage of up to $u_o = 100$ V with a current of 2 A and a resistance of 50 Ω with frequencies of up to f = 10 MHz is used to provide the process with electrical current. The pulse amplitude, -width, and -frequency can all be adjusted.

The µ-electrodes require a substrate material that has a high thermal conductivity and a high melting point that lead to a higher heat dissipation into the µ-electrode, which in turn leads to considerably lower electrode wear rates [Ferr07]. In addition, high bending strength is required to make µ-electrodes with a small diameter and a high electrode length possible. Tungsten and graphite are usually used for the task; here KFM 308 tungsten carbide is used.

5.2.2 Minimum quantity lubrication system

The first supplying method, decided upon, was flooding the machining zone via an available MQL system; only minimal quantities of MWF were used, however, these minimal quantities are a flood supply for MPGTs with a diameter of 50 µm. Since the machine tool is not capsuled from its environment and is located in a clean room, a MWF safe for both the user and the machinery is needed. Sodium dodecyl sulfate (SDS) is a surfactant and detergent that has lubricating qualities; it is cheap, causes no health hazards in small quantities and is still used in the soap and shampoo industry [Smul00] [Arra17a]. Therefore, SDS was chosen as the primary MWF for the investigations in chapter 7.

A Venturi minimum quantity lubrication system (MQL) that sprays a liquid/air aerosol on to the machining zone is used in for the experimental setup, a schematic of the process is presented in Figure 5-6. Inside the MQL system, pressured air moves through a narrowed cross-section, creating a small vacuum inside a liquid tank. The liquid is suctioned into the MQL system and is then transported to the contact zone. Positive air pressure of 0.65 bar was used during the experiments.

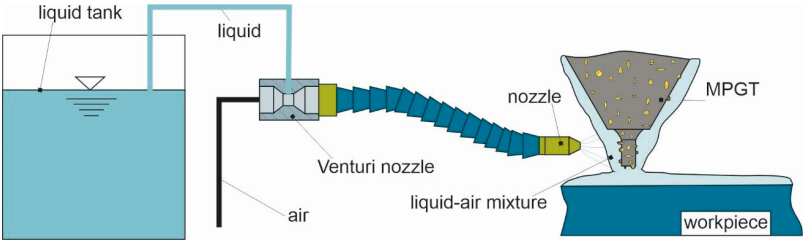

Figure 5-6: MQL system with a Venturi principle

This experimental setup required a pre-machining step that was conducted before micro grinding. The workpiece was machined with a larger grinding pencil tool to eliminate all the mounting related errors. The grinding pencil had a diameter of 3 mm and was operated with a rotational speed of 30,000 rpm, a feed rate of 10 mm/min, and a depth of cut of 20 µm. The workpiece required no polishing process prior to being glued to a workpiece mounting unit.

5.2.3 Submerged cutting pool

The prerequisites considered when designing this submerged cutting pool were that the device has to fit in the ultra-precision four axes machine tool, it must allow the usage of a dynamometer as well as an AE-Sensor all while considering the line of view of the camera. Submerged cutting allows the user to use almost any type of MWF without having to capsule the machine tool from the environment – a necessity for in house developed machine tools that are prone to constant changes. Figure 5-7 shows the resulting module. As mentioned in section 5.1.2, the module can align the surface of the workpiece, so that it does not need any pre-grinding. A sharp-edged polished workpiece is mounted in the setup. A measuring probe is used to measure the alignment of the workpiece. The X-Y table is used to move the workpiece, and the Z-axis is used to move the measuring probe. The principle of the alignment system is that of a three-point support system. Two micrometer screws represent two vertically moving support points

that push against a fixed joint. The micrometer screws themselves are mounted to the lubrication pool and need to push the pool upwards. To do so, a spring element made out of polytetrafluoroethylene (PTFE) presses the pool downwards, against the micrometer screws to produce traction.

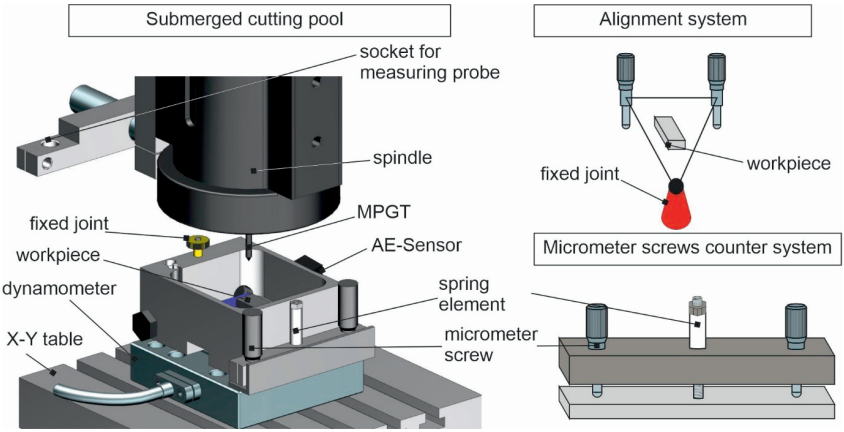

Figure 5-7: Submerged cutting pool

5.3 Machine Tools: Spindle Related Errors

An ideal spindle only has one degree of freedom and that is the rotation around its axis [Anan12]. Any movement in the remaining five degrees of freedom is classified as run-out error and is, therefore, undesired. Run-out errors may result from the spindle's design and manufacturing or from external influences such as thermal gradients, applied forces, or external vibrations [Mars09]. A fundamental distinction in motion errors is that some are harmonic of the basic rotor speed-synchronous motion error and some are not – these are called asynchronous motion errors [Ward15].

Figure 5-8 depicts an exemplary schematic of a spindle used for this thesis. The image illustrates two of the major errors that can occur during spindle rotation. The first being an error in tool rotation that is caused by a small imbalance in the air bearing system that carries the rotor inside the spindle. This imbalance causes the whole rotor to not rotate in line with the main axis – instead, the rotation is eccentric. The straightness of the substrates adds to this eccentricity, a problem often seen with substrates of lower quality. Eccentricity adds to the width of microchannels produced by micro end mills and MPGTs or increases the size of micro holes in microdrilling operations. In addition, to the radial component, the tool also moves in the axial direction, adding a small change in depth of cut. This eccentricity changes in a nonlinear fashion with increasing rotational speeds. Besides, the run-out value changes with the rotational angle so that the rotatory motion of the tool is not entirely circular.

Another type of error is the clamping error of MPGTs. The microstructure of the tool shaft surface and that of the collet chucks are not ideal; there will always be protrusions that cause mounted tools to add an additional clamping error to the run-out. This clamping error causes the tool itself to not rotate in line with its rotor. BOHLEY et al. measured the total run-out error

of a spindle to identify the amount of displacement caused by reclamping errors in a 2D-system and discovered that values of over 5 µm could occur. Of course, BOHLEY et al. also mentions that it is vital to reclamp tools in the same angular position to reduce reclamping error [Bohl16]. As mentioned in section 5.1.2, the machine tool used for this dissertation can correct this type of error to a certain extent.

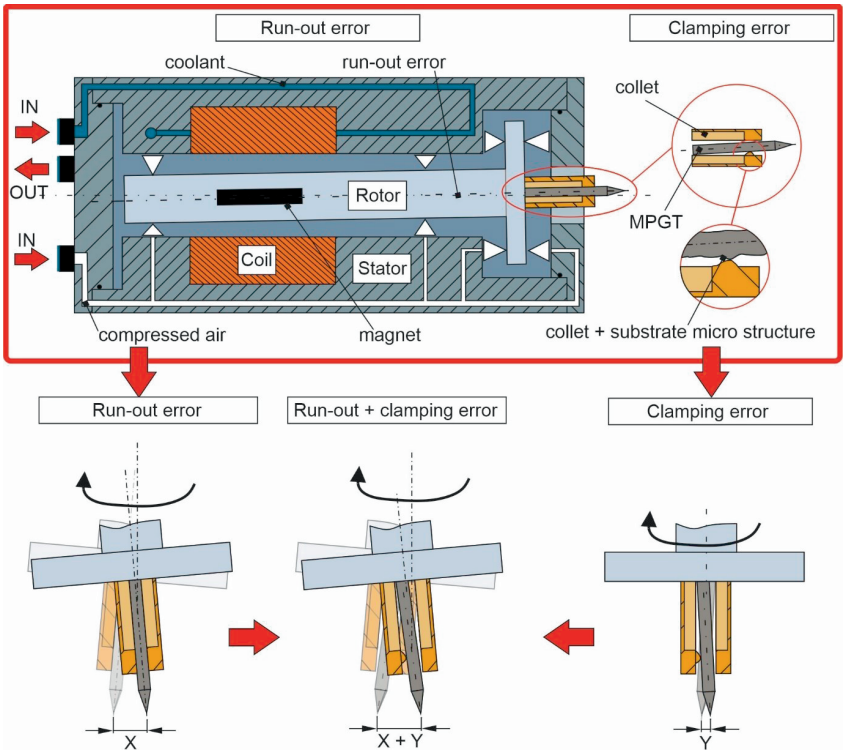

Figure 5-8: Errors related to spindle

A third error that can occur is thermal expansion/compression of the stator. While the spindle is located in a temperature-controlled clean room (20 °C ± 1 °C), the spindle itself is not exempt from thermal effects. The spindle requires a coolant that flushes through canals in the stator housing. Even the smallest fluctuation in the temperature of this coolant can cause thermal expansion/compression. The rotor thermally expands during the process; this thermal expansion depends on rotational speed and cannot be eliminated. The tool itself is affected by both an axial and radial run-out component. The radial run-out error may cause a slight increase/decrease in channel width, which adds/decreases stress on the tool. An axial run-out error, on the other hand, will decrease/increase the depth at which a tool cuts into material. The influence of thermal expansion on the run-out of the spindle is almost insignificant for the axial component, however, this change in temperature can change the depth of cut by up to a few micrometers.

5.4 Consumables

5.4.1 Substrate Materials

Table 5-2 lists the cemented carbide substrates that were used in this dissertation. KFM209 was the initial substrate material that has been used in all previous research on MPGTs as well as the research conducted for sections 8.1 – 8.4; until recently, it was also one of the main substrates used to manufacture micro end mills at our institute. PN90 and KFM308, the newest substrate materials for micro end mills at our institute, were used because their dimensions suited the µEDM experimental setup; KFM308 was used as a µelectrode material, and KFM308 was used as the MPGT tool substrate. KFM308 was later replaced with tooling steel. The KFM series is manufactured at *Konrad Micro Drill* and the PN series at *Sandvik,* Table 5-2 lists their properties according to their manufacturers.

Table 5-2: Cemented carbide specifications

Grade	Hardness *HV30*	Tungsten carbide + additives *wt.%*	Cobalt *wt.%*	Grain size *µm*	Bending Strength *N/mm²*	Density *g/cm³*	Dimensions ØDxL *mm*
KFM209	1920	92%	8%	0.2	4800	14.4	3.125x33
KFM308	1970	92%	8%	0.3	4300	14.6	3x28
PN90	1950	91%	9%	0.2	4700	14.55	3x40

Tool substrates made of HS0-4-1 high-speed tool steel (HSS) substrates with a hardness of about 700 HV30 were also used [DIN99] – Table 5-3 shows the material composition. To avoid confusion, each case study performed will indicate the material of the substrate.

Table 5-3: HS0-4-1 high-speed tool steel specifications [Wegs13]

C *wt.%*	Si *wt.%* ≤	Mn *wt.%* ≤	P *wt.%* ≤	S *wt.%* ≤	Cr *wt.%* ≤	Mo *wt.%* ≤	Other *wt.%* ≤
0.77 – 0.85	0.65	0.4	0.03	0.03	3.9 – 4.4	4 – 4.5	Rest

5.4.2 Workpiece

The workpiece material used was 16MnCr5 – also described as 1.7131 in the German material catalog and AISI 5115 in the American Iron and Steel Institute (AISI) – is a chrome-manganese alloyed case hardening steel according to DIN EN 10084 [DIN98]. The initial hardness of 16MnCr5 is 218 HV30 with a tensile strength value of up to 1180 N/mm^2. Table 5-4 lists the material composition.

Table 5-4: 16MnCr5 material composition [Wegs13]

C *wt.%* ≤	Si *wt.%* ≤	Mn *wt.%* ≤	P *wt.%* ≤	S *wt.%* ≤	Cr *wt.%* ≤	Iron *wt.%*
0.19	0.4	1.3	0.025	0,035	1.1	Rest

The workpieces are cut and machined to have the dimensions: 20 mm x 10 mm x 5 mm. The workpieces are then sent to a hardening shop and are hardened to have a hardness of 665 HV30

[DIN85] and tensile strength of approx. 2220 N/mm^2 through their entire cross-section – tensile strength is determined according to DIN EN 50150 [DIN00]. The workpieces are then polished to have a surface roughness R_z of less than 50 nm.

Figure 5-9 illustrates a workpiece glued onto its mounting unit. A scribing laser is used to mark the workpieces with its code number as well as its path markings and numbers for the later following machining experiments. An L-shaped calibration path is left without Laser markings to leave space for the measuring probe used in the submerged cutting pool system. The workpiece mounting unit has channels in which glue can flow. The whole unit can be directly mounted to the submerged cutting unit or mounted directly on the machine tool.

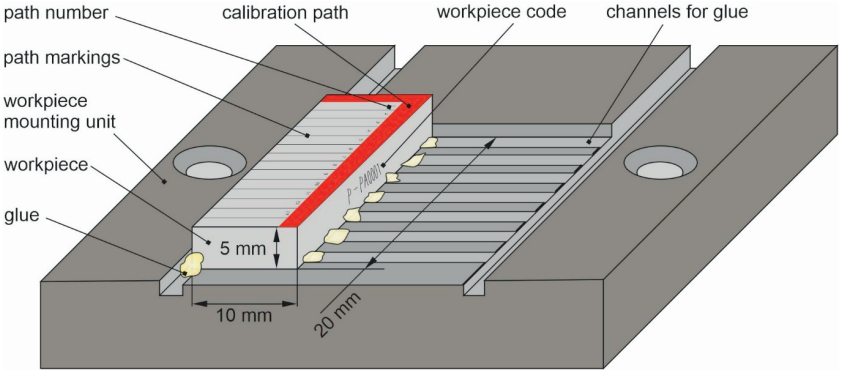

Figure 5-9: Workpiece mounting unit

5.4.3 Metalworking Fluids

In the MQL system, an aerosol made of air and a water-based solution that consists of water and sodium dodecyl sulfate (SDS) is sprayed on the machining zone. In submerged grinding, the MWF is simply added to the pool. A list of all MWFs used in the dissertation is presented in Table 5-5.

Table 5-5: MWFs used for submerged cutting experiments.

MWF	Manufacturer	Basis	Kinematic viscosity at 20 °C in mm^2 s^{-1}
Twinmax	*Steidle GmbH*	Plant	180 [Stei18]
Lubrimax Edel C	*Steidle GmbH*	Plant	88 [Stei18]
Canola oil	*Brökelmann & Co., Oelmühle GmbH & Co.*	Plant	78.7 [Spic07]
DiaMond 80	*Oelheld GmbH*	Ester	3 [Oelh18]
Petrofer Isocut R – 10 HM	*Petrofer Chemie, H.R. Fischer GmbH & Co. KG*	Ester	10.8 (at 40 °C) [Petr18]
SDS (0.02 wt%)	-	Water	1
SDS (1 wt%)	-	Water	1
SDS (5 wt%)	-	Water	1

5.5 Evaluation Technology

5.5.1 Optical microscope

The microscope was manufactured by Leitz (Ergolux AMC), and it uses a halogen bulb as light source to illuminate the workpiece in a bright and dark field contrast method. Leitz NPL Fluotar lenses with a magnification of 5x, 10x, 20x and 50x are used. This magnification is enough for an initial substrate/tool/microstructure inspection; however, it does not substitute for a Scanning electron microscope (SEM) or a confocal microscope.

5.5.2 Confocal microscope

A confocal microscope that is manufactured by Nanofocus is used to measure the surface roughness and shape of microchannels. The microscope uses a lens to focus light beams, emitted by a high-performance LED light source on the surface that is measured. The light is reflected and filtered, showing only the focal plane. By vertically shifting the lens, a stack of images is generated to produce the entire topography of the microchannels. The image stacks are then put together to generate three-dimensional models [Nano18]. The image software MountainsMap by DigitalSurf is used to analyse the microchannels.

5.5.3 Scanning electron microscope

A scanning electron microscope from Thermo Fischer Scientific (FEI Quanta 600) was used to visualize the tool topography and to analyze material compositions. The microscope is equipped with an EDX (energy-dispersive X-ray spectroscopy) and EBSD (electron backscattering) system and can operate in both low and high vacuum. EDX for material analysis and EBSD is used to draw conclusions about crystal structures. SEM is used to check the quality of the MPGTs (grain distribution, quality of the nickel layer) and to evaluate microchannels.

6 Manufacturing Micro Pencil Grinding Tools

In the presented work, a grinding process is used to machine the substrate's geometry, and an electroless plating process is used to coat the abrasive grits on both cemented carbide and tooling steel substrates.

6.1 Manufacturing MPGT Geometries

6.1.1 Tool grinding process

Figure 6-1 illustrates the tool grinding steps required to manufacture MPGT substrate geometries on the cylindrical tool grinding unit in section 5.1.1. Before using the tool grinding process described in Figure 3-4, the substrates were machined via a larger conventional tool grinding machine tool, changing the cylindrical geometry of the substrates to a conical geometry with an angle of approx. 40°. The conical geometry reduces material that has to be removed via the dicing blade and ensures sufficient illumination when observing the cutting process. The end face of the cylindrical tooltip was the first surface that was machined. Following that, the substrate diameter was manufactured while the substrate rotates around its axis at a rotational speed of 100 rpm. The final diameter of the tooltip was machined in multiple steps, to reduce the process forces on the dicing blade and to achieve a better surface quality on the final product. The feed rates that were used to manufacture the end face and the first diameters was 2 mm/min. The feed rate to manufacture the final diameter was 1 mm/min.

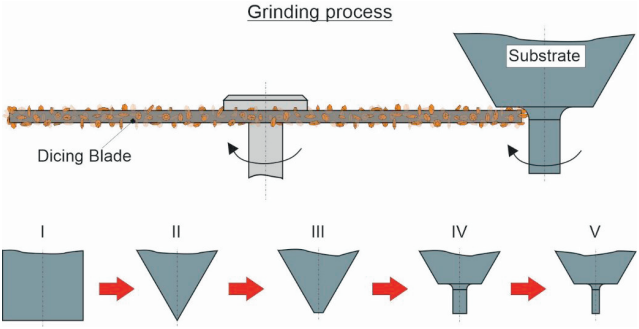

Figure 6-1: Tool grinding process

The diameter of the cylindrical substrate tip is adjusted according to grit size and planed bond thickness. For instance, if a monolayered MPGT – that is an MPGT with a single layer of grits – with a diameter d_{MPGT} of 50 µm has an average grit size of 2 µm is manufactured, a substrate diameter d_s of 46 µm is required. Multilayered MPGTs – that is MPGTs with multiple layers of grits – require a lower diameter and a longer coating time to make up for the difference in diameters. Diameters for substrate tips made for multilayered MPGTs were universally kept at 38 µm ± 2 µm. The length of each substrate tip was adjusted according to its foreseen application. The area to be coated was limited by adding an electrically inert shrink tube for the coating process. Figure 6-2 illustrates the geometry of a standard MPGT-substrate and an equation that calculates its maximum diameter for monolayered MPGTs.

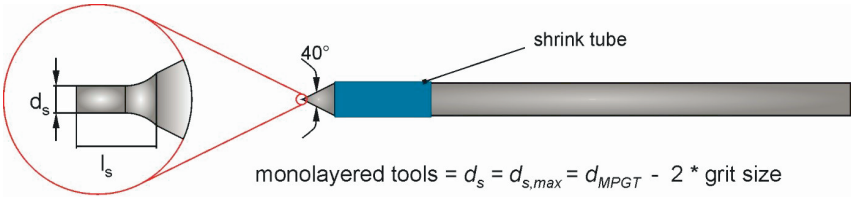

Figure 6-2: Geometry of a substrate

6.1.2 Deburring

As the substrate material was switched from cemented carbide to tooling steel, a new problem arose; burr formed at the edges of the tool. By fine-tuning the grinding program and the aid of some cleaning clay, this burr was kept to a minimum (<1 µm). However, the burr still influenced the quality of the product. Adding to the problem, when cavities were manufactured using the developed µEDM process, additional re-solidified material formed around the edges of the cavity. We tried using an ECM method but found that it only served to manufacture small cavities on the substrate surface and removed less burr than anticipated (more on the topic in section 6.3.2).

A mechanical option was developed in which cleaning clay infused with abrasive grits for deburring purposes was used. CBN grits of different grit sizes (5-10 µm, 20-30 µm) were embedded in a small piece of cleaning clay – see Figure 6-3. After the tool grinding process, the modified cleaning clay was placed on the tooltip while substrates are still clamped and rotating in the spindle with a low rotational speed. The cleaning clay was pulled parallel to the bottom surface of the substrates, with a finger gently pressing towards the tooltip. Pressing towards the tooltip guides the cleaning clay towards the area that needs to be deburred.

This process also gives the substrate rounded edges with a radius that increases, the longer the process is performed. Also, it smoothens the surfaces, almost removing all grinding marks from the substrate manufacturing process. After removing both the burr and the grinding marks, the substrate is deemed too smooth for an effective coating process and requires roughening – this is where the ECM process is used.

Figure 6-3: Deburring processes and influence of burr on abrasive layer

6.2 Manufacturing Cavities for MPGTs[2]

A parameter study was conducted with the system presented in section 5.2.1. The study determines the influence of supply voltage u_o and pulse duration t_i on the cavity diameter d_M and cavity depth h_m. Figure 6-4 depicts a schematic showing the process parameters. A feed rate v_e of 1 µm/min and a rotational speed of 15,000 rpm were used for this experimental study. This slow feed rate was used to prevent the two electrodes from colliding at lower supply voltages u_o, and pulse durations t_i, as the material removal rate is directly proportional to these two parameters. Distilled water with an electrical conductivity value of $\kappa < 5$ µS cm^3 was used as a working medium.

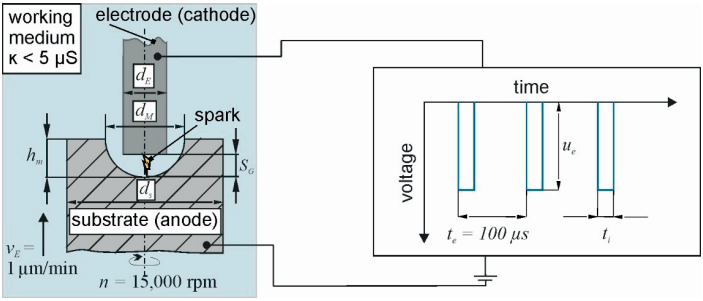

Figure 6-4: µEDM parameter schematic

A constant discharge duration t_e of 100 µs was used. The diameter of the substrate varied according to the process parameters. Experiments with larger pulse durations t_i and larger supply voltages u_o required larger substrate diameter as the size of the cavities increased and became larger than the substrate diameter. The µ-electrodes had an initial diameter of 5 µm and a length of 200 µm. The length and the diameter of each µelectrode were measured before each use. The determining process result was the so-called spark gap S_G. The spark gap can be calculated by subtracting the electrode diameter d_E from the final cavity diameter d_M. The spark gap is calculated as follows:

$$S_G = \frac{d_M - d_E}{2} \tag{12}$$

The supply voltage u_o was investigated with a constant pulse duration of $t_i = 0.3$ µs. A supply voltage u_o range of 40 – 100 V was investigated. Figure 6-5 shows the results of the test series. The size of the spark gap S_G had a proportionally progressive increase when increasing supply voltage u_o. The largest spark gap was measured at $S_G = 40$ µm and was achieved with a supply voltage of $u_o = 100$ V. The smallest spark gap was measured at $S_G = 5$ µm using $u_o = 40$ V.

To increase the effect, pulse duration has on the size of a cavity, a supply voltage of 50 V was used instead of 40 V during the ensuing investigation. A pulse duration range of 0.2 – 0.4 µs was investigated. Figure 6-5 shows the results of the test series. As determined before, the spark gap S_G increased with increasing pulse duration t_i. A spark gap of 4 µm was achieved at a pulse duration of 0.2 µs. While smaller pulse durations t_i are possible, a slower feed rate is required as the chance of collision between electrodes due to small vibrations increases.

[2] Results from this section have been previously published in [Arra19c] .

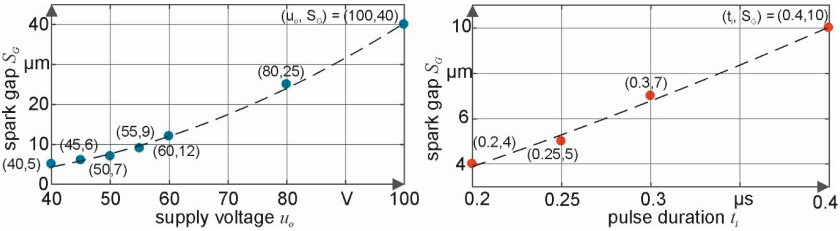

Figure 6-5: Diagram showing influence of discharge voltage and pulse duration on spark gap

A supply voltage of 45 V, a pulse duration of 0.25 µs, and feed rate v_E = 2 µm/min were ultimately chosen to produce the cavities needed for the MPGTs used in machining experiments. With adjusted parameters, a spark gap S_G of 4-5 µm could be achieved. This slight increase in supply voltage u_o and the pulse duration t_i made a higher feed rate possible, decreased process time, and made the process much more stable while maintaining small cavity diameters. Cavity diameters varied in a range of 13-20 µm. This deviation occurred because of changing µ-electrode diameters, run-out errors of substrates, and the positioning errors between electrodes [Arra19c]. Substrate diameter, cavity diameter, and the thickness of the abrasive layer have to be compatible. A too thick abrasive layer can completely cover cavities that are not large enough. For instance, an abrasive layer that is 5 µm thick would reduce a cavity diameter of 20 µm to 10 µm, because phosphorous nickel would grow uniformly around the circumference.

Figure 6-6 shows a substrate before and after producing a cavity. Inside the cavity, re-solidified residues cover the surface of the cavity; this is a sign that the system could benefit from a better flushing system. In literature, flushing mechanisms were improved by adding a µ-electrode rotation [Shab11], µ-electrode vibration [Yu09] or an orbital movement pattern while moving one electrode towards the other [Bamb09].

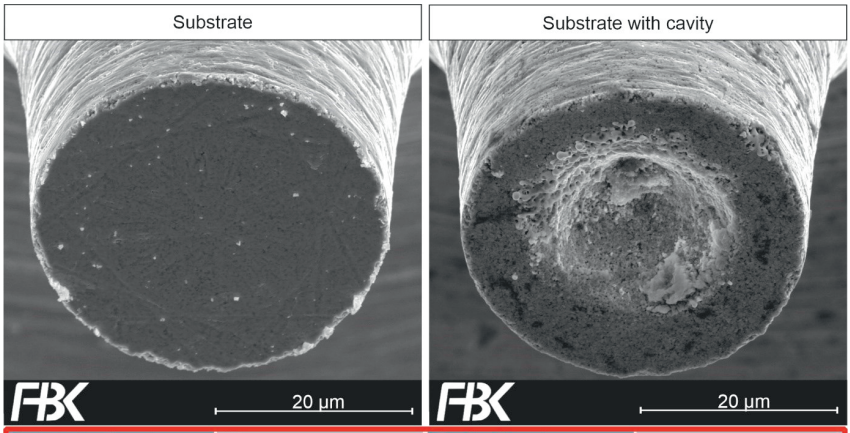

Substrate diameter	36 µm	Cavity diameter	19 µm
µ-electrode diameter	6-8 µm	Supply voltage	45 V
Rotational speed	15,000 rpm	Discharge duration	100 µs
Feed rate	0.002 mm/min	Pulse duration	0.25 µs

Figure 6-6: Substrate with cavity

The same parameters were successfully used on the HS0-4-1 tooling steel substrates. The only downside was that burr formed on the cavity edges, which was remedied via additional deburring.

6.3 Electroless plating of MPGTs[3]

There are two major parts to a coating process; surface treatment and the coating process itself. Bad surface treatment can cause the desired nickel layer to suffer from various deformities or worse, an abrasive layer that appears to be of the utmost quality on its outer layer, but has terrible adhesion to its base body.

Before starting surface treatment, each substrate is inspected for defects as well as manufacturing residues via an optical microscope (specifications in section 5.5.1). Larger manufacturing residues and even some burr can be removed with cleaning clay. A micrometer eyepiece is used to measure the substrates tooltip diameters with an accuracy of approx. 1 µm. Following that, shrink tubes are put on each substrate to limit the area that is coated to approximately 20 mm^2 (Figure 6-2 in section 6.1)

The methodology presented in this section is based on the processes presented in section 3.3. While electroless plating was ultimately chosen for tool manufacturing, a similar methodology can also be used for electroplating. As a matter of fact, this method has been used to manufacture MPGTs made with both coating processes.

6.3.1 Experimental setup

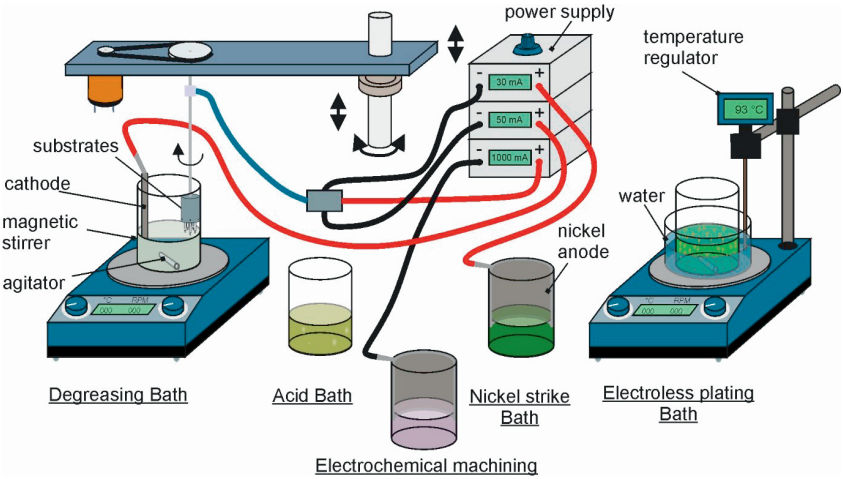

Figure 6-7: Electroless plating experimental setup

Figure 6-7 shows a schematic of the experimental setup used for the electroless plating process. The coating includes the following six process steps, in sequence; degreasing, electrochemical machining (ECM), pickling, electroplating, and electroless plating. During all sequences, the substrates are moved from one solution to the next via a slide bearing. A clamp determines the height of the device. Five substrates can be coated simultaneously with their grit population

[3] Results from this section have been previously published in [Arra16a, Arra16b, Arra17b, Arra18, Arra19b] .

unaffected. A slide bearing device that contains a gear reduction system that regulates the substrate rotational speed in a range of 0.33-46 rpm is used to ensure an evenly distributed grit population.

6.3.2 Substrate preparation and surface treatment processes

Degreasing processes

The degreasing solution is a mixture of distilled water and sodium hydroxide. This alkaline solution removes manufacturing residues, oil and fat layers from the surface of the substrate. A cathodic degreasing process is conducted with 50 g/L sodium hydroxide at a temperature of 40-50 °C. The processing time was two minutes at a current density of 5 A/dm^2. A nickel anode was used, adding nickel ions to the solution.

Electrochemical machining (ECM)

As mentioned earlier (section 6.3.1), ECM is the second step in surface treatment. After failing to effectively remove burrs from the substrate edges, we noticed that as a side effect, the process produced cavities on the surface (Figure 6-8). As mentioned in section 3.4.2, carbides inside tooling steel are electrically inert and cannot be dissolved by electrochemical means; this results in small cavities on the substrate surface. Apart from the cavities, the surface seemed to be much smoother. During electroless plating, nickel grows into these cavities, giving the abrasive layer an interlock. Only HSS substrates in this dissertation are treated with this process.

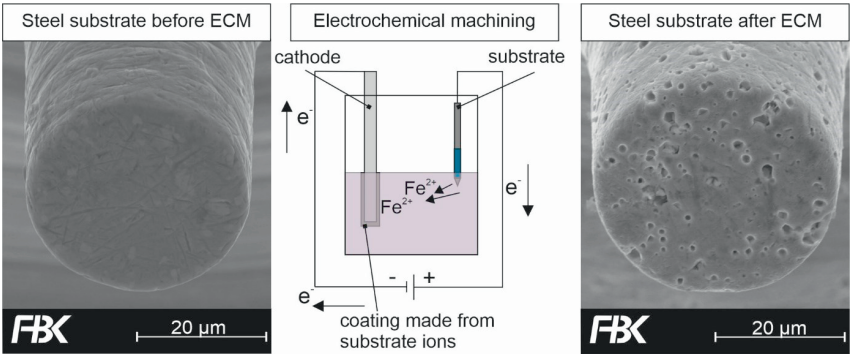

Figure 6-8: Electrochemical machining (ECM)

This process functions similarly to an electroplating process but in reverse. Material is removed from the substrate by ionic reduction and is added to a cathode. The water-based solution is made out of 30 g/L sodium tungstate and 20 g/L sodium hydroxide – according to a recipe developed by YEH [Yeh01]. Substrates are processed individually at room temperature, with a current density of I = 50 A/dm^2 and a polishing time of 30 seconds. After the ECM, no cleaning clay should be used, as residues will be interlocked in the cavities. In addition, the surface is highly sensitive to corrosion, which is why the next step has to be conducted immediately.

Pickling process

Following the ECM process, the substrate is immersed in an acidic solution to first of all, neutralize the degreasing and the ECM solution. Both the upcoming electroplating and the electroless plating solutions are weak acids (pH value 4-7) that can react with alkaline residues from

previous solutions: observations showed lump formations in the electroplating electrolyte when drops from the degreasing solution were added. Secondly, and more importantly, the acidic solution removes passivation layers that formed on the surface of the substrate via air oxidation. Iron (III) oxide on the surface of substrates can block ongoing coating processes. Therefore, the substrates are not allowed to have a dry moment between coating and pickling.

Two types of etching solutions have been used during this thesis: one used on cemented carbide substrates with 10 g/L HCl with distilled water and a second one for HSS that is made of 10% HCl. The low HCl concentration for cemented carbide was chosen because a weaker reaction to the following coating processes has been observed at higher HCl concentrations. HCl is volatile, it evaporates at higher temperatures, steadily decreasing the HCl concentration in the solution, which is why it is used at room temperatures.

Nickel-Strike electroplating process

Following the etching process, the substrates receive a thin, exceptionally adhesive, and wear-resistant nickel layer. This coating helps to initiate the autocatalytic chemical reduction process on the substrate surface [Mall90]. In experiments with cemented carbide substrates, it was observed that nickel formation could not be achieved during the electroless plating process without this pre-coating process. An electric cycle is created between the substrate and the nickel anode [Bren47]. In this electric cycle, the substrate is the cathode and the nickel electrode acts as an anode. This thin nickel layer is applied to the substrate using a Wood's nickel strike solution at room temperature. The solution consists of distilled water, 250 g/L nickel chloride as well as 10 g/l hydrochloric acid for cemented carbide substrates and 50 g/L for steel substrates. The substrates are plated with a 3 A/dm^2 current density and a coating time of 60-90 seconds. The inert shrink tubes are used to mask part of the substrate to concentrate the electroplating process on a defined area. This assures that the area to be coated is constantly immersed in the solution, allowing for constant current densities despite differing immersion depths of the substrates.

6.3.3 Electroless plating

The electroless plating solution is heated up to 87 °C ± 1 °C. The pH value in the solution is adjusted using hydrochloric acid (HCl) and kept in the range of 5.2-5.4. The beaker containing the electroless plating solution is placed in a larger beaker filled with water to increase temperature stability during the process [Arra16b]; a sensor regulates the temperature in this larger beaker. A temperature difference of approximately 7 K was measured between the water and the plating solution in the beakers. 100 ml plating solution was prepared for each experiment in a beaker that has an inner diameter of 66 mm and a glass thickness of 2 mm. The components used for this solution are listed in Table 6-1. The recipe used for this electroless plating solution was developed from a similar one published by PARK et al. [Park10]. The component concentration of thiourea and the abrasive grit concentrations will be discussed in the next two subsections.

Table 6-1: Composition of electroless plating solution

Component	Concentration [g/L]
Nickel sulfate ($NiSO_4 \cdot 6H_2O$)	30
Sodium hypophosphite ($NaPO_2H_2$)	20
Sodium acetate (CH_3COONa)	20
Thiourea (CH_4N_2S)	0.0001 – 0.0011
Hydrochloric acid (HCl)	Adapted to pH-value
Abrasive grits	Adapted to grit size

During the main coating time, the substrates are placed up to the middle of the shrink tube into the solution. The magnetic stirrer rotates the agitator with approximately 60-150 rpm, whirling up the dormant abrasive grits at the bottom of the beaker. The rotational speed of the agitator is adjusted to the grit size in the solution, as the weight of the grits may either cause them to remain at the bottom of the beaker or float at the surface of the solution. Because of centrifugal forces, the trajectories of the abrasive grits tend to be closer to the rim of the beaker, which is why the substrates are placed closer to the rim. A constant nickel growth coats abrasive grits that impact the cylindrical tooltip. When the magnetic stirrer stops rotating, the abrasive grits drop to the bottom of the beaker while nickel is still growing at a constant rate. This allows the coated abrasive grits to be embedded further with an additional nickel layer with a thickness that is influenced only by the embedment time.

In the upcoming two subsections the influence of the stabilizer component thiourea, as well as the electroless plating parameters, are investigated in detail. KFM209 was the substrate material in both studies. The goal of the study was to achieve monolayered MPGTs with sufficient grit protrusion and exceptional surface topology. Figure 6-9 shows a schematic of a monolayered abrasive layer with all of its components. The image also shows the effect electrochemical machining has on the process. As mentioned before, the cavities help the abrasive layer to interlock.

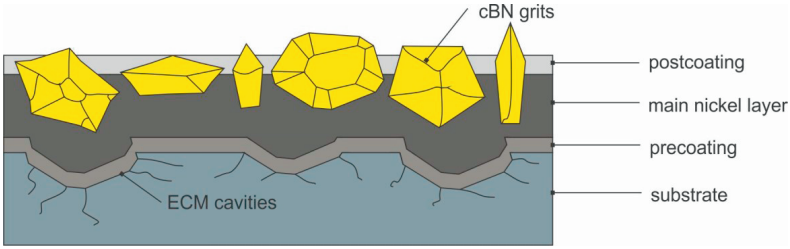

Figure 6-9: Monolayered abrasive layer

6.3.4 Stabilizer concentration study

In general, the solution is less sensitive to smaller variations in every component in the solution except for the thiourea concentration. Small variations in the thiourea concentration can either cause the plating solution to decompose early or hinder nickel deposition completely [Cheo04]. Thiourea concentrations in a range of 0.1-1.1 mg/L were investigated. The main coating time was 15 minutes, and the surface treatment was for cemented carbide substrates. The evaluation was based on the optical characteristics of nickel layers and possible deposition rates. A beaker

containing a 100 ml plating solution was used for the investigation. Three substrates for each thiourea concentration were coated. Figure 6-10 shows SEM images of coated substrate surfaces that illustrates the difference in quality for different thiourea concentrations. Figure 6-11 shows the nickel deposition rate achieved with this thiourea concentration.

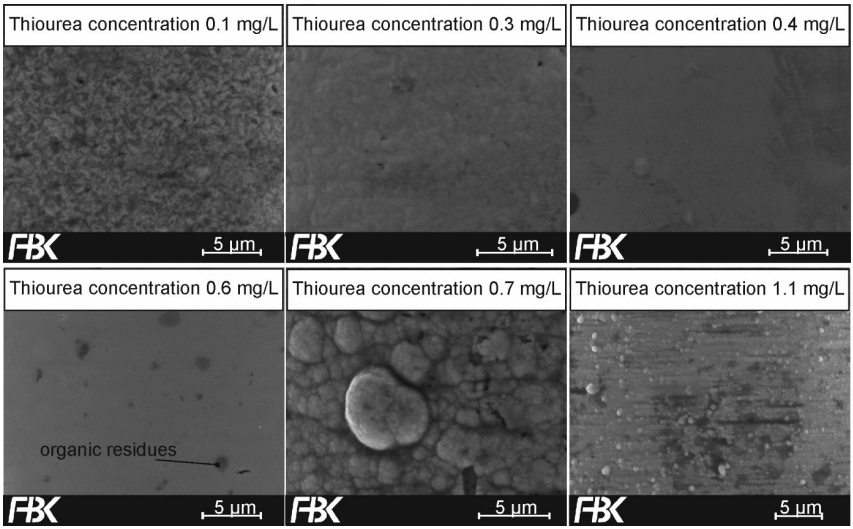

Figure 6-10: Influence of thiourea concentration on surface quality of coating

At a thiourea concentration of 1.1 mg/L, almost no nickel deposition occurred – the grinding marks from the manufacturing process are still visible. Thiourea concentrations in the range of 0.7-0.9 mg/L lead to a formation of a rough, uneven nickel layer with an almost cauliflower-like structure. Besides, nickel deposition rates in a broad range of 5-16 µm were documented, making the results irreproducible. When using concentrations below 0.3 mg/L have a rough, porous inhomogeneous surface at a lower nickel deposition rate. The range of 0.3-0.6 mg/L showed a much more even nickel layer with less porous surfaces and less nodal formation than with previous concentration ranges.

Diligent handling of the stabilizer thiourea is necessary, as only a narrow concentration range enables a successful coating process and an even narrower range to achieve a coating with good surface quality. In terms of ideal surface quality, a thiourea concentration of 0.4-0.5 mg/L was determined to be the most consistent. Some substrates coated with a concentration of 0.3 mg/L proved to be more porous and other substrates coated with a 0.6 mg/L tended to have the same rough, uneven surface as ones coated with a 0.7 mg/L concentration. The maximum nickel deposition rate was documented at a mean value of 21 µm/h ± 4.1 µm/h using a thiourea concentration of 0.4 g/L. The nickel deposition rate was determined by using an optical microscope (specifications in section 5.5.1) and its micrometer eyepiece to measure the diameter of the substrate's tooltip before and after the coating process.

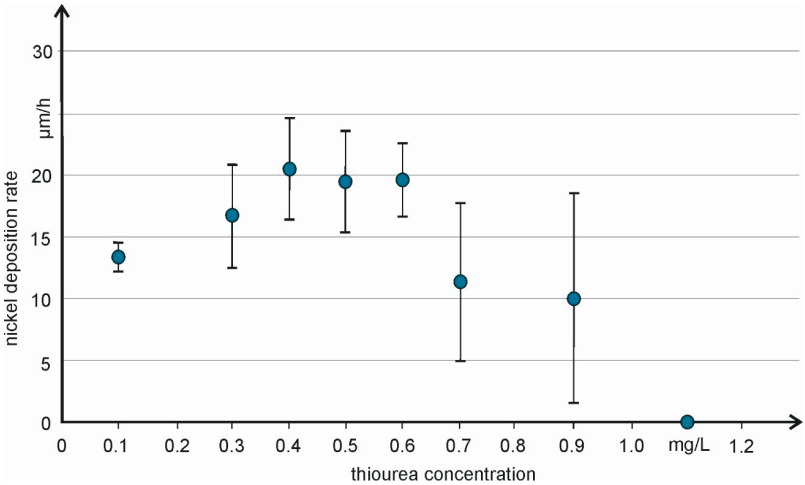

Figure 6-11: Influence of thiourea on the nickel deposition rate

A quantitative EDX analysis shows that phosphorous contents of 1-4 wt.% can be achieved. According to the literature study conducted in section 3.3.4, when a phosphorous content reaches values below 7 wt%, the layer has a microcrystalline structure. The range achieved for tools in this work have especially high hardness values, but a low tensile strength.

6.3.5 Abrasive grit evaluation study

Having achieved process reliability for electroless plating, it was time to add abrasive grits to the Ni-P layer and determine the best parameters to produce abrasive layers for MPGTs using grits of different sizes. Grit concentration in the solution, substrate rotational speed, and grit embedment time were the investigated parameters here. A grit size with a constant range of 1-2 µm was chosen to initiate the study. Parameters for monolayered MPGTs have been investigated for different grit sizes and are made available in section 6.3.7 (Table 6-2). Every experiment was conducted at least three times with a single substrate per solution.

In the first study, the effect of grit concentration in the solution on the grit density in the abrasive layer was investigated. Doing this study first was vital as it has led to a reduction in abrasive grits usage. Also, grit density directly influences the evaluation process of the other studies. To give an example, an overdose in grit concentration may support lump formation on the bottom surface of MPGTs. The desired product is an MPGT with a Ni-P layer thickness of approximately 1 µm and a lump-free, dense abrasive layer that provides enough chip space between grits. Following the diagram presented in Figure 6-11, a main coating time of 150 s and an embedment time of 30 s were chosen. A constant substrate rotational speed of 1.5 rpm was configured. Grits were whirled up in the solution with a rotational speed that is high enough for abrasive grits to float in the solution but low enough to prevent a large eddy from forming at the center of the beaker – as mentioned in 6.3.3, it is adapted to grit size. Figure 6-12 depicts three MPGTs, coated with three different grit concentrations; 150 mg/l, 500 mg/l, and 1000 mg/l. Adding only a small amount of 15 mg to a 100 mL solution was enough to produce a semi-operational MPGT. As depicted in Figure 6-12, a direct correlation could be established

between the grit concentration added to the solution and the grit density on the finished product. It was determined that a grit concentration range of 0.5-1 g/L is sufficient to manufacture MPGTs with a grit size of 1-2 µm. A grit concentration of 0.5 g/L was chosen for the remainder of the investigations.

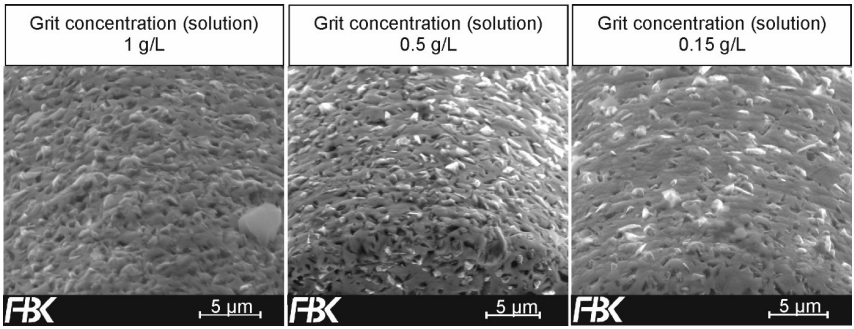

Figure 6-12: Varying grit concentrations in coating solution

Finding the right balance between grit protrusion and high grit retention forces is essential for successful micro grinding operations. Three embedment times were examined: 30 s, 60 s, and 120 s – Figure 6-13 illustrates the results. 120 s proved to be a too high embedment time the grits are, for the most part, wholly covered with a Ni-P layer. Embedment times of 30 s and 60 s produced sufficient results. 60 s was used in the final part of this grit study.

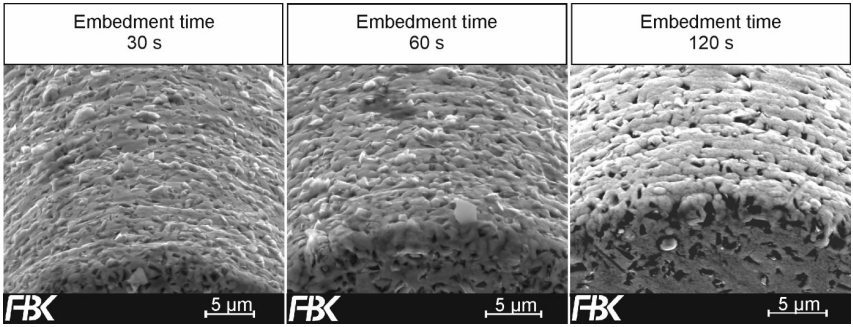

Figure 6-13: Influence of embedment time

Next, the rotational speed of the substrate is investigated; the initial rotational speed was 1.5 rpm. Figure 6-14 shows the 5 rotational speeds investigated, covering a range of 1.5-46 rpm. With progressing rotational speed, a sort of nodal formation is occurring on the surface of the substrates. The rotational speeds should, therefore, be chosen below 9 rpm, depending on the grit size. For larger grits, a slower rotational speed is preferred as it increases contact time between the substrate surface and incoming grits. For smaller grits, used to produce smaller tools like the MPGTs with diameters below 5 µm presented in section 6.3.7, a higher rotational speed is necessary as the coating process is rather short.

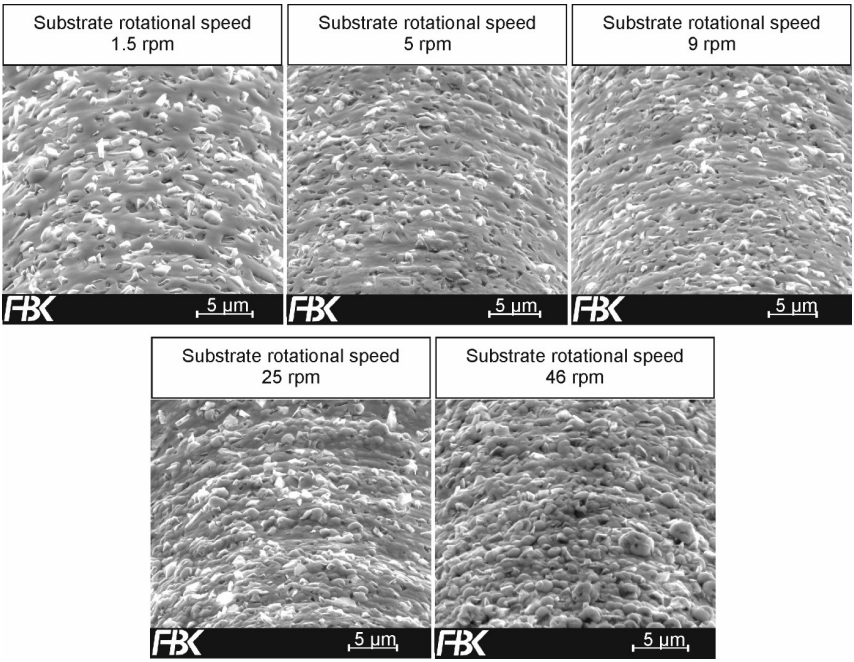

Figure 6-14: Influence of substrate rotational speed

An additional investigation was carried out for non-rotating substrates. The assumption was that the behavior of the boundary layer influences the diffusion of the solution; this causes the substrate to experience an almost laminar flow on the flow side and a turbulent one on the backwater side. These considerations are taken from a macroscopic point of view and are illustrated in Figure 6-15. The flow side of the substrate was coated with a smooth, even nickel layer, just as seen in Figure 6-10 for a 0.4 mg/L thiourea concentration. The backwater side shows a rough, uneven surface structure similar to the one in the 0.7 mg/L thiourea; this leads to the conclusion that there is a correlation between the substrate rotation during electroless plating and the surface topology. The backwater observation is also commonly known in literature [Oert11], [Schl06].

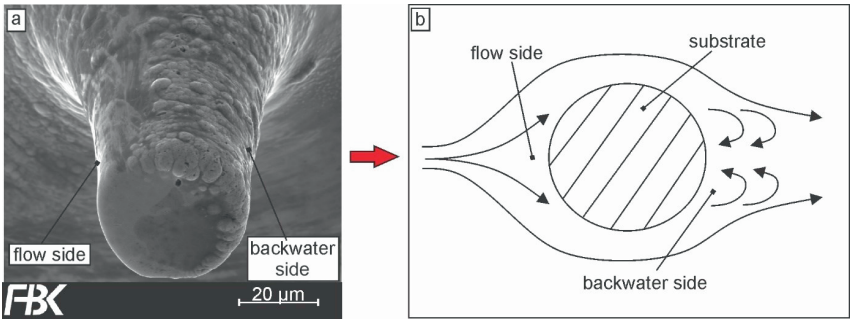

Figure 6-15: a) substrate topography with 0 rpm rotational speed, b) Backwater area according to [Schl06],

6.3.6 Abrasive grit adhesion to the substrate surface

Several theories are considered to explain how grits that impact the substrate surface remain there long enough to be coated. The main issue here is that abrasive grits are under the influence of forces that occur because of sedimentation and the current in the solution – forces that move grits away from the substrate. Yet, it seems that there are stronger forces that keep the abrasive grits in place long enough for a phosphorous nickel layer to form. There are of course the Van der Waals forces that help small abrasive grits to adhere to the substrate surface long enough for a phosphorous nickel layer to form around them. Adsorption effects can be provoked by adding a surfactant to the plating solution. During this study, 1 g/L of the surfactant Sodium Dodecyl Sulfate has been added to the solution to test the effect on grit density on the tool bottom. The result was that adsorption occurred between the grits themselves. Large grit populations accumulated at the center of the plating solution. A surfactant that prevents interaction between the grits themselves is needed to make use of this effect.

A third mechanism that occurs during the plating process is small hydraulic abrasion. Particles suspended in a working medium under the influence of fluid flow act upon surfaces they impact on, mechanically. This mechanical impact can be categorized into impact and sliding abrasion. Material is removed over time through small scale deformation, cutting, fatigue cracking or a combination of all – Figure 6-16 shows an impact erosion model based on a model developed by GUO et al. [Guo02]. While these material removal mechanisms occur, constant nickel growth would compensate for small grooves that happen due to erosion. The theory is that upon impact, abrasive grits stay in contact long enough to start grit embedment by the ensuing growth of the phosphorous nickels layer. The parameters that influence this process are the grit velocity as well as its angle, its hardness, its shape factor, and the grit concentration in the solution. A higher concentration, for example, means that more particles strike the surface of the substrate and increasing the chance for grits to be embedded into the phosphorous nickel layer. On the other hand, a too high concentration may increase the chance for grit collusions to occurring. Collusion between grit decreases grit velocities, changes their trajectory so they may not collide with the substrate at all and may even damage the grits themselves.

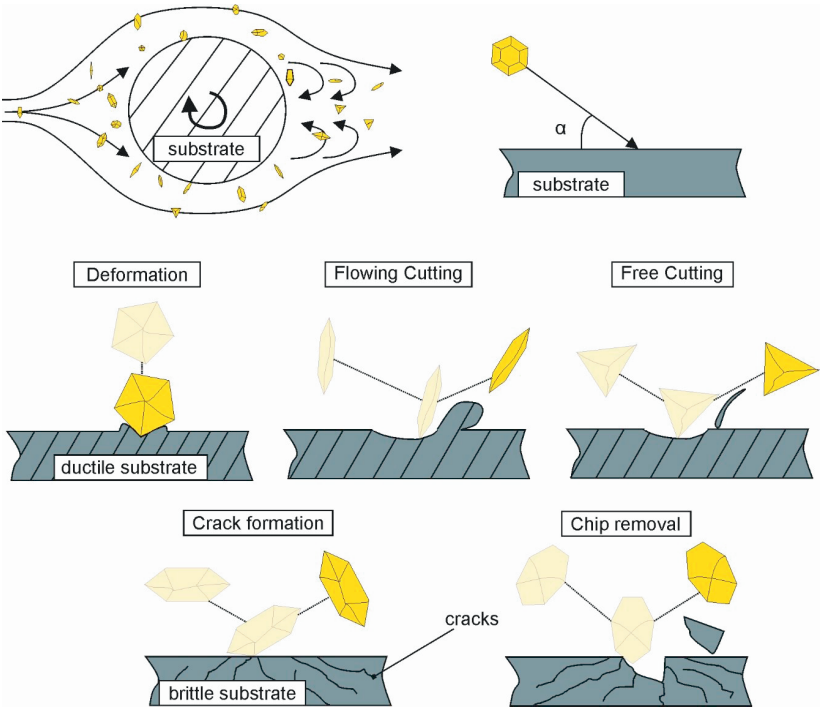

Figure 6-16: Hydraulic erosion mechanisms based on a model developed by GUO et al. [GUO02], simulating grit behaviour during electroless plating

6.3.7 The product

Table 6-2 lists the suggested plating parameters to manufacture monolayered MPGTs with different grit sizes. The minimum plating time is the time needed to embed the grits to about approximately 30%-50%. In the embedment phase, the grits reach a nickel layer thickness of approximately 50%-80% of coated grit size.

Table 6-2: Coating parameters for monolayered MPGTs with diameters < 50 µm

Grit Size in µm	Minimum plating time in min	Embedment time in min	Optimal grit concentration (solution) in g/L
1-2	2	0.5-1	0.5-1
2-4	3	1.5-2	4
3-6	5	2-3	8
5-10	10	3-4	15
6-12	12	4	20
8-16	15	5	23

Generally speaking, the grit size is the most significant limitation to the plating process. It is easier to control a plating process with smaller grits because the grits are relatively small when compared to the area to populate on the substrate; this can be seen in Figure 6-17.

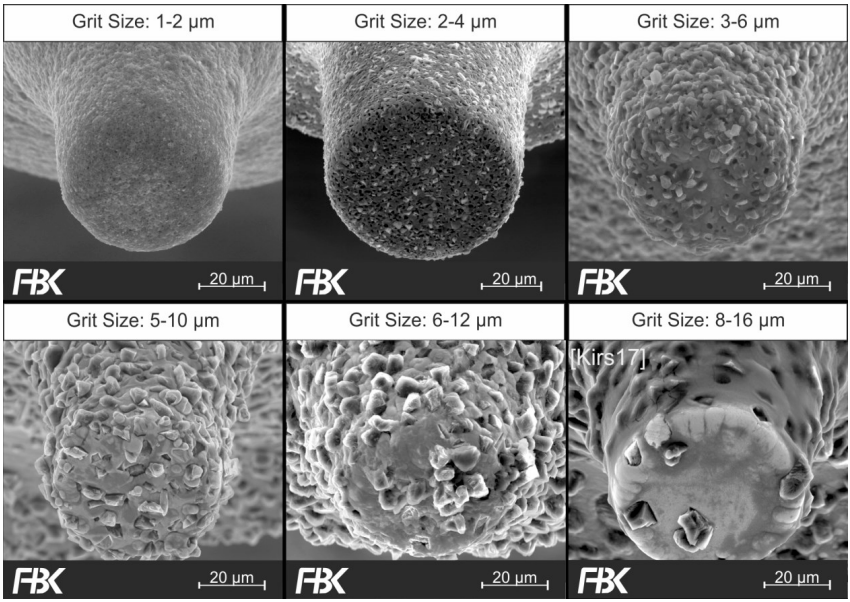

Figure 6-17: Electroless plated MPGTs with different grit sizes

The uniformity of the grit distribution diminishes with rising grit sizes. For example, a grit size of 8-16 µm is too large for the given substrate diameter of 36 µm to achieve a feasible grit density. Also, larger grits require a much larger grit concentration increasing the costs of the manufacturing process tremendously. The minimal grit concentration required to manufacture MPGTs with a grit size of 8-16 µm is 23 g/l. In comparison, for a grit size of 1-2 µm, a concentration of 0.15 g/l is sufficient to manufacture an MPGT with a diameter of 50 µm [Kirs17]. Experimental results revealed the grit size of 6-12 µm to be the largest grit size to deliver MPGTs with sufficient grit concentration. Figure 6-18 shows MPGTs with a cavity in the three grit sizes: 1-2 µm, 3-6 µm, and 5-10 µm. The cavity was manufactured using the µEDM process mentioned in section 6.2. The tools are used in chapter 8.

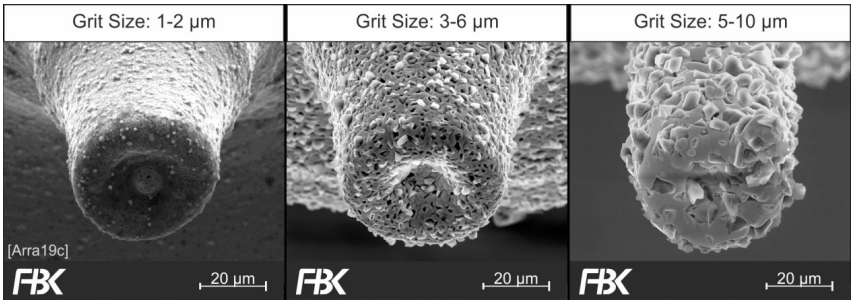

Figure 6-18: MPGTs with cavities

Figure 6-19 shows MPGTs with diameters smaller than 5 µm. The substrate was machined down to a diameter of 2-3 µm at a tip length of 250 µm. The dicing blades that have been used to manufacture them caused this high aspect ratio. Because of the large radius on dicing blades, only a small portion of the substrate has a cylindrical shape. The main coating time was 3 minutes for all grit sizes; this means that tools coated with a large grit size are monolayered tools and tools coated with a small grit size a multilayered tool. The embedment time was 15 s for a 0.5-1 µm grit size, 20 s for a 0.75-1.5 µm grit size and 30 s for a 1-2 µm grit size. Manufacturing residues and loose grits are usually removed via cleaning clay. Using cleaning clay on MPGTs with a diameter of ~5 µm would bend the tooltip. It was observed that even the force produced by a soft piece of tissue, grazing the tool-tip is enough to bend them.

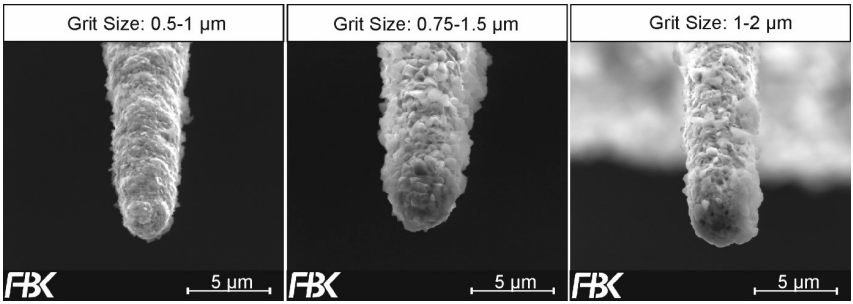

Figure 6-19: MPGTs with diameters < 5 µm

One would think that larger tools with larger grit sizes are easier to manufacture than smaller ones; however, this is far from true. These larger grits are heavier and require a higher rotational speed from the magnetic stirrer. Higher rotational speeds mean that these grits impact the substrate at a higher velocity, making it harder for them to stick to the surface. Much larger quantities of grits are required to manufacture tools with larger grit sizes. Figure 40 shows an example of such MPGTs with two different grit sizes. For a grit size of 20-30 µm, a recommended grit concentration of 50-70 g/L is added to the solution, and for a grit size of 6-12 µm the same as with the smaller tools.

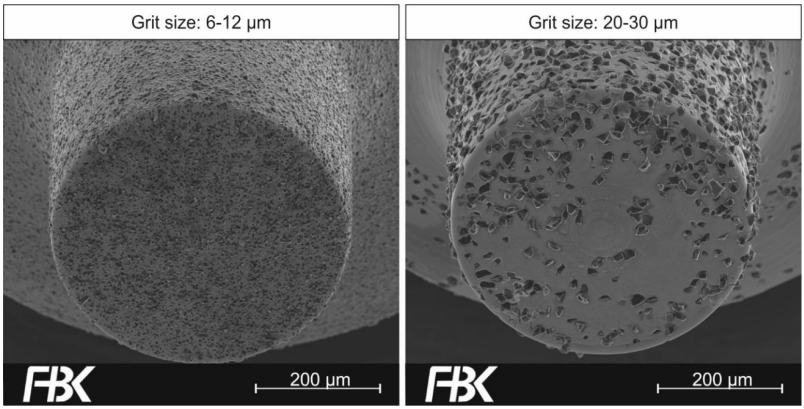

Figure 6-20: MPGTs with a diameter of 400 µm

6.3.8 Electroless plating troubleshooting

Tables 6-3 to 6-5 contain some of the most prominent defects that were observed over the course of this Dissertation. These tables should serve as a troubleshooting for the process presented in section 6.3.

Table 6-3: Coating defects with electroless plating method (part 1)

Description	Cause	Example
Bare spots on the nickel layer	This defect occurred exclusively with MPGTs made of tooling steel substrates. A slow transition between the pickling and the electroplating step in the pre-treatment caused this systematic defect. The substrate needs a swifter transition between pre-treatment steps to prevent it from becoming dry.	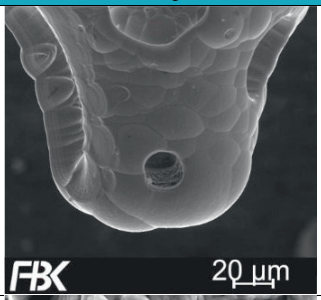
Layer formation that prevents nickel growth	This layer is made of a sodium compound that forms when the degreasing solution changes to an opaquer color. In most cases, this layer hinders nickel growth completely.	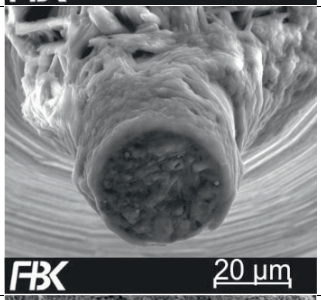
Spontaneous de-composition	As mentioned in section 3.3.4, at the end of the solution life, the solution has a rapid, spontaneous metal deposition on all active surfaces. This solution life can be expanded by adding a higher stabilizer concentration that masks smaller active particles in the solution.	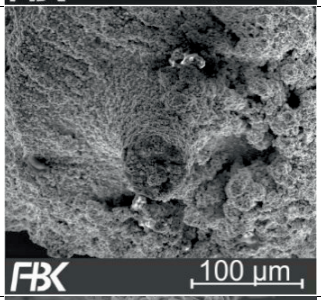
Lump formation that grows away from the substrate	A systematic defect that occurred when tooling steel substrates became magnetic.	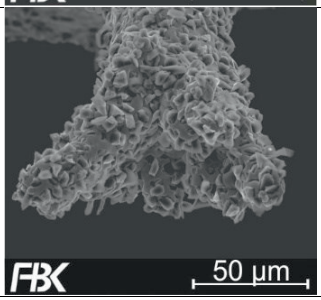

Table 6-4: Coating defects with electroless plating method (part 2)

Description	Cause	Example
Lump formation on the Ni-P layer	This defect occurs when a foreign particle is coated on the substrate surface. A certain reject rate is calculated with each batch of electroless plated MPGTs.	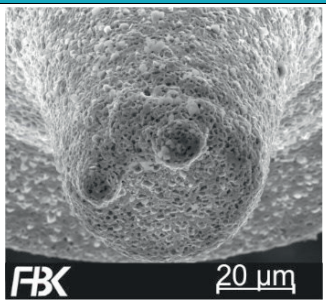
Cracks in the Ni-P layer	This defect was systematic and occurred when the electrolyte used for precoating is contaminated. EDX analysis showed an increased phosphorous content in cracked areas.	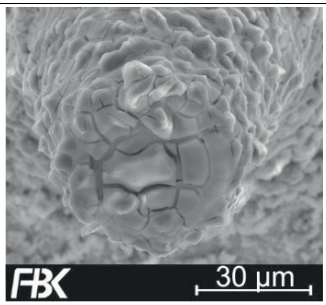
Lack in nickel growth	A lack of nickel growth occurs either because of an incorrect electroless plating solution composition or because of an erroneous pre-treatment. In this dissertation, the error occurred mostly when the electrolyte from the precoating solution reached the end of its life.	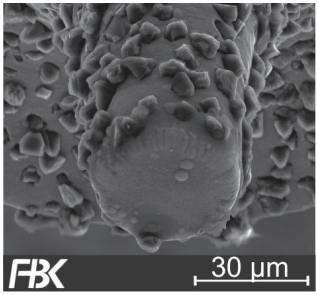
Lack of grit embedment	Grits on the upper surface are barely coated as they lack proper embedment; this occurs either from a lack of embedding time or a too-high grit concentration. If a grit concentration is too high, the grit embedment time will not be sufficient to coat the grits on the upper surface properly.	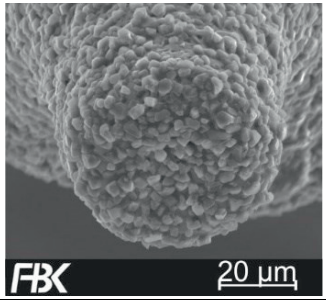

Table 6-5: Coating defects with electroless plating method (part 3)

Description	Cause	Example
Ni-P accumulation on edges	This defect occurred exclusively with MPGTs made of a tooling steel base body. Burr on the substrate causes higher nickel growth on the edges, causing non-uniform abrasive layers.	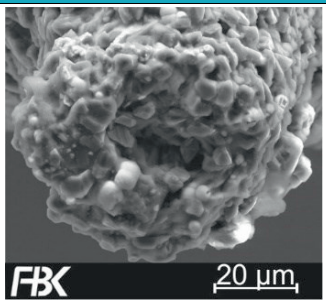
Non-uniform nickel growth	Non-uniform nickel growth is mostly the result of a too turbulent liquid flow. This can happen as a result of too high rotational speeds (tool as well as solution) or too high process temperatures (depicted tool).	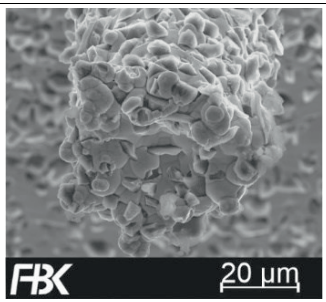

7 Micro Grinding: Experimental Procedures

Experimental procedures for the upcoming machining experiments are discussed in this chapter. The different process kinematics for different MWF supplying methods, measuring techniques to determine adhesions as well as microchannel topography, and a methodology to evaluate case studies are all presented in this chapter.

7.1 Process Kinematics

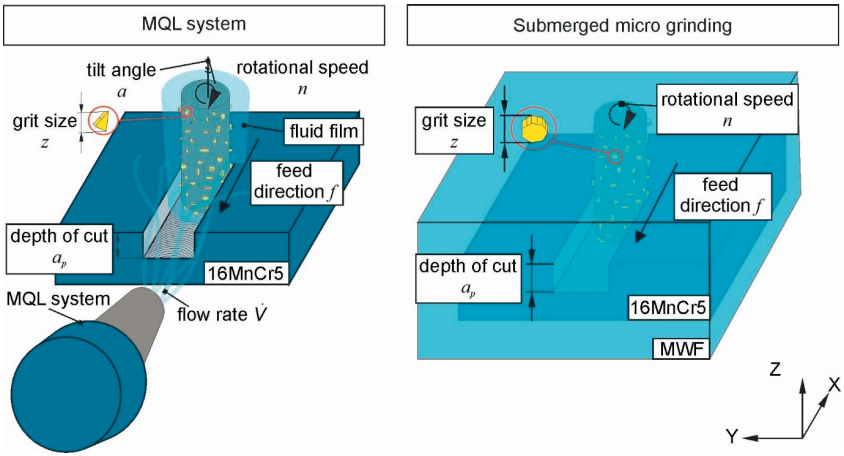

Figure 7-1: process kinematics for MQL system and submerged grinding

Two types of MWF fluid supplying methods are used in this dissertation, a MQL System and a submerged cutting system. Both systems have their own process preparation steps, but have the same process kinematics; Figure 7-1 shows the process kinematics of both. The tool rotates clockwise around its axis, while the workpiece moves with a defined feed rate towards it. In the Z-axis, the contact point between the MPGT and the workpiece is determined manually by moving the tool towards the workpiece surface using a slow feed rate (0.01 mm/min). Once contact occurs, the operator can observe chip removal with the built-in camera system. The tool is then moved beyond the edge of the workpiece. After configuring the MPGT to the desired depth of cut, the process is started [Arra19a].

7.1.1 MPGTs with an inclination angle

As mentioned in the state of the art (section 2.2.5), a method that was used to reduce substructures in machined microchannels was adding an inclination angle to MPGTs by tilting the spindle. The rotational axis of the ultra-precision four axes machine tool presented in section 5.1.2, is used to add an inclination angle. Adding an inclination angle to the process should concentrate the bulk of the machining effort on the grits at the circumference of the abrasive layer, reducing the involvement of the grits at the MPGT pivot (see Figure 7-2).

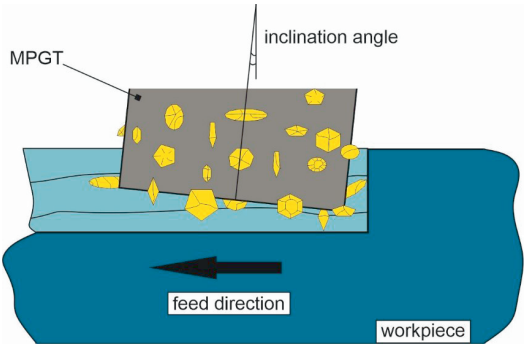

Figure 7-2: influence of inclination angles

7.1.2 MPGTs with Cavities

A second method that reduces substructures was mentioned in the state-of-the-art (section 2.2.5): micro grinding with MPGTs that have a cavity. Studies using MPGTs with cavities were initiated to improve MPGTs in three ways: reduce adhesions, minimize substructures, and increase tool life. If there are no grits at the pivot of MPGTs, the minimal cutting speed of the remaining grits increases, potentially increasing tool life. A cavity at the pivot of the tool would mean that fewer adhesions would develop as adhesions gather mostly at the pivot. A cavity also means that most grits gather at the circumference of the tool; this reduces the effect of grit protrusion differences that influence the depth of substructures. Adding to this, a cavity increases the coated area, interlocking the abrasive layer. A negative point, however, is the reduced grit density due to a reduced substrate area.

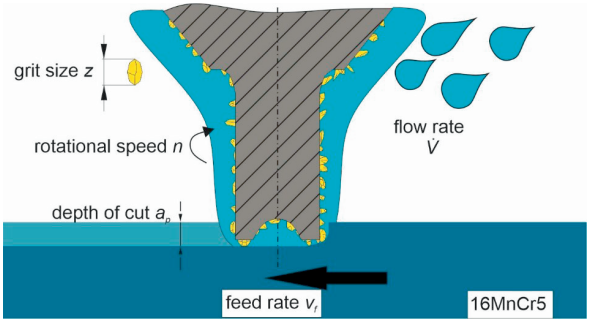

Figure 7-3: Process parameters used for MPGTs with cavity

7.1.3 Creep feed and pendulum grinding methods

Two types of machining methods have been used during the course of this dissertation: a creep feed grinding method and a pendulum grinding method. Figure 7-4 shows a comparison between both processes. In experiments conducted with a creep feed grinding method, microchannels were machined in one grinding step. A low feed rate and a comparatively higher depth of cut were employed.

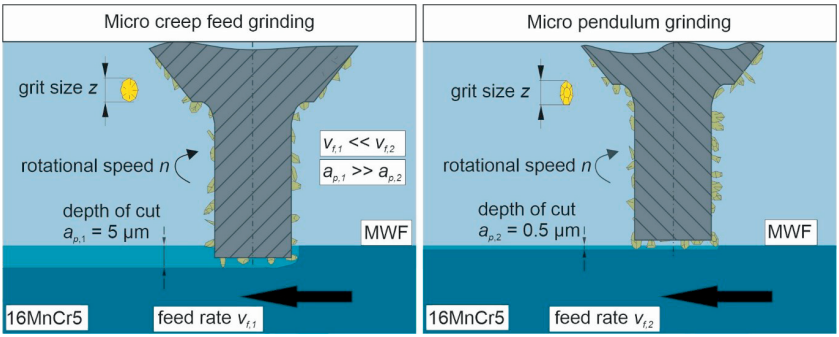

Figure 7-4: Pendulum grinding and creep feed grinding

The pendulum grinding process has a much faster feed rate and a much smaller depth of cut; creep feed grinding experiments were conducted with a depth of cut of 5 µm and pendulum grinding experiments with 0.5 µm.

A second pendulum movement was added to the process. In order to attempt machining deeper channels, the channel has to be wider than the tool itself to allow more MWF to flow into the machining zone; this allows for better lubrication and better chip removal. The feed direction moves the tool in a rectangular fashion. The microchannel becomes 4 µm wider doing so. The Z-axis is only used to move the tool downwards, eliminating errors caused by the backlash of the linear axes. Figure 7-5 shows a schematic of the method.

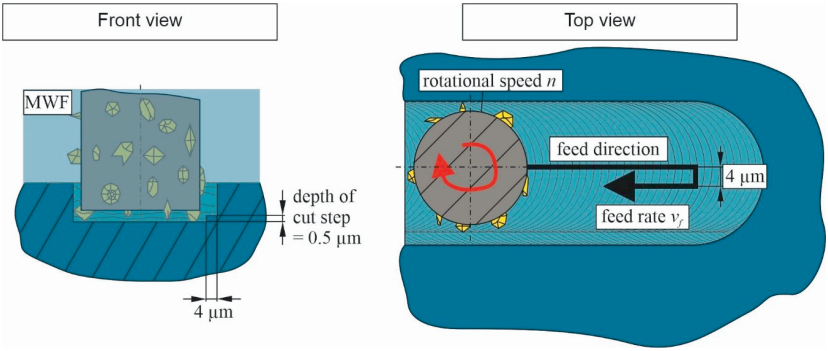

Figure 7-5: Micro pendulum grinding method for deeper channels

7.2 Microchannel Analysis

Microchannel analysis was conducted using the confocal microscope that was introduced in section 5.5.2. The confocal microscope was used to measure microchannels to make a 3D-topography model that can be evaluated. Among the results obtained from the confocal measurements are the channel dimensions, channel form, and roughness values.

Topographies of microchannels were measured with 20x and 60x magnification lenses that have a numerical aperture of NA_{20x} = 0.9 and NA_{60x} = 0.4 respectively; 60x magnification was used when roughness values are measured and 20x for applications in which a higher quantity of

data was required. Missing data points that result from the finite numerical aperture or artefacts on the surfaces were interpolated using linear interpolation. A plane leveling of the first order was applied to the areal measurement data to minimize the sum of the squared distances. Profiles located at the center of microchannels with a length of 400 µm were extracted manually from the areal data. Calculation of 2D roughness parameters included a limitation of the bandwidth using a Gaussian-filter (0.008 µm) [DIN12] [DIN97] (lc = 80 µm; ls = 0 µm).

To estimate the surface quality, the arithmetical mean roughness value R_a [DIN09], was calculated according to DIN EN ISO 4288. The first segment was chosen to be at the entry point of each microchannel.

7.3 Material Analysis of Adhesions on MPGTs

The analysis of MPGTs after machining their respective microchannels showed a layer of iron adhesions covering the bottom surface of MPGTs. Energy-dispersive X-ray spectroscopy (EDX) was used to conduct a material analysis on the abrasive layer, measuring the percentage of iron adhesions on the surface. Figure 7-6 marks the reference area that is measured in EDX measurements.

The percentage of adhesions at the bottom of MPGTs cannot be quantified. The adhesions at the bottom of MPGTs depend on the size, position, orientation, density, and wear of its abrasive grits. The unique characteristics of MPGTs will cause deviations between tools used for the same experimental case. In addition, adhesions may partially detach from the abrasive layer, distorting the measured value. Figure 7-6 shows the difference between measuring the reference area and three samples within the area. A portion of the adhesive layer detached from the abrasive layer at the center of the MPGT. As a result, sample 1 which is closest to the pivot has only 2.33 wt.% iron adhesions. Sample 2 which is further away from the pivot has 83.09 wt.% iron adhesions. In comparison, the reference area has a total of 29.46 wt.% iron adhesions.

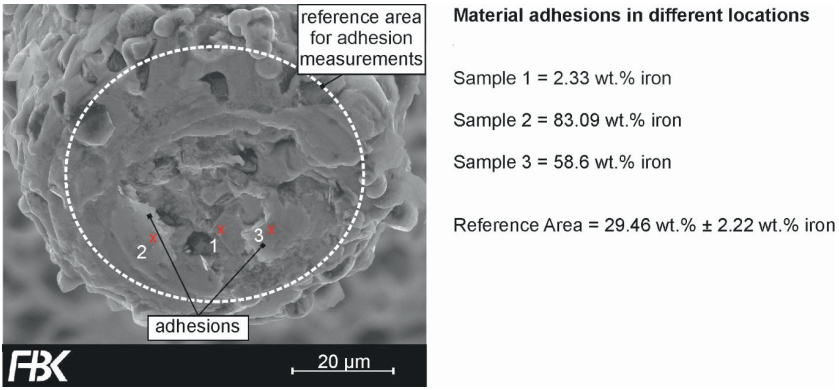

Figure 7-6: Reference area for EDX measurement [Arra20]

7.4 Analysis of Variance

Larger parameter studies are evaluated via Analysis of variance (ANOVA). ANOVA is a collection of statistical models that are carried out to establish the significance of process parameters. This method creates an empirical relation between investigated parameters to determine

the significance of process parameters. A test result is statistically significant when the likelihood of it occurring by chance is insignificantly minuscule.

In ANOVA, experimental results are compared with the null hypothesis – a hypothesis that describes the absence of a relationship between a factor and an outcome [Wass16]. In ANOVA the null hypothesis is correct until proven otherwise [Ratn16]. The probability-value (p-value) determines the probability of the null hypothesis to be false. According to the p-value, a set of data is considered significant when a significance level of over 95% or a p-value of 0.05 is reached. Despite there being other factors that are used to determine the significance of parameters, in this dissertation the evaluation criteria were limited to the p-value.

8 Micro Grinding: An Application Analysis of MPGTs

An application analysis in the use of MPGTs is presented. This chapter intends to highlight the problems occurring when using MPGTs for micromachining. All experiments are performed on hardened 16MnCr5 steel.

The very first problem we encountered after the abrasive layer study, presented in section 6.3 was that the abrasive layer broke off upon entry during machining experiments (see Figure 8-1). Upon closer inspection with an optical microscope, the microchannels exhibited a bluish annealing color – often referred to as grinding burn [Malk08]. TARASOV states that grinding burn in steel workpieces results from the formation of an oxide layer and is characterized by a bluish color [Tara50]. According to ECKSTEIN, a bluish color on a steel workpiece surface occurs at temperatures between 200 °C – 400 °C. [Ecks87]. Figure 8-1 lists the annealing colors in a range of 200 °C – 360 °C.

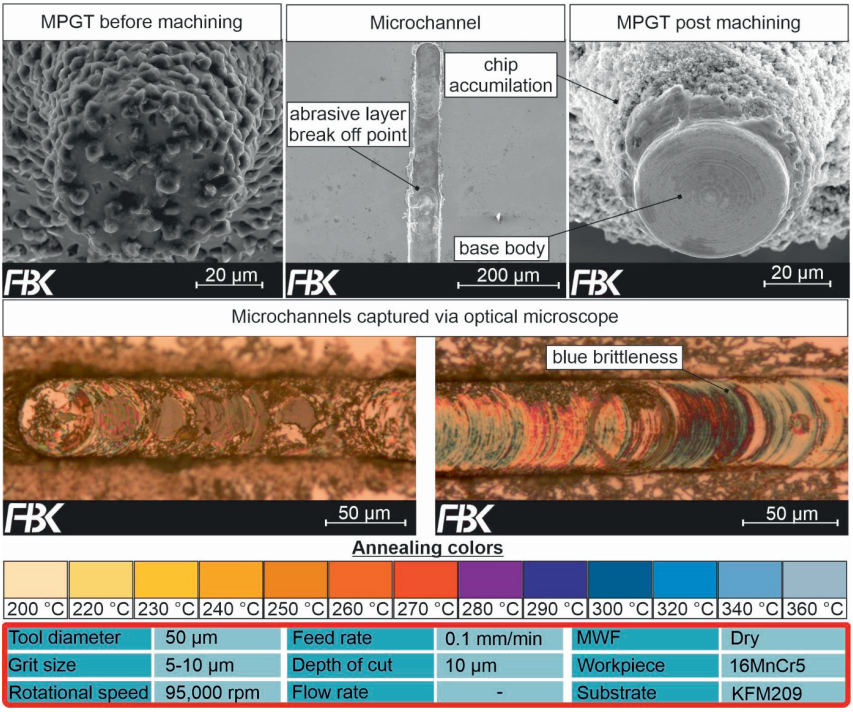

Figure 8-1: Dry micro grinding experiment with annealing color scale from [Fisc01]

These initial machining experiments proved that we lacked machining parameters, tool specifications, and most importantly a way to supply the process with metalworking fluid (MWF) – which is the first thing that will be investigated in this chapter. Two MWF supplying methods were tested: a MQL system combined with water-based SDS solutions and a submerged cutting pool in which several MWFs were tested – among tested MWFs, the same water-based SDS solutions that were used for the MQL system.

A parameter study is conducted with both systems to determine which parameters influence the process the most. The parameter studies will also serve to highlight the problems micro grinding with MPGTs has. Wear mechanisms and causes for substructures are determined based on these micro grinding experiments.

Case studies that employ MPGTs with an inclination angle, as well as MPGTs with a cavity, are conducted. Both these process modifications are conducted to test if they reduce substructures and if they increase tool life.

8.1 Micro Grinding with Sodium Dodecyl Sulfate: Feasibility Analysis[4]

Based on the dry machining experiments conducted in the prelude to chapter 8, temperatures in the range of 200 – 400 °C caused an early tool failure. To solve this problem distilled water and distilled water mixed with 0.02 wt.% SDS were used as MWF. Since both are water-based, a high cooling effect was expected during machining. The surfactant SDS was expected to increase the MWFs wetting properties while adding lubricity. Table 8-1 lists the experiments conducted in this section; the case numbering will be continuing throughout the dissertation to connect all cases. The ultra-precision four axes machine tool combined with the Venturi MQL system was used for this study. The tests were executed with a rotational speed of 30,000 rpm at feed rates of 0.05 mm/min and 0.1 mm/min. The projected microchannels were 0.5 mm long and 5 µm deep. MPGTs with a single layer of grits were used in this experimental series. A size of 2-4 µm was used with an abrasive layer thickness of 1-2 µm. Each experiment was repeated three times.

Table 8-1: Test series for MQL system test

Case	Feed rate in mm/min	Metal working fluid
Case 1	0.05	Dry
Case 2	0.1	Dry
Case 3	0.05	Water
Case 4	0.1	Water
Case 5	0.05	SDS
Case 6	0.1	SDS

8.1.1 Wear analysis

Figure 8-2 shows MPGTs after machining their microchannels for cases conducted with a feed rate of 0.05 mm/min – the images for 0.1 mm/min looked similar. Both the water-cooled cases and the dry machining cases failed to complete an entire microchannel. The abrasive layer broke off and similar to a scratch test, the cemented carbide base body pushed the much softer 16MnCr5 material aside, producing a microchannel despite lacking an abrasive layer. The abrasive layer breakoff point is marked in the SEM images of the microchannels (see Figure 8-2). Also, worth mentioning are the breakouts on the edges of the microchannels that can be seen in these scratched microchannels.

Despite only using minimal quantities of SDS, five of six experiments executed with SDS, produced a microchannel, almost without tool failure; the one failed experiment was conducted with a feed rate of 0.1 mm/min and failed 10 µm before completing the 0.5 mm cutting path.

[4] Results in this section have been previously published in [Arra17a] .

Tool wear was slightly higher for cases in which machining was carried out with a higher feed rate.

Energy-dispersive X-ray analysis (EDX) was performed for the five MPGTs that withstood the case study to determine the iron adhesion on the face side of the abrasive layer. In addition, the bottom surface of the microchannels was inspected for nickel adhesions. The analysis showed no signs of nickel adhesions at the bottom of microchannels but showed an iron concentration of 28.65 wt.% ± 5.1 wt.% for cases performed with a feed rate of 0.05 mm/min (Figure 8-2 shows one of these analyses) and 50.05 wt.% ± 0.78 wt.% for a case machined with a feed rate of 0.1 mm/min.

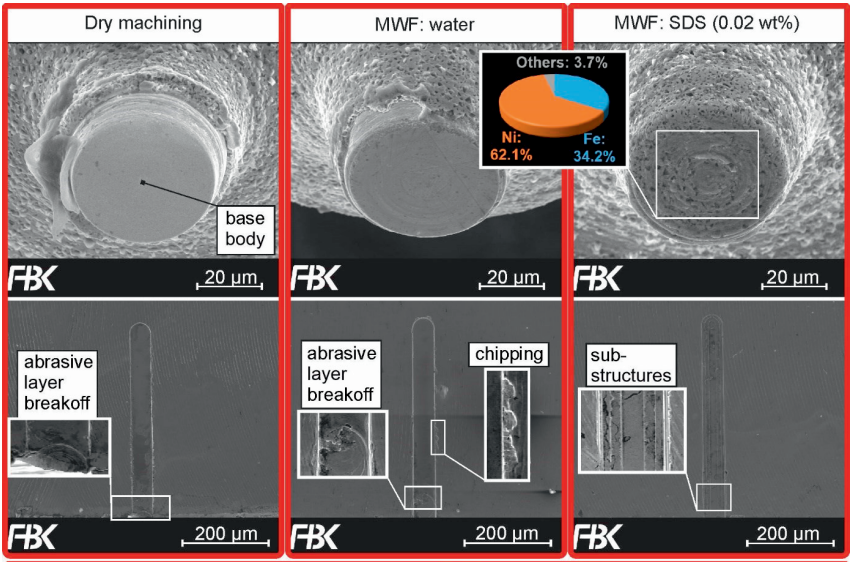

Tool diameter	50 µm	Feed rate	0.05 mm/min	MWF	Dry/water/SDS
Grit size	2-4 µm	Depth of cut	5 µm	Workpiece	16MnCr5
Rotational speed	30,000 rpm	Flow rate	0/60 ml/h	Substrate	KFM209

Figure 8-2: MQL system case study

8.1.2 Structure analysis

Figure 8-3 shows the mean roughness values R_a of each of the six cases with their respective standard deviations. The bottom surface of each microchannel was measured regardless of the achieved cutting path length. The lowest roughness values were documented for cases 5 and 6 – with the lowest Ra values being at case 6.

More revealing than the roughness values are the reconstructed models from the confocal microscope. Figure 8-4 presents a comparison between a dry machining case and a case in which SDS (0.02 wt%) was used. Channels machined dry resemble a scratch test. The microchannels manufactured with SDS (0.02 wt%) on the other hand, have almost burr-free edges with a bottom surface that resembles the characteristics of the tool that machined them. The pivot point of the MPGT is visible in the channel and on the tool that machined that channel. The channel also shows the exact moment at which the abrasive layer was damaged upon entry and also the

extent to which run-out influenced the process. The pivot on the tool is far off-center, and the microchannel has a step-like structure that is a direct result of this. The manifestation of these characteristics or substructures is unique to each MPGT.

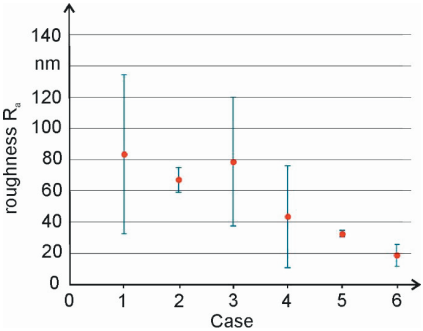

Figure 8-3: Roughness values R_a

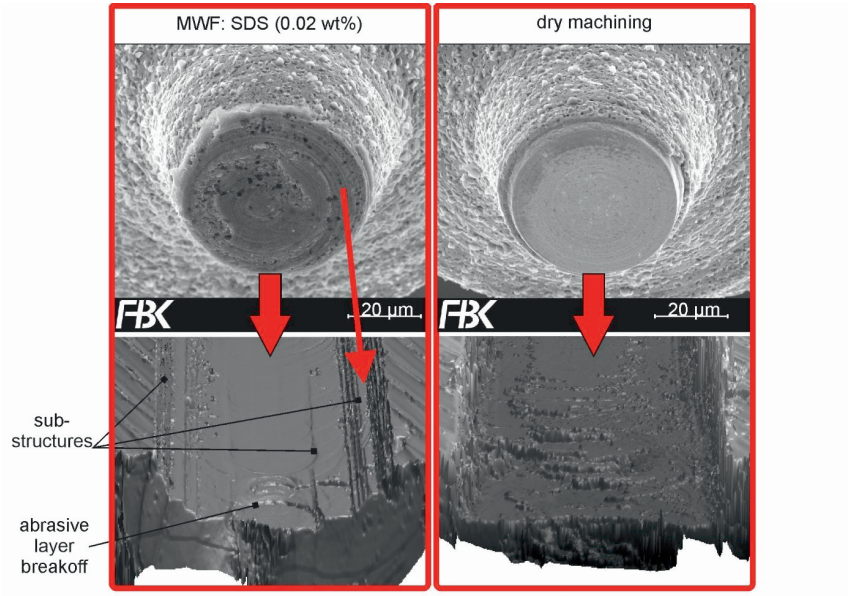

Tool diameter	50 µm	Feed rate	0.1 mm/min	MWF	Dry/water/SDS
Grit size	2-4 µm	Depth of cut	5 µm	Workpiece	16MnCr5
Rotational speed	30,000 rpm	Flow rate	0/60 ml/h	Substrate	KFM209

Figure 8-4: Structure analysis for machining dry and with SDS (0.02 wt.%)

8.1.3 Conclusions

A comparison between dry machining, water-cooled machining, and machining with SDS was conducted in this section. Constant parameters with two different feed rates were used to vali-

date the process. The cutting path achieved with dry machining and the water-cooled experiments is close to zero. Despite only using small quantities of SDS – a concentration of 0.02 wt.% – almost all tools completed their assigned cutting path. Tool failure occurred with one of the tools used with the higher feed rate (0.1 mm/min). EDX analysis showed that almost twice as much iron adhesions occurred when a feed rate of 0.1 mm/min was used than when a feed rate of 0.05 mm/min was used. For given tool specifications, a linear connection between feed rate and iron adhesions can be assumed. This connection is highlighted in the state-of-the-art: a higher feed rate translates to a higher chip thickness which translates to higher process forces. The normal forces that press against the tool increase adhesions. Higher amounts of iron adhesions translate to less grit protrusion, which, in turn, translates to higher operating temperatures – explaining the single tool failure in case 6. A higher concentration of SDS should decrease the iron adhesions even further, making higher feed rates possible.

Another issue that might have caused reduced tool life is using a monolayered MPGT with a nickel layer thickness of 1-2 µm. Figure 8-5 shows a multilayered MPGT that machined a U-shaped structure. A rotational speed of 50,000 rpm and a feed rate of 0.1 mm/min were used. The depth of cut was 7 µm, at a structure length of 1 mm and a structure width of 0.15 mm – amounting to a 2.15 mm long channel. Despite showing signs of wear, the MPGT is still functional. MPGTs coated with this coating method seem to have a self-sharpening effect that helps new emerging grits to gain a good enough protrusion. Using multilayered MPGTs attributes to much better tool life because it makes MPGTs much more stable.

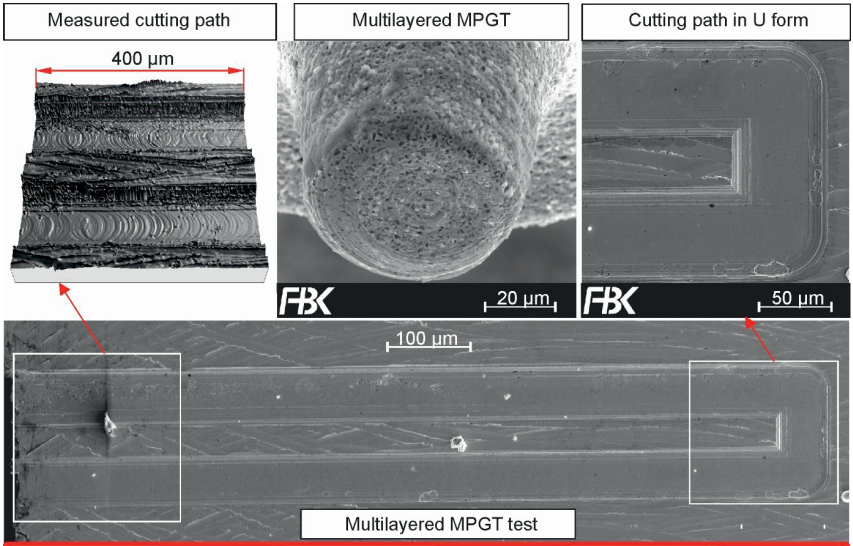

Tool diameter	50 µm	Feed rate	0.1 mm/min	MWF	SDS (0.02 wt.%)
Grit size	2-4 µm	Depth of cut	7 µm	Workpiece	16MnCr5
Rotational speed	50,000 rpm	Flow rate	60 ml/h	Substrate	KFM209

Figure 8-5: a) arcs measured using confocal microscopic images, b) multilayered MPGT post machining and c) U-shaped microstructure

The 3D-topographies extracted from the confocal microscope showed that cases 1-4 resemble a scratch test more than a machining process – material was removed in a ripping motion due to a lack of cutting edges and chips adhered to the bottom surface of the microchannel. Microchannels in cases 5 and 6 had a much smoother surface. Despite that, some of the microchannels showed substructures at the bottom surface and the side surfaces. These substructures seemed to be influenced by tool specifications, tool wear, and run-out. Further investigations are required to determine the causes of these substructures.

Microchannels in cases 5 and 6 had much smoother surfaces and therefore, much better roughness values. The roughness values seemed to improve with increasing feed rate, which could be attributed to grits engaging more in sliding and ploughing actions at lower feed rates. Due to tool failure, the roughness values in cases 1-4 proved to be unreliable.

8.2 Substructure Mechanisms

One of the most fascinating aspects of this type of micro grinding process is the fact that every MPGT is unique in its characteristics; this means that every microchannel machined with MPGTs is also unique. Seeing as tool wear changes the fundamental tool characteristics while the machining process is in progression, even two microchannels manufactured with the same MPGT might have completely different features or substructures as they are called. If we add to this the process parameters as well as errors stemming from the machine tool, the environment, and the user himself, we will have much more difficulty predicting the bottom surface of microchannels.

While the same can be said about almost any grinding tool, here substructures influence the function of the entire microchannel.

In this section, the most significant influences that cause substructures are discussed.

8.2.1 Influence of tool characteristics

The characteristics of microchannels are unique for each MPGT and can only be replicated with great difficulty. They are influenced by the size, density, protrusion, and positioning of abrasive grits on MPGTs [Arra19a]. Figure 8-6 shows one of the more extreme examples of one of the microchannels machined in the case study that is introduced in section 8.3 (case 10) as well as the parameters used to machine the channel. The channel is 4 µm deep at the center and has a step-like structure with each step being a micrometer higher than the last. This means that if a microchannel with a cutting depth of 4 is required, the functionality of the microchannel is affected. Figure 8-6 also illustrates a theoretical case in which a similar microchannel is machined. The MPGT used in this scenario has unique, distinct grits at the bottom surface that have different protrusions as well as different positions. The grit closest to the pivot is protruding much more than the other grits. If this MPGT is used in a micro grinding process, that grit would either break off at the start of the process or manufacture a smaller channel inside the microchannel. This smaller channel is a substructure and its dimensions depend on the position of the grit, the protrusion difference with the other grits, and run-out error. In our example, this smaller channel was 2 x c wide and b – a deep. The next grit with the highest protruding cutting edge produces the next step.

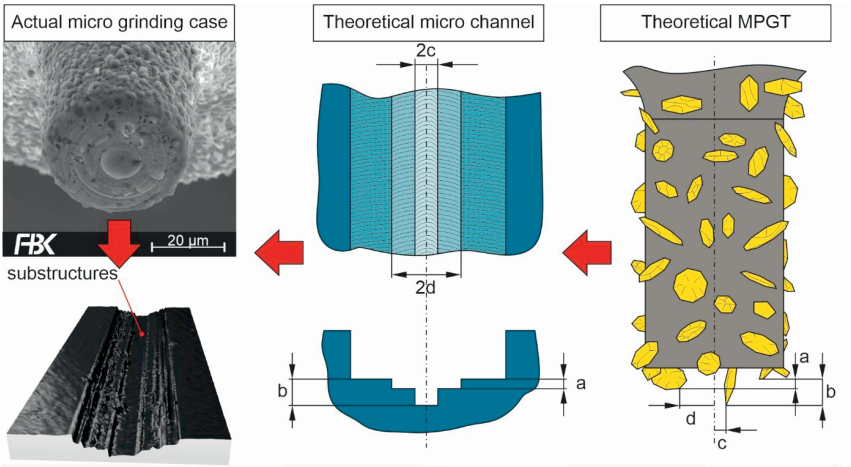

Tool diameter	50 µm	Feed rate	0.2 mm/min	MWF	SDS (1 wt.%)
Grit size	3-6 µm	Depth of cut	5 µm	Workpiece	16MnCr5
Rotational speed	30,000 rpm	Channel length	1 mm	Substrate	KFM209
Inclination angle	0°	Flow rate	100 ml/h		

Figure 8-6: Theoretical case demonstrating substructures based on tool specifications

8.2.2 Influence of tool wear and run-out error

Upon starting a micro grinding process, MPGTs go through many changes during the machining process. Even if MPGTs starts out with a well-balanced grit distribution with a balanced grit protrusion, tool wear will change the tool throughout the machining process.

In Figure 8-7 illustrates the same microchannel presented in Figure 8-4 (section 8.1.2). This channel shows the effect of tool wear and run-out errors perfectly. As the MPGT starts the machining process, loose grits break off the abrasive layer, causing abrasive wear to the nickel coating, changing its form. A run-out error causes an eccentric rotation, damaging one side of the tool more than the other. If a two-dimensional case is considered and the tool is split in half, each half would manufacture an utterly different microchannel with its unique substructures. Since it is an eccentric rotation and both sides have a completely different form, a step-like structure is developed at the edges.

As mentioned in section 8.4, less abrasive wear and more material adhesion occur at the pivot of the MPGT. A side effect of these material adhesions is that they form a protective layer for grits at the pivot of the MPGT. While the grits on the circumference lose in protrusion during micro grinding, grits at the pivot remain at roughly the same cutting depth. This means that even if smaller channels are missing at the start of the process, they will most likely occur later and they will gradually increase in depth.

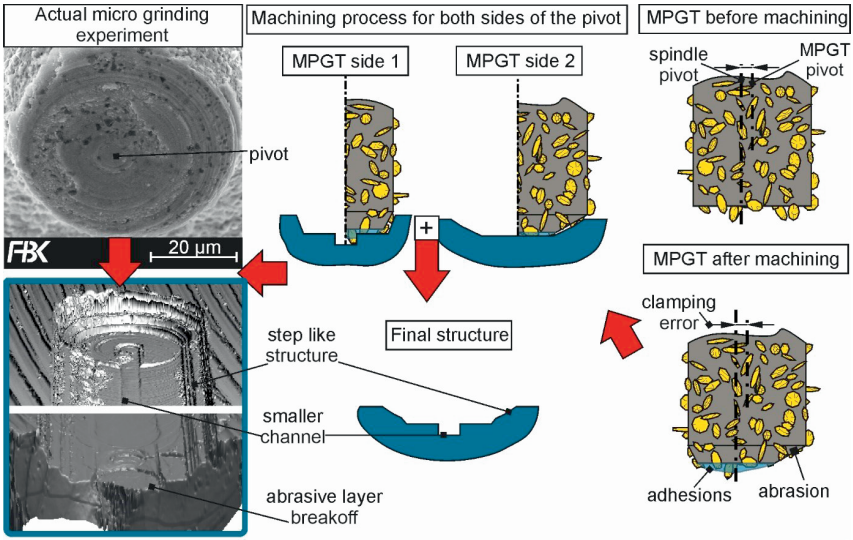

Tool diameter	50 µm	Feed rate	0.1 mm/min	MWF	SDS (1 wt.%)
Grit size	2-4 µm	Depth of cut	5 µm	Workpiece	16MnCr5
Rotational speed	30,000 rpm	Channel length	1 mm	Substrate	KFM209
Inclination angle	0°	Flow rate	100 ml/h		

Figure 8-7: Influence of tool wear and clamping error on the development of substructures

8.2.3 Influence of process parameters

So far, process parameters seem to only have one influence that was documented: grinding marks. Figure 8-8 features microchannels machined with an MPGT that has a diameter of 400 µm and a grit size of 20-30 µm. Larger MPGTs enable much higher feed rates at given machining conditions. Channels with a cutting path of 3 mm and a depth of cut of 10 µm were machined at a variety of feed rates. SEM images of the bottom surface of these channels showed repeating patterns in the grinding marks. Once measured it became apparent that these repeating patterns have a feed rate dependent, almost constant distance. This means that one grit is protruding much more than all the other grits and is producing this grinding mark pattern. If the milling equation for feed rate per rotation (f_z) is used to calculate the theoretical distance between two grinding marks, it will give us the same distance measured.

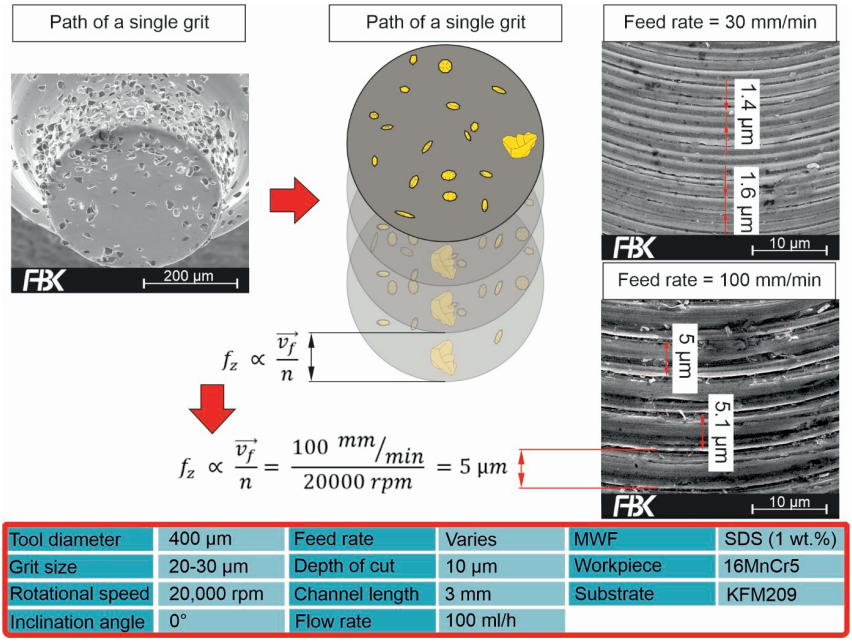

Tool diameter	400 µm	Feed rate	Varies	MWF	SDS (1 wt.%)
Grit size	20-30 µm	Depth of cut	10 µm	Workpiece	16MnCr5
Rotational speed	20,000 rpm	Channel length	3 mm	Substrate	KFM209
Inclination angle	0°	Flow rate	100 ml/h		

Figure 8-8: Influence of process parameters on substructures

8.3 Parameter Studies with a Minimum Quantity Lubrication System

What was learned from section 8.1 is that under current tool specifications and process parameters, the process only works in the presence of MWFs. Also, a keyword here is "parameters"; we still have to pinpoint which parameters need to be adjusted to maximize performance. Other researchers conducted micro grinding experiments in the past, apart from ENGMANN, none machined steel workpieces and none did so with MPGTs that have a diameter of 50 µm, a diameter that is half that of what PARK et al. used to machine silicon in his study [Park10]. Only feed rates of 0.05 mm/min and 0.1 mm/min were used in the last study, one of the MPGTs used in the experiment even failed to complete a cutting path of 0.5 mm – a cutting path far below what is needed for potential, industrial applications. The parameters: grit size and rotational speed needed to be investigated while combined with different feed rates. In addition, the effect of an inclined spindle and MPGTs with a cavity needs to be determined.

8.3.1 Experimental plan

Three case studies were conducted for this section. The first being a full factorial case study and the other two are studies based on the results obtained from the study. The full factorial case study consisted of four parameters at two levels and was conducted with each case being repeated three times. The effect of process parameters and grit size on tool performance were identified. Grit protrusion, position, and density were not explored in this study, as it is only difficult to control these parameters precisely. That being said, the same manufacturing parameters have been used to produce tools with the same grit size; deficient tools were sorted out.

As done in the previous study, the tool performance was evaluated by measuring the achieved cutting path and the surface roughness on the bottom surfaces of microchannels. The cutting path was limited to 1 mm at a 5 µm depth of cut. Additionally, multilayered MPGTs with a nickel layer thickness of 6-7 µm were used, which contain multiple layers of grits.

Table 8-2 presents the parameters of the performed case study – a total of 16 cases and 48 experiments with a new tool for each. The numbering of the cases is in continuation with the case study in section 8.1.

In the second study, MPGTs with a cavity were used with the same parameters as case 18. Case 18 was chosen because it delivered the best surface quality without tool inclination. The 3D-topographies of machined microchannels were then compared to those produced by cases 18 and 22. Table 8-3 lists the cases in the second case study. The third study was conducted with the parameters in Table 8-4 The achieved cutting path before tool failure, roughness values and the size of formed burr, were all evaluation criteria.

Table 8-2. Full factorial case study

Case	(A) Grit size in µm	(B) Feed rate in mm/min	(C) Inclination angle in °	(D) Rotational speed in rpm
Case 7	1-2	0.1	0	30,000
Case 8	3-6	0.1	0	30,000
Case 9	1-2	0.2	0	30,000
Case 10	3-6	0.2	0	30,000
Case 11	1-2	0.1	2	30,000
Case 12	3-6	0.1	2	30,000
Case 13	1-2	0.2	2	30,000
Case 14	3-6	0.2	2	30,000
Case 15	1-2	0.1	0	50,000
Case 16	3-6	0.1	0	50,000
Case 17	1-2	0.2	0	50,000
Case 18	3-6	0.2	0	50,000
Case 19	1-2	0.1	2	50,000
Case 20	3-6	0.1	2	50,000
Case 21	1-2	0.2	2	50,000
Case 22	3-6	0.2	2	50,000

Table 8-3. Second case study to test the effect of a cavity at the pivot of MPGTs

Case	Grit size in µm	Feed rate in mm/min	Inclination angle in °	Rotational speed in rpm	Cavity
Case 18	3-6	0.2	0	50,000	None
Case 22	3-6	0.2	2	50,000	None
Case 23	3-6	0.2	0	50,000	Cavity

Table 8-4. Third case study to test the limits of the improved process

Case	Grit size in µm	Feed rate in mm/min	Inclination angle in °	Rotational speed in rpm
Case 24	5-10	1	0	30,000
Case 25	5-10	2	0	30,000
Case 26	5-10	4	0	30,000

8.3.2 Full factorial case study[5]

The evaluation process for the experiments in the full factorial case study (Table 8-2), was conducted via Analysis of variance (ANOVA). Due to the strong correlation between the selected variables with tool life, it was possible to analyze at a 95% confidence interval and a p-value of ≤ 0.05. The surface roughness, on the other hand, has p-values that surpass the threshold of ≤ 0.05. High initial tool damage for smaller grit sizes as well as adhesions that clog the abrasive layer of the tool upon entry have a high influence on surface roughness. Taking this into consideration, the threshold was increased to ≤ 0.1 [Arra19a].

Using ANOVA, the main effects and interaction plots are detected to identify the influence of individual parameters and their interacting effects on the process responses. Figure 8-9 shows the main effects as a function of tool life, and Figure 8-10 shows the interactions between two parameters – only the most influential interactions are depicted. The software produced a median point for each parameter.

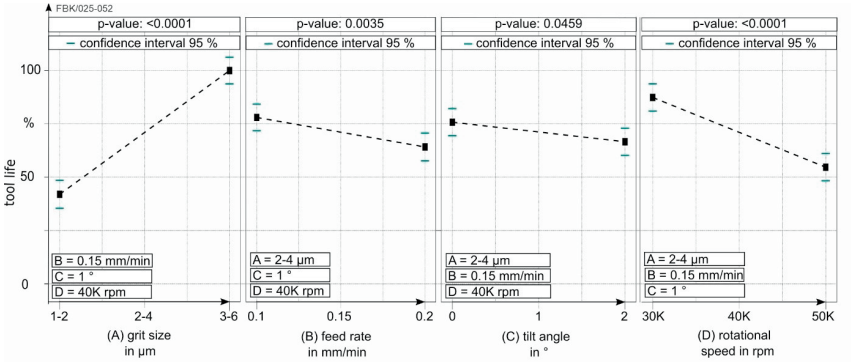

Figure 8-9: Main effects of the four investigated parameters on cutting path

[5] Results in this section have previously been published in [Arra19a]

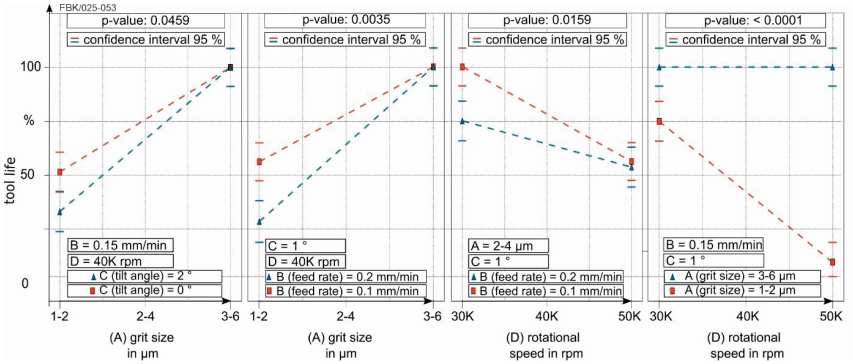

Figure 8-10: Effects of the most relevant interactions on cutting path

The influence of grit size dwarfs the influence of every other factor. The importance of a large grit size is especially visible in the interactions between parameters; no tool failure happened with the larger grits. The second most influential parameter was rotational speed. The magnitude of the effect rotational speed has on the process becomes apparent when viewing the interaction between grit size and rotational speed. When using 50,000 rpm at a grit size of 1-2 µm the tool life drops almost down to zero. Inclination angle and feed rate both have a negative effect on the process.

Figure 8-11 depicts exemplary microchannels and their respective tools after the machining process. Cases 9, 10, 21 and 22 are shown, all of which cases conducted with a feed rate of 0.2 mm/min. Case 21 is the case with the worst parameters in the entire study – an image depicting tool failure is presented. When tool failure occurs, a large portion of the abrasive layer is torn off the substrate.

As with the previous study, most tools showed larger amounts of adhesions post-machining while most microchannels had substructures. Larger grits caused material adhesions to build a small plateau at the pivot of the tool which increased in size when the tool was inclined.

When comparing surface roughness values, p-values between 0.05 and 0.1 were calculated for all parameters except for the grit size, which had a p-value of 0.64. Grit size was, therefore, taken out of the calculations. Figure 8-12 shows the effects of the factors: rotational speed, inclination angle, and feed rate as well as their most significant interactions.

Figure 8-13 shows 3D-topographies of cases 7, 8, 18, and 22 (parameters included in the figure), presenting distinct differences related to parameter variations. The representative images of cases 7 and 8 show that grit size has little to no influence on the structure – provided, of course, that the same machining conditions were used and the abrasive layer was still intact. A significant improvement in structure quality was documented for cases 18 and 22, cases in which both the rotational speed and the feed rate have been increased simultaneously. In case 22 the inclination angle was also changed, which is reflected by the orientation of the grinding marks (Figure 8-13) [Arra19a]. The origin of these substructures was elaborated in section 8.2.

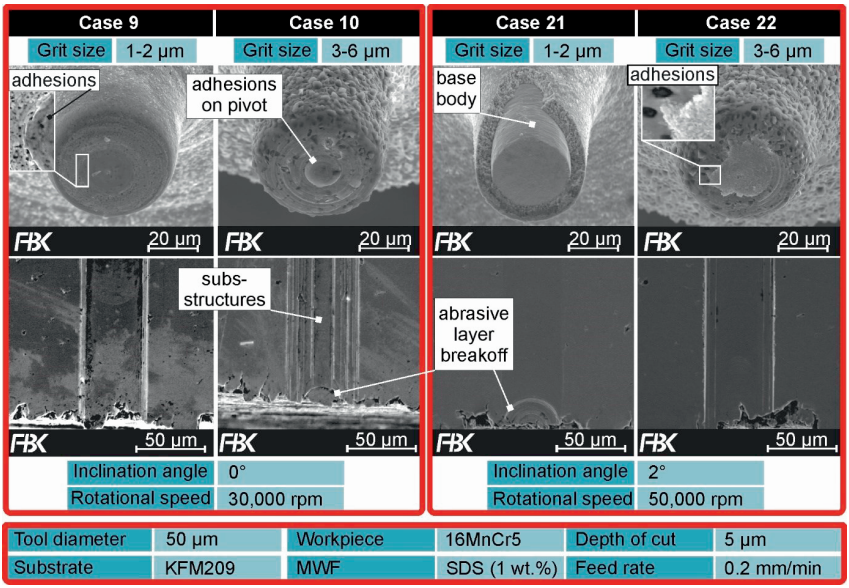

Figure 8-11: Post-process images of MPGT and machined structure for the cases: a) 9, b) 10, c) 21 and d) 22

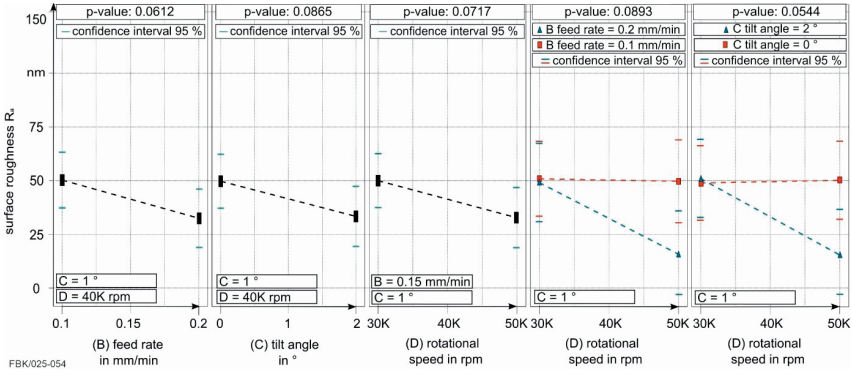

Figure 8-12: Effects of rotational speed (D), feed rate (B) and tilt angle (C) on surface roughness and their interactions

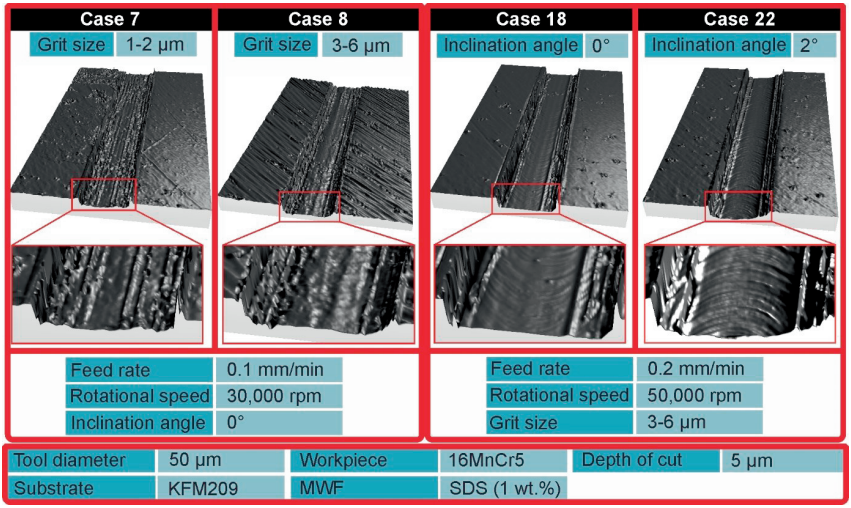

Figure 8-13: Confocal microscopic images of machined structures: case 7, case 8, case 18 and case 22

8.3.3 Case Study for MPGTs with Cavities[6]

This study was initiated to improve MPGTs in three ways: reduce adhesions, minimize substructures, and increase tool life. If there are no grits at the pivot of MPGTs, the minimal cutting speed of the remaining grits increases, potentially increasing tool life. A cavity also means that most grits gather at the circumference of the tool; this reduces the effect of grit protrusion differences that influence the size of substructures. Adding to this, a cavity increases the coated area effectively interlocking the abrasive layer. A negative point, however, is the reduced number of potentially active grits.

MPGTs with cavities were used to machine two additional microchannels with the same parameters as case 18. The parameters used were a rotational speed of v_c = 50,000 rpm, a feed rate of v_f = 0.2 mm/min, a depth of cut of a_p = 5 µm, and a grit size of 3-6 µm. Figure 8-14 shows SEM images in which machined microchannels are compared with microchannels from cases 18 and 22. All microchannels contained substructures at the center of the cross-section; however, regular MPGTs produce by far the deepest, most influential substructures. While still present, substructures were much shallower in the other two cases. Inclined MPGTs produced microchannels with the least substructures, however, the cross-section of these microchannels changed from the desired rectangular shape to a more concave form. According to the study performed in section 8.3.2, an inclination also reduces tool life. Despite not being able to remove substructures from microchannels completely, a cavity reduced the depth of substructures. The small channel at the center of the depicted microchannel, for example, has a depth of about 300 nm – an improvement when compared to the left channel in Figure 8-14, which is approximately 700 nm deep.

EDX measurements showed a high decrease in iron adhesions at the abrasive layer of MPGTs with cavities. Adhesions seemed to almost exclusively form in the cavity. As seen in Figure

[6] Results in this section have previously been published in [Arra19c]

8-14, the grits of regular MPGTs are almost entirely covered with a layer of adhesions, while the cutting edges of MPGTs with cavities are still visible.

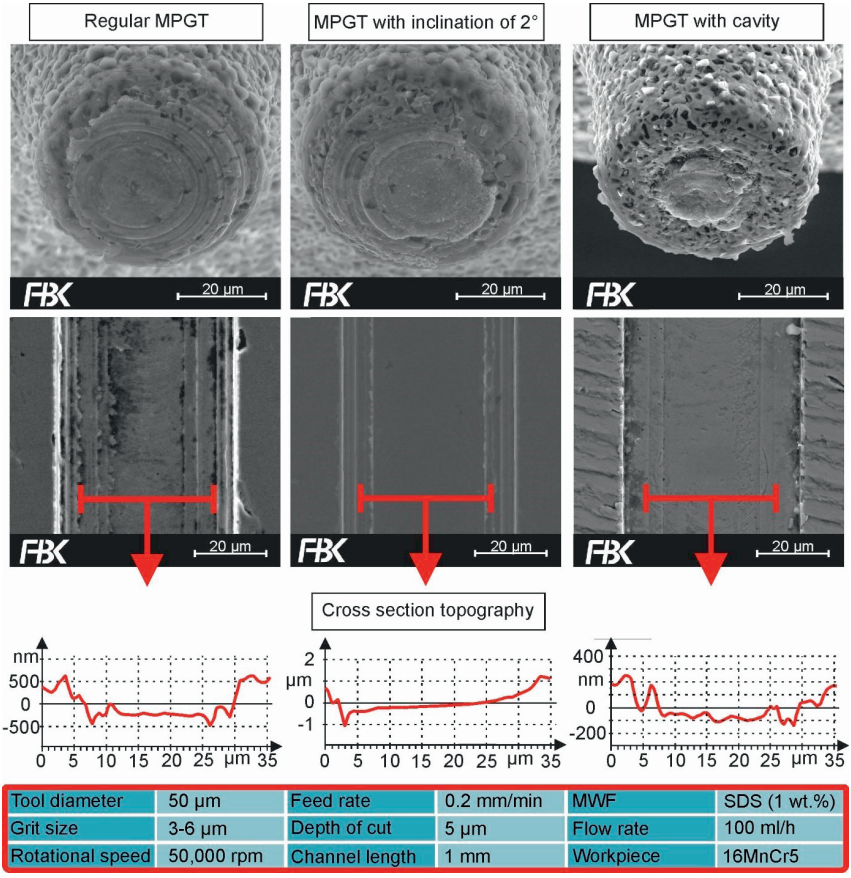

Tool diameter	50 µm	Feed rate	0.2 mm/min	MWF	SDS (1 wt.%)
Grit size	3-6 µm	Depth of cut	5 µm	Flow rate	100 ml/h
Rotational speed	50,000 rpm	Channel length	1 mm	Workpiece	16MnCr5

Figure 8-14: Performance comparison between optimized MPGTs and regular MPGTs

8.3.4 Tool life analysis with larger grits[7]

The full factorial case study showed that the best tool life is achieved at a rotational speed of 30,000 rpm, an inclination angle of 0° and grit size of 3-6 µm, with the grit size having the highest influence. Three more cases are presented, in which MPGTs with a grit size of 5-10 µm were used to demonstrate the new capabilities of the process and to deliver a basis on which upcoming case studies are built. In this case study, higher feed rates (≥ 1 mm/min) are used, and the experiments were conducted until tool failure.

[7] Results in this section have previously been published in [Arra19a] .

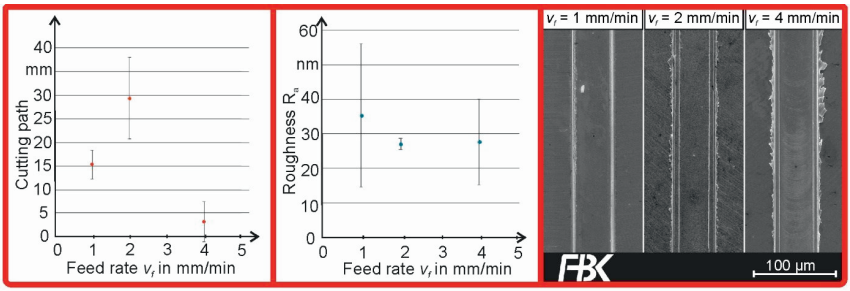

Tool diameter	50 µm	Feed rate	Varies	MWF	SDS (1 wt.%)
Grit size	5-10 µm	Depth of cut	5 µm	Workpiece	16MnCr5
Rotational speed	30,000 rpm	Flow rate	100 ml/h	Substrate	KFM209

Figure 8-15: Results of case study: achieved cutting path, roughness values R_a and burr formation with different feed rates

Table 8-4 shows the kinematic conditions for the new cases. Each case was performed at least two times. The resulting microchannels, as well as diagrams of achieved cutting paths and roughness values R_a, are depicted in Figure 8-15. After increasing grit size and feed rate, a considerable amount of burr formed around the edges of the microchannels. Three microchannels have been picked to demonstrate the effect of feed rate on burr formation. While the bottom surface of the microchannel depends more on the position, the protrusion, the density, and the condition of abrasive grits, the burr formation seems to depend more on process parameters.

The lowest produced roughness value R_a was 18.9 nm with a feed rate of 4 mm/min; however, the cutting path achieved was estimated at 0.14 mm. The longest cutting path achieved was measured at 35.4 mm and was machined with a feed rate of 2 mm/min. Different MPGTs that were used in the same case delivered different results. The standard deviation for all results was much higher than in previous cases, performed with smaller grits.

Both the tool life and possible feed rates improved after adjusting the grit size, the inclination angle, and the rotational speed. To test the process in the machining of complex closed structures, the shape of a house was machined with a feed rate of 2 mm/min – depicted in Figure 8-16. The accumulated channel was 4.215 mm long and was machined without interruption. This complex structure presents the challenge that the tool changes machining direction upon finishing each line. All straight and diagonal feed directions are covered. An image of the MPGT that manufactured the structure is also depicted in Figure 8-16.

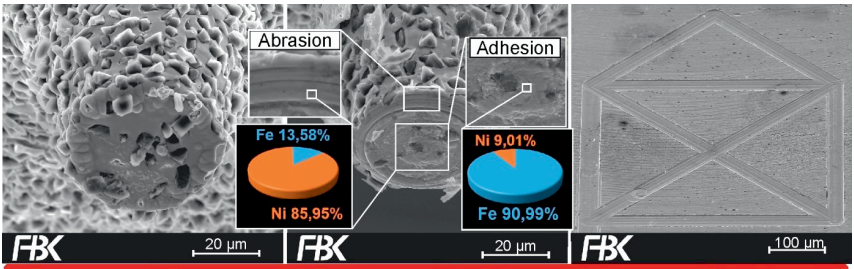

Tool diameter	50 µm	Feed rate	2 mm/min	MWF	SDS (1 wt.%)
Grit size	5-10 µm	Depth of cut	5 µm	Workpiece	16MnCr5
Rotational speed	30,000 rpm	Flow rate	100 ml/h	Substrate	KFM209

Figure 8-16: Complex micro channel in the shape of a house and the MPGT that machined it

8.3.5 Conclusions

The studies in this section were conducted using a MQL system with SDS (1 wt.%) as MWF. A parameter study to determine the effect of grit size, rotational speed, and inclination angle on tool life and surface quality was performed. Based on the results of this parameter study, the effect of a cavity at the pivot of MPGTs was tested. Finally, a second, smaller case study in which the best parameters from the previous study were used with varying feed rates to test MPGTs until failure.

The effect of grit size on tool life

The first study concluded that larger grit sizes increase tool life, while rotational speed and inclination angle reduce tool life. A high percentage of MPGTs with a grit size of 1-2 µm could not complete the entire cutting path, with some even failing upon entry. When combined with higher rotational speeds, MPGTs with a grit size of 1-2 µm had the worst results, reaching a tool life of almost zero. It is assumed that due to the low protrusion of smaller grits, adhesions can easily clog the abrasive layer. In addition, smaller grits on the circumference can sustain far lower mechanical impact than larger ones, causing even more damage to the circumference.

These negative aspects of smaller grits make larger grits much more favorable in this process. MPGTs with a grit size of 3-6 µm completed the whole cutting path without fail – this also applied to all cases in which an inclination was used (cases 12, 14, 20, 22). Adhesions still form on abrasive layers with larger grit sizes, however, larger grit protrusions make it more difficult to completely clog them. A small plateau made of iron adhesions was developing at the pivot of MPGTs when larger grits were used. Adhesions also seemed to develop on the circumference when an inclination was used. When MPGTs with a cavity was used, iron adhesions gathered mostly in the cavity, leaving the cutting edges of the abrasive layer almost free of iron adhesions.

The effect of rotational speed on tool life

Tool failure at higher rotational speeds is a strange phenomenon because it is the total opposite of other machining processes. When comparing to conventional machining processes, the maximum uncut chip thickness $h_{cu,max}$ is far too for low chip removal to occur, which would explain the reduced tool life. However, due to the immensely reduced cutting edge radii of individual

grits, this is not the case. Instead, the probable cause for tool failure is the clogging of the abrasive layer due to adhesions. These adhesions occur due to short term friction welding processes of chips that accumulate at the face side of the tool [Laue80]. When the abrasive layer is clogged, friction increases, producing higher process temperatures and forces [Kloc09]. A high enough temperature would loosen and ablate the abrasive layer from the cemented carbide base body. Higher rotational speeds would increase heat generation during machining, increasing the likelihood of tool failure [Laue80]. In conclusion, material adhesions cause more rapid wear progression on the abrasive layer by breaking out single grits or even entire grit populations. Tool wear mechanisms are further discussed in section 8.4.

The effect of an inclination angle on tool life

As discussed in Figure 7-2, an inclination angle, reliefs grits located at the pivot of the tool while increasing the focus more on grits on the circumference; this is, of course, the hypothetical scenario, however, in practice, an inclination angle seems to influence the tool life negatively. A likely cause is that grits closer to the circumference do most of the cutting during the process and therefore, have the most abrasive wear and the most grit chippings due to mechanical impacts. As previously mentioned in the state-of-the-art, MPGTs tend to become tapered at the face side of the tool because of immense wear on the circumference. Using an inclination on MPGTs increases the process forces on the abrasive grits on the circumference, decreasing tool life; this is especially true for MPGTs with smaller grits that have less volume to boot.

Results from using a grit size of 5-10 µm

In the second study, no inclination angle was added, a rotational speed of 30,000 rpm was configured, and the grit size of 5-10 µm was used to maximize achievable cutting paths. A feed rate of 2 mm/min produced the highest cutting path at 35.4 mm. The depth of cut decreased during machining until a value of zero was reached, at which point the abrasive layer was torn off. A high difference in performance between MPGTs that machined the same case was documented. Performance differences can be led back to each tool having a unique abrasive layer. A process characteristic that is especially important in MPGTs with larger grit sizes that occupy the bottom surface of the tool in much smaller numbers. While higher standard deviations are a given, the decreased amount of grits at the bottom of the tool has the benefit that a more accurate wear analysis is possible. Tool wear mechanisms will be further discussed in the next section (8.4).

Surface quality analysis

The roughness values of the full factorial study were determined and the data was compiled into a diagram. The p-values for all parameters and their interactions were higher than 0.05, which is why the threshold was increased to 0.1. Rotational speed, inclination angle, and feed rate had p-values between 0.05-0.1, while grit size was deemed less relevant for roughness values. The best roughness values were achieved in cases in which feed rate and rotational speed were simultaneously increased as well as in cases in which rotational speed and inclination angle were simultaneously increased. The standard deviations for roughness values between microchannels in the same case are larger than in the previous section, this was especially visible in the second case study. Larger grit sizes caused a far higher deviation in roughness values than they did in tool life. In addition, when compared to the study performed in section 8.1, the improvements possible with further parameter modifications are only incremental.

Substructure analysis showed that no significant changes are achieved from changing grit sizes, as substructures are more affected by grit density, orientation, protrusion, and tool wear rather than by their size. An inclination angle reduced substructures but caused a concave bottom surface. MPGTs with a cavity tremendously reduced the depth of the substructures. It can be assumed that the diameter of the cavity directly influences the size of the substructures – larger cavities result in more even microchannels. However, a larger cavity may also result in a less stable substrate that provides less area for grits to adhere to during the coating process; meaning that a lesser number of grits adhere to the bottom surface of the abrasive layer. Further discussions about substructures are presented in section 8.2.

8.4 Development of a Tool Wear Mechanism Theorem

Per the state of the art, tool wear is further explored in this section. To investigate tool wear further, an experiment was conducted with four separate tools, using the same parameters that were used for case 25 in section 8.3: a grit size of 5-10 µm, a rotational speed of 30,000 rpm and a feed rate of 2 mm/min. The tools were used to machine 2 mm long and 5 µm deep microchannels. After completing each microchannel, the tools were inspected via SEM. Consecutively, another channel was machined with each MPGT. In this study, the progressing wear mechanisms on each grit on the bottom surface of the abrasive layer is examined. The experiment was halted after grinding four channels, each (one of the tools was only used on three channels). It became clear that iron adhesions have a strong influence on the machining process in general.

Another point that is discussed in this section is the use of tooling steel instead of cemented carbide. A comparison between both substrate materials has previously been presented in section 3.1.

8.4.1 Life cycle of MPGTs while micro grinding 16MnCr5

Figure 8-17 shows the results, obtained from one of the substrates. The first image shows the MPGT after machining two consecutive microchannels. The cutting path is almost as long as the cutting path of the shape of a house in section 8.3.4 (Figure 8-16). The MPGT has been reclamped twice, yet it still shows similar wear mechanisms as in section 2.3.1 – high adhesions at the pivot of the tool and more abrasive wear, grit chipping and attrition at the circumference. Abrasive wear seems to be stronger on one side of the circumference than on the other. Run-out of the spindle and uneven grit distributions could be the reason for that unsymmetrical abrasive wear.

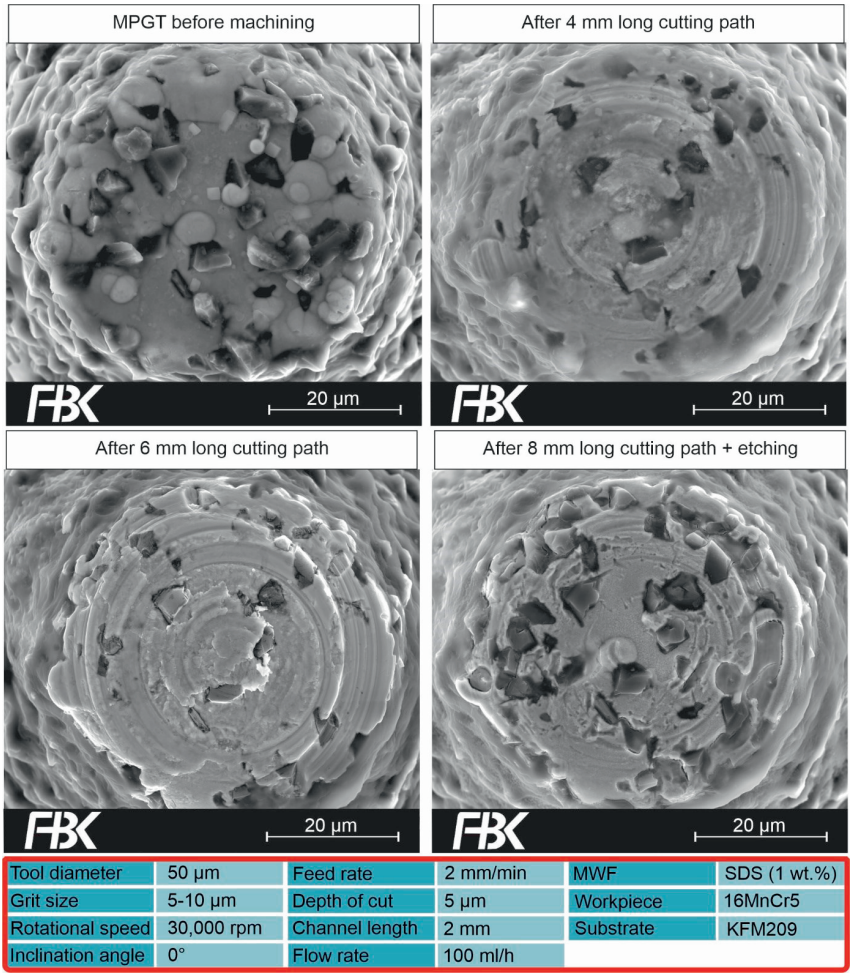

Tool diameter	50 µm	Feed rate	2 mm/min	MWF	SDS (1 wt.%)
Grit size	5-10 µm	Depth of cut	5 µm	Workpiece	16MnCr5
Rotational speed	30,000 rpm	Channel length	2 mm	Substrate	KFM209
Inclination angle	0°	Flow rate	100 ml/h		

Figure 8-17: Wear analysis for MPGTs

After machining an additional microchannel (now 6 mm cutting path), abrasive wear increased at the pivot of the tool with some of the adhesions even breaking off. The circumference area was damaged further by high abrasive wear. With increased abrasive wear that reduces grit protrusion at the circumference and adhesions that protect grits at the pivot, the bottom of the MPGT will slowly take the shape of a hemisphere.

After machining the fourth microchannel, the tool was put in a solution that consists of 3% nitric acid and 97% ethanol for 5 minutes. The solution etched the layer of adhesions off of the tool surface. The last SEM image shows that many grits were covered entirely with a layer of adhesions and could not participate in the machining process, confirming previous theories.

8.4.2 Life cycle of cBN grits while micro grinding 16MnCr5

Despite not conducting the experiment until tool failure, the images delivered valuable information about some of the individual grits on the tool bottom surface. Four grits were tracked during the whole process to quantify different wear mechanisms. Due to adhesions, it is quite difficult to count the grits on the bottom of the abrasive layer as it is unclear if a layer of adhesions is covering some of the grits or if they broke off. Figure 8-18 details the damage that four grits took during the process.

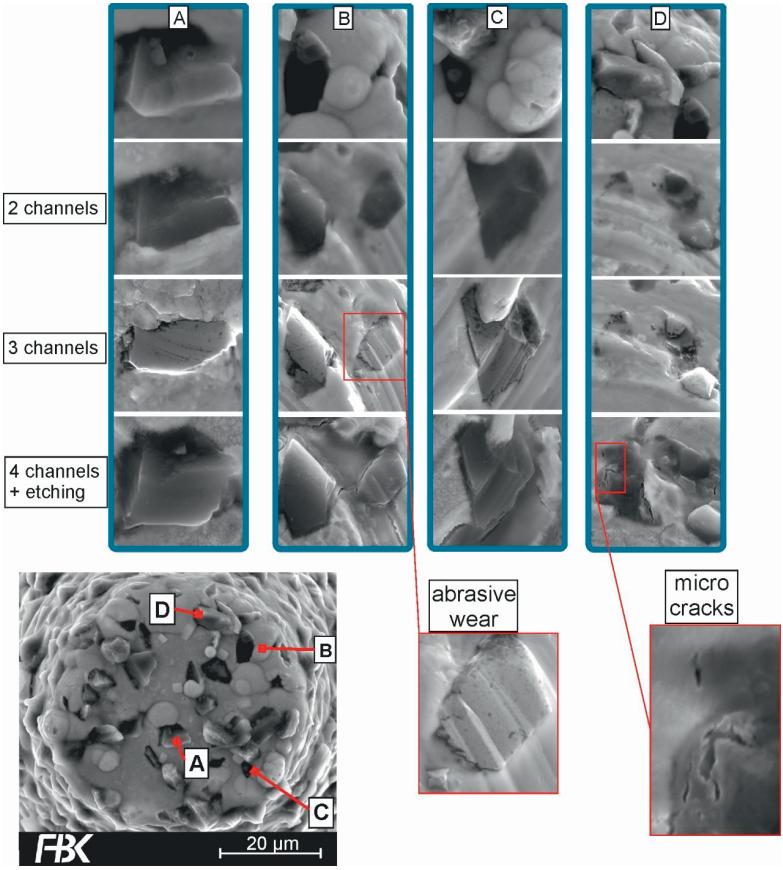

Figure 8-18: Life cycle of single grits

Grit A is close to the pivot of the tool; the main wear mechanism here is attrition that progresses on the right side of the grit, most likely because the right side protruded more. The grits at the pivot are the final grits engaged, therefore, they remove much less material than grits at the circumference. Grits at the pivot have a relatively low cutting speed, with some coming closer to a scratching test. Grits at the pivot endure far lower mechanical impacts.

The grits in B, C, and D are closer to the circumference. Grits at the circumference remove the most material, meaning that they remove material with the largest chip thickness and the highest process forces; this causes high abrasive wear and mechanical impacts. All of the tracked grits were influenced by that abrasive ring that formed. In B a second grit that was completely covered emerged after a 4 mm cutting path – a third of the other grit was removed over an 8 mm cutting path. Grit C was almost completely covered at the start of the process. Abrasion not only uncovered that grit but also removed part of it, creating a step-like structure on the grit itself. The grit in D almost broke off completely, with the remnant chunks of the grits covered with adhesions. Following the etching process, it became clear that fragments of the grit remained. These remnant chunks showed signs of microcracks occurring during the process.

A topic that was previously discussed in section 2.4.2, is the increase of wear on cBN grits when water-based MWFs are used. This effect could not be seen in the experiments conducted so far. It is assumed that the process is not performed long enough for this chemical affinity to have a significant effect.

8.4.3 The influence of substrate material

During the course of this dissertation, it was established that cemented carbide might not be the most adhesive substrate material for a metallic abrasive layer – the abrasive layer failure mechanisms presented in the previous sections, strongly underline this.

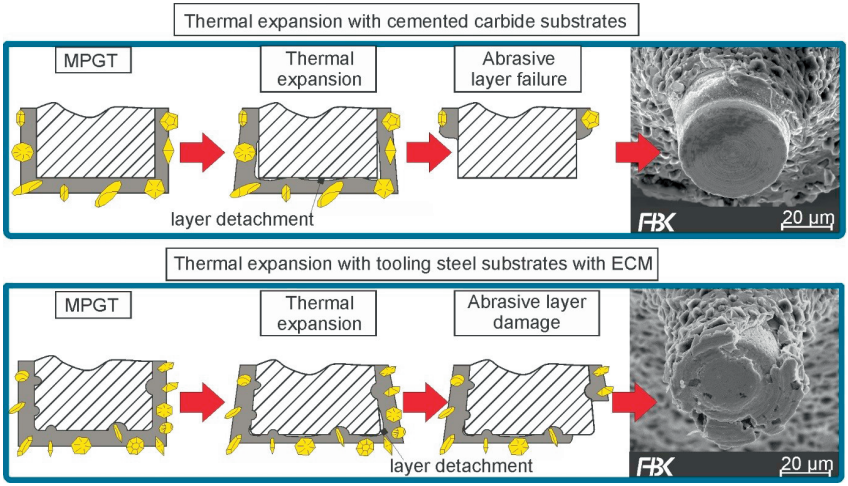

Figure 8-19: Thermal expansion on abrasive layer

While machining results proved that further parameter optimizations and a different MWF are required to improve the process a different substrate material could allow MPGTs to sustain even higher temperatures. A schematic of the theory behind tool failure for both cemented carbide and tooling steel is presented in Figure 8-19. For cemented carbide, higher temperatures cause the bottom portion of the abrasive layer to detach due to thermal expansion. As mentioned in the state-of-the-art (section 3.1), cemented carbide has a much lower thermal expansion coefficient. Tooling steel, on the other hand, has a similar thermal expansion coefficient to nickel, guaranteeing better adhesion for the abrasive layer at higher temperatures. In addition, the small

cavities manufactured with the ECM process further increase adhesion as the abrasive layer interlocks itself further in the substrate surface. The example presented in Figure 8-19 demonstrates that even if a portion of the abrasive layer detaches from the substrate, the adhesion of the rest of the abrasive layer remains strong.

8.5 Metalworking Fluid Study with a Submerged Cutting System[8]

In this study, the method developed by BRUDEK et al. was implemented for the micro grinding process [Brud06]. Submerged cutting allows the user to use almost any type of MWF without having to capsule the machine tool from the environment – a necessity for in house developed machine tools that are prone to constant changes. The experimental setup for this was developed for the ultra-precision four axes machine tool and was also implemented on the Nano Grinding Center (NGC). The sole goal of this study was to explore the effect of different MWFs on the bottom surface of MPGTs. Table 8-5 lists the MWFs used in this case study with its process parameters and grit size. Three microchannels with a depth of cut of 5 µm and a channel length of 3 mm were machined using each MWFs. The rotational speed was kept at 30,000 rpm and the feed rate at 1 mm/min. MPGTs were coated with a grit size of 5-10 µm – without a cavity as we want to explore the effect of MWFs on the pivot area after all.

Table 8-5: MWFs used for submerged cutting experiments.

Case	MWF	Grit size in µm	Feed rate in mm/min	Rotational speed in rpm	Kinematic viscosity at 20 °C in $mm^2 s^{-1}$
Case 27	*Twinmax*	5-10	1	30,000	180 [Stei18]
Case 28	*Lubrimax Edel C*	5-10	1	30,000	88 [Stei18]
Case 29	*Canola oil*	5-10	1	30,000	78.7 [Spic07]
Case 30	*DiaMond 80*	5-10	1	30,000	3 [Oelh18]
Case 31	*Petrofer Iso-cut R – 10 HM*	5-10	1	30,000	10.8 (at 40 °C) [Petr18]
Case 32	SDS (1 wt.%)	5-10	1	30,000	1
Case 33	SDS (5 wt.%)	5-10	1	30,000	1

8.5.1 Wear analysis

MPGTs were evaluated based on SEM images taken before and after machining each microchannel with qualitative EDX analysis performed of each. The machined channel length, the roughness values, and the actual cutting depth had no relevance to the study as there was no complete tool failure in this study. There were, however, two cases in which a small portion of the abrasive layer detached off the base body; a case conducted with *Petrofer Isocut R – 10 HM* and a case conducted with *DiaMond 80*.

In terms of adhesions, the best results could be achieved using the *Twinmax* and *Lubrimax Edel C* MWFs, Table 8-6 shows the results of every MPGT used in the study. The worst performances were achieved using *Petrofer Isocut R10 – HM* and *DiaMond 80*, followed closely by SDS with a 5 wt.%.

Figure 8-20 shows a representative tool for each case. The tools used in the image show the symptoms that occurred on at least two of the three tools used for each case. The difference

[8] Results in this section have been previously published in [Arra20]

between applied MWFs becomes clear upon the comparison. The MWF that contain SDS with 5 wt.% performed worse than that with 1 wt.%, which is why it is not shown. Similar to the results from the previous studies (chapter 7), adhesions gathered at the pivot area of the tool. In the experiments with SDS (1 wt.%), the supplying method already showed improvements as there were not nearly as many adhesions on the three inspected tools as there were in previous studies. Abrasive wear, attrition, and microcracks, however, were still present; as with tools from the previous chapter, an outer ring formed on almost every tool used in all seven cases.

Grits on MPGTs that were used with *Twinmax* and *Lubrimax Edel C*, show signs of micro-chipping and abrasion yet have their full protrusions. Visually, these two cases show no sign of adhesions on the tool bottom (Figure 8-20).

Table 8-6: Iron adhesions measured via EDX on the bottom surface of MPGTs

Iron adhesions measured in wt.%			
MWF	**Tool 1**	**Tool 2**	**Tool 3**
SDS (1 wt%)	29.49 ± 2.22	26.3 ± 1.58	15.99 ± 0.74
SDS (5 wt%)	36.3 ± 3.39	40.45 ± 2.13	38.79 ± 2.31
DiaMond 80	39.86 ± 6.35	58.18 ± 0.44	14.7 ± 1.92
Petrofer Isocut R10 – HM	51.18 ± 1.63	48.73 ± 2.19	25.38 ± 6.27
Twinmax	5.56 ± 0.37	7.23 ± 1.56	39.95 ± 0.61
Lubrimax Edel C	26 ± 0.45	3.24 ± 0.38	5.04 ± 0.21
Canola oil	23.62 ± 3.42	38.98 ± 1.15	12.55 ± 1.66

The mean depth of cut for all microchannels was measured at about 1.5 mm in cutting length. Figure 8-21 illustrates a diagram that shows both the mean values with their respective standard deviation for all cases. The mean values of all microchannels except for the ones machined with *DiaMond 80* have similar results, roughly ranging between 3-4 µm in mean values. Micro grinding experiments in which *DiaMond 80* was used, experienced the largest deviation between actual and set depth of cut.

Despite adjusting the Z-axis to a cutting depth of 5 µm, several influences can reduce or increase that depth of cut. To zero the contact point between tool surface and workpiece surface, the tool is moved in 0.5 µm steps towards the workpiece while the user views the whole process through a video-microscope. Once chip formation occurs, the Z-Axis is zeroed and the tool is moved to the start position, where the machining process can begin. This means that the exact depth the tool reached once it scratched the surface might be 0.5 µm – 1 µm off, not considering the backlash of the Z-axis. Upon entry, the tool loses grits that are not sufficiently embedded. These grits might be the grits that caused the chip formation during the scratch process.

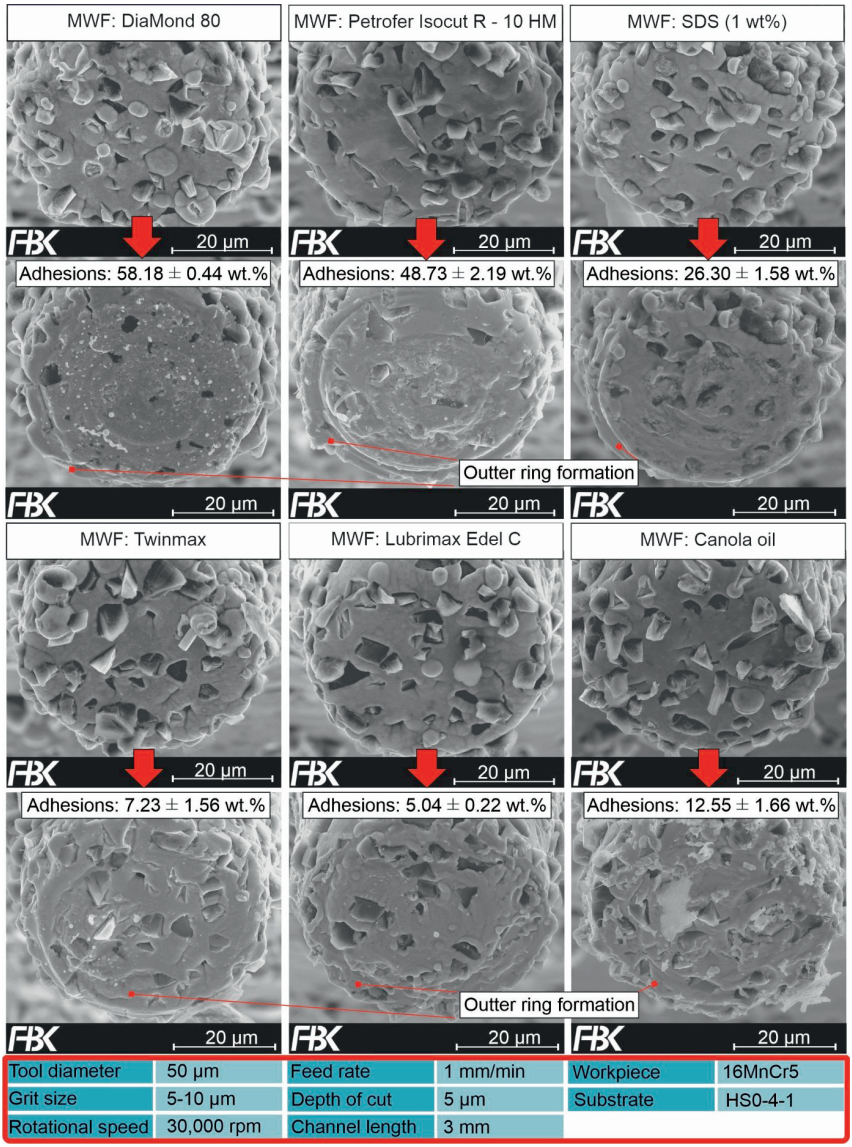

Figure 8-20: Wear analysis for MPGTs used in submerged cutting

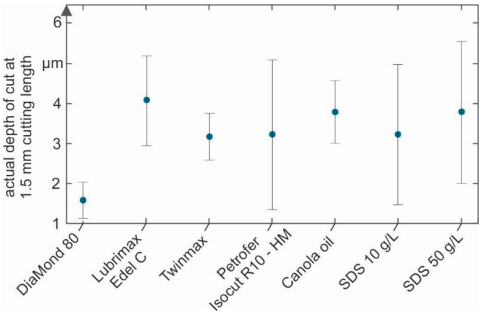

Figure 8-21: Actual depth of cut at a cutting length of 1.5mm

8.5.2 Conclusions

A submerged cutting process was implemented for our micro grinding process. Seven different MWFs from the state of the art and the previous sections were used in a micro grinding experiment with the intention of determining the effect different MWFs have on tool wear. In particular, tool wear of the adhesive nature. It was assumed in section 8.3 that adhesions cause higher rotational speeds to have a negative effect on the process.

Tool wear

The best results were achieved using MWFs that have a high viscosity – *Lubrimax Edel C* and *Twinmax*. Viscosity describes the resistance a fluid has shear and tensile stresses, informally defined as "thickness" for liquids. Thicker MWFs have a higher viscosity, higher lubricity, and higher-pressure absorption capacity. A resistant lubricating film forms between the abrasive grits and the workpiece surface during machining; this minimizes ensuing temperatures that result from friction. Canola oil has a viscosity as high as *Lubrimax Edel C* has, however, it lacks the additives that improve its performance [Arra20].

MPGTs used with *Lubrimax Edel C* and *Twinmax* only showed minimal adhesive wear. High abrasive wear for grit populations closer to the circumference remained regardless of the MWF used. The third best MWF was SDS with 1 wt.%, which has been used in the last two sections. SDS was used for two reasons, to test if a different MWF supplying method delivers similar results – which it did – and to test if a higher SDS concentration (5 wt.%) is better for the process. SDS with 1 wt.% outperformed canola oil despite the difference in viscosity; it is assumed that reduced surface tension is the reason for this slight edge. SDS with 5 wt.% caused more adhesions on the bottom surface of MPGTs. It is assumed that a certain threshold for SDS concentration was passed, causing a negative effect on the MWF. Higher SDS concentrations cause more foaming to the solution. Foaming means that gas is added to the micelles of the MWF which is unfavorable to mechanical machining.

Depth of cut analysis

The depth of cut analysis served to highlight one problem with the current micro grinding process: tool wear decreases the actual depth of microchannels tremendously. It has been previously shown that upon entry, many MPGTs sustain damage on their abrasive layer, which causes this decrease in depth of cut. This damage to the abrasive layer is caused by too high

process forces. These process forces can be reduced by reducing feed rate, increasing rotational speed and/or depth of cut.

Outlook to the next section

Twinmax and *Lubrimax Edel C* performed best in terms of reducing iron adhesions to a minimum. In order to determine which of the two MWFs performs better and to minimize the depth of cut error, a micro pendulum grinding process was implemented. The results will be presented in the next section.

8.6 Case Studies with a Micro Pendulum Grinding Method

Micro pendulum grinding has been introduced in section 7.1.3. Two pendulum movements are conducted to decrease process forces and increase the influx of MWF to the machining zone. Much higher feed rates are possible while maintaining a relatively high process accuracy.

The process can also be used to machine much deeper microchannels than before. The problem we faced so far was that the abrasive layer of MPGTs broke off less than 1 mm into the micro grinding process whenever cutting depths of 10 µm and above were attempted. Here, microchannels reaching aspect ratios >1 (that is approx. a 50 µm deep channel) are easily achievable. Figure 8-22 illustrates a microchannel that is 3 mm long and 48.2 µm deep. The microchannel was machined with a rotational speed of 30,000 rpm, a feed rate of 30 mm, and depth of cut of 0.5 µm.

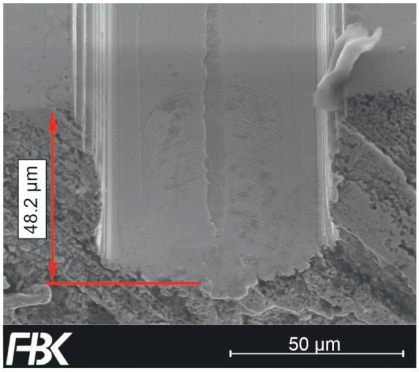

Tool diameter	50 µm	Feed rate	30 mm/min	Workpiece	16MnCr5
Grit size	5-10 µm	Depth of cut	0.5 µm	Substrate	HS0-4-1
Rotational speed	30,000 rpm	MWF	Twinmax		

Figure 8-22: Microchannel with high aspect ratio machined with pendulum grinding [Arra20]

Machining deeper channels was used as an endurance test for MPGTs in this section. With this endurance test, another parameter study is started to test the new limits of the current process. Two MWFs that reduce iron adhesions to a minimum have been identified: *Twinmax* and *Lubrimax Edel C* – now we can determine which is better suited for the process. Different rotational speeds and different grit sizes need to be tested. If the plan worked correctly, an increase in rotational speed should have a positive effect on the process again. What is also interesting is finding out how reducing adhesions with MWF stacks with the adhesions reducing effect conjured by a cavity that is manufactured via EDM.

8.6.1 Endurance test and experimental plan

Figure 8-23 illustrates two microchannels that were machined according to the presented micro pendulum grinding method. The goal was machining a 5 mm long microchannel with a microchannel depth of 50 µm. The right side of the figure shows a tool that failed to complete its task. The tool itself lost the abrasive layer at the bottom and was flattened while continuously moving downwards. The substrate material HS0-4-1 is barely harder than the workpiece material and cannot remove material. Therefore, once the abrasive layer breaks off the bottom of the tool, material is not removed but ploughed and squeezed – this affects grinding marks, roughness peaks, and substructures. The achieved microchannel depth can be used as a direct indicator of the performance of MPGTs.

The left images show an MPGT that completed its task while staying intact and the microchannel it machined. The MPGT started forming a hemisphere-like shape at the bottom of the tool, due to higher tool wear at the circumference. The microchannel is, therefore, much narrower at the bottom, showing clear substructures. Direct indicators for successful grinding operations are the grinding marks at the bottom of the microchannel. As will be mentioned in section 8.2.3, grinding marks follow the same equation for feed rate per rotation (f_z) that is used in micromilling, as one grit always cuts deeper the rest. In the case presented in Figure 8-23, a rotational speed of 30,000 rpm and a feed rate of 30 mm/min produce a feed rate per rotation of 1 µm. The distance measured between the grinding marks of all structures confirms the theory for MPGTs with a diameter of 50 µm.

Based on these results, a parameter study is conducted by which the effect of a few key parameters is determined. An endurance test has been designed to determine the effect of grit size, MWF, rotational speeds, and cavities on this newly developed micro grinding process. In order to do so, a microchannel with a cutting path of 5 mm and a microchannel depth of 50 µm was machined with the methodology described above. Eight microchannels were machined with each parameter combination, as the process has proven to have high standard deviations in previous sections. Both the microchannel depth and the number of tools to withstand the endurance test were used as evaluation criteria. A constant feed rate of 30 mm/min with a depth of cut of 0.5 µm is used. Table 8-7 shows a list of all cases in this parameter study. The base parameters for this study are a grit size of 5-10 µm, a rotational speed of 30,000 rpm, and the MWF *Twinmax*. Experiments are performed on the ultra-precision four axes machine tool, presented in section 5.1.2.

In the study presented in section 8.5, the MWFs *Twinmax* and *Lubrimax Edel C* showed the least amount of adhesions on the abrasive layer. It was assumed that both these MWFs perform equally well. To determine which of the two MWFs is better, the endurance test is performed.

The grit size was previously determined to have a positive effect on the process. The grit sizes 4-8 µm, 5-10 µm, and 6-12 µm are tested to determine which delivers the best results. The study is conducted to identify the maximum grit size that can be used with MPGTs that have a diameter of 50 µm. It is a study that determines when grit density outweighs the effect of grit size for a given diameter.

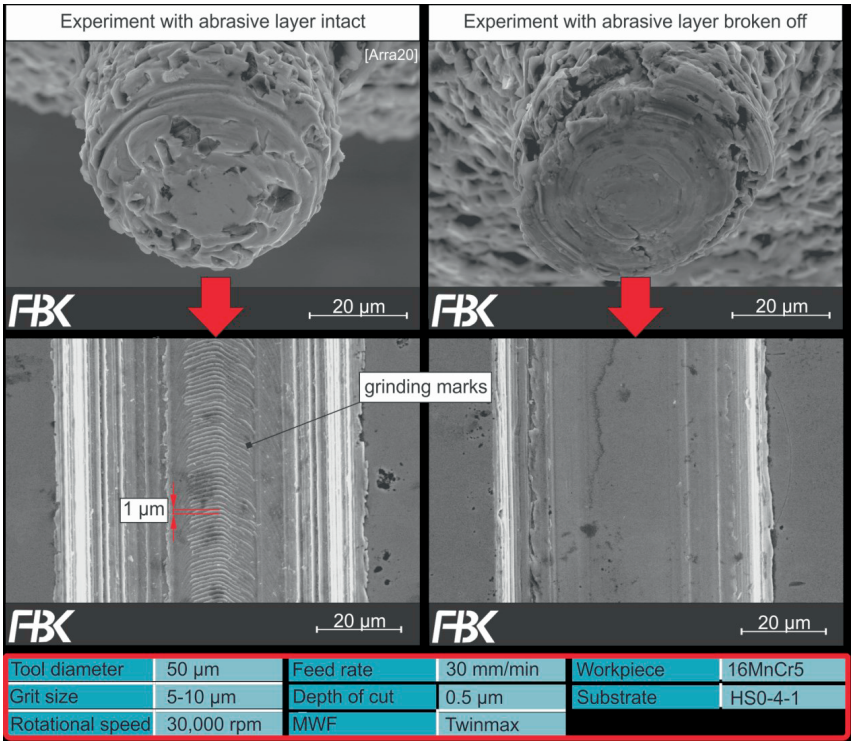

Figure 8-23: Microchannels with high aspect ratio

Higher rotational speeds have previously shown negative effects on the process. It was assumed that the clogging of the abrasive layer with material adhesions caused more heat generation, causing the abrasive layer to detach from the previously used cemented carbide base body; this is not the case anymore. Micro grinding experiments with the rotational speeds of 10,000 rpm, 30,000 rpm, and 50,000 rpm were conducted.

The effect of a cavity at the pivot of MPGT will be determined by a tool life test. In section 8.3.3, it was proven that a cavity reduces substructures while providing a reasonably good tool life – at least for a grit size of 3-6 µm that is. The grit size of 3-6 µm is unsuitable for high-performance machining, prompting us to use a grit size of 5-10 µm instead. The study will determine if the benefits of a cavity, outweigh the reduced number of active grits.

A final case study is conducted to see if feed rates of 120 mm/min and 240 mm/min are possible using the current technology. The case study is conducted on the Nano Grinding Center (NGC), which is presented in section 5.1.3. A rotational speed of 120,000 rpm is chosen for the task at hand – the rotational speed is chosen due to its favorable run-out error of about 2 µm. Combined with the chosen feed rates, the tool moves 1 µm per rotation at a feed rate of 120 mm/min and 2 µm per rotation at a feed rate of 240 mm/min. The results are compared to those from case 34 to test if the results are constant when using the same speed ratio.

Table 8-7: Parameter combinations for micro pendulum grinding endurance test

Case	MWF	Grit size in µm	Rotational speed in rpm	Feed rate in mm/min	Cavity
Case 34	*Twinmax*	5-10	30,000	30	None
Case 35	*Lubrimax Edel C*	5-10	30,000	30	None
Case 36	*Twinmax*	4-8	30,000	30	None
Case 37	*Twinmax*	6-12	30,000	30	None
Case 38	*Twinmax*	5-10	10,000	30	None
Case 39	*Twinmax*	5-10	50,000	30	None
Case 40	*Twinmax*	5-10	30,000	30	With cavity
Case 41	*Twinmax*	5-10	120,000	120	None
Case 42	*Twinmax*	5-10	120,000	240	None

8.6.2 Micro pendulum grinding endurance test

The effect of MWFs[9]

Figure 8-24 shows the endurance test applied using the MWFs *Lubrimax Edel C* and *Twinmax*. Experiments conducted with *Lubrimax Edel C* reached a mean microchannel depth of 33.3 µm ± 10.4 µm, with two of the tools retaining their abrasive layer. Microchannels machined with *Twinmax* reached a microchannel depth of 35.9 µm ± 13.2 µm with four tools out of eight, still having an intact abrasive layer, post-machining. The mean microchannel depth for both cases is close in value and cannot be used as a sole evaluation criterium. A p-value of 0.673 was calculated via a t-test, deeming the parameter as insignificant. However, twice the amount of MPGTs completed the entire microchannel without tool failure when *Twinmax* was used, giving *Twinmax* a slight edge over *Lubrimax Edel C*.

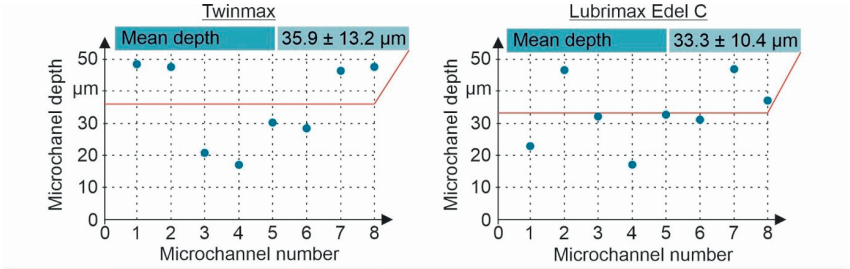

Figure 8-24: Endurance test analysis with different MWFs

[9] Effect of MWFs have been previously published in [Arra20]

The effect of grit size

Figure 8-25 illustrates the endurance test with three different grit sizes – the results for the grit size 5-10 µm are the same as *Twinmax* in Figure 8-24. MPGTs coated with abrasive grits of size 4-8 µm, reached a mean depth of 12.9 µm ± 6.2 µm with all tools failing to complete the entire microchannel depth. MPGTs coated with a grit size of 6-12 µm achieved a mean depth of 29.4 µm ± 12.4 µm with one tool sustaining the experiment. An ANOVA test was conducted to compare the three cases, the results are listed in Figure 8-25. The p-value between the grit sizes 5-10 µm and 6-12 µm proved to be insignificant while the other two p-values were significant. As with the MWF analysis, the experiment was influenced by the microchannel depth, chosen for the study. More MPGTs that embedded a grit size of 5-10 µm retained their abrasive layer after the experiments than those embedded with a grit size of 6-12 µm. Case studies in which a higher volume is removed would have shifted the p-value further down.

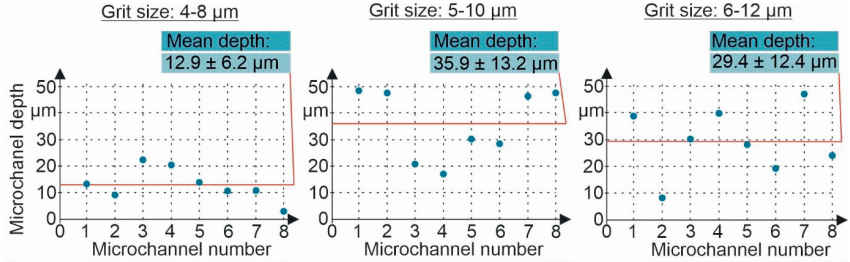

Tool diameter	50 µm	Feed rate	30 mm/min	Workpiece	16MnCr5
		Depth of cut	0.5 µm	Substrate	HS0-4-1
		Rotational speed	30,000 rpm	MWF	Twinmax

Compared grit sizes	p-value	Significance
4-8 µm and 5-10 µm	0.0012	Significant
4-8 µm and 6-12 µm	0.0047	Significant
5-10 µm and 6-12 µm	0.3311	Insignificant

Figure 8-25: Endurance test analysis with different grit sizes

The effect of rotational speed

Figure 8-26 illustrates the endurance test with three different rotational speeds – the results for the rotational speed of 30,000 rpm are the same as *Twinmax* in Figure 8-24. A direct relationship between rotational speed and microchannel depth was proven. The p-values proved that the interacting parameter variations were significant. Five of the tools used for the experiments conducted with a rotational speed of 50,000 rpm sustained the experiment. The difference between the mean values of experiments conducted with 30,000 rpm and 50,000 rpm would probably shift further up in favor of the latter if a deeper microchannel depth was chosen for the study.

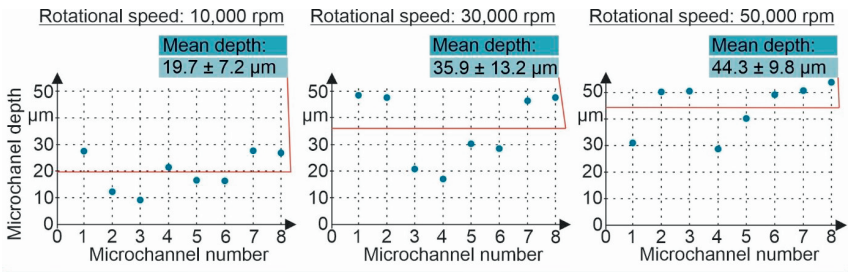

Tool diameter	50 µm	Feed rate	30 mm/min	Workpiece	16MnCr5
Rotational speed	30,000 rpm	Depth of cut	0.5 µm	Substrate	HS0-4-1
				MWF	Twinmax

Compared rotational speeds	p-value	Significance
10,000 rpm and 30,000 rpm	0.0110	Significant
30,000 rpm and 50,000 rpm	0.0498	Significant
10,000 rpm and 50,000 rpm	0.0001	Significant

Figure 8-26: Endurance test analysis with different rotational speeds

The effect of a cavity manufactured via µEDM

Figure 8-26 illustrates an endurance test performed for MPGTs with and without cavities – the results for tools without a cavity are the same as *Twinmax* in Figure 8-24. A cavity most definitely decreases the tool life for current machining conditions. The p-value shows a significant effect on the process.

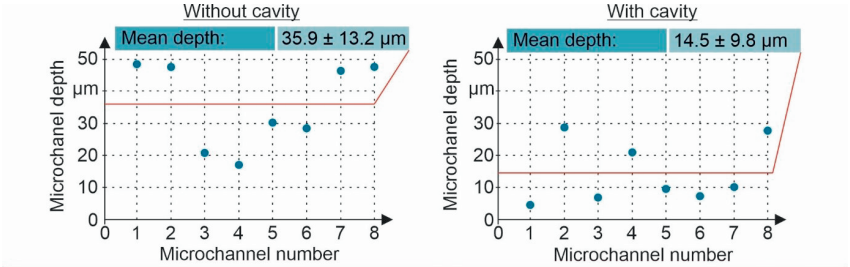

Tool diameter	50 µm	Feed rate	30 mm/min	Workpiece	16MnCr5
Grit size	5-10 µm	Depth of cut	0.5 µm	Substrate	HS0-4-1
		Rotational speed	30,000 rpm	MWF	Twinmax

Compared MPGTs	p-value	Significance
With and without cavity	0.0024	Significant

Figure 8-27: Endurance test for MPGTs with and without a cavity

The effect of higher feed rates at a higher rotational speed

The tools used in case 41 move at the same feed per rotation as the tools used in case 34. Figure 8-28 presents the results of both cases in comparison. While case 34 has a much higher mean microchannel depth, the p-value indicates the variance as insignificant. However, as stated earlier, case 34 exhibits four tools that completed the machining experiment while still intact – in case 41, every MPGT was damaged during the machining experiments.

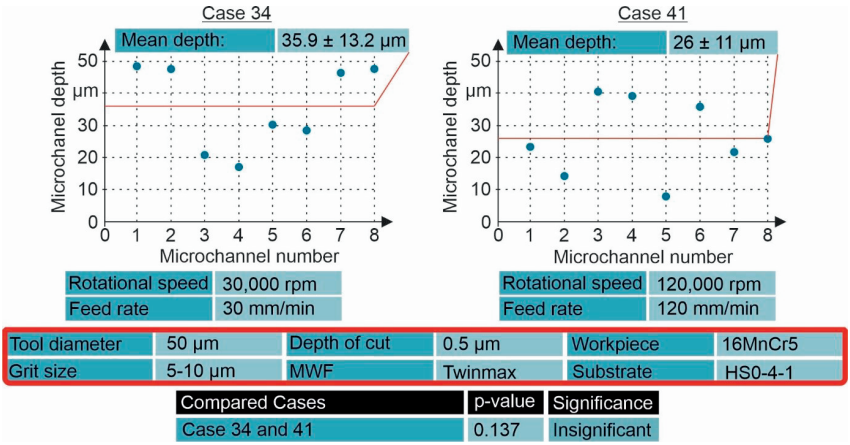

Figure 8-28: Endurance test analysis for cases 34 and 41

Performance comparison for two different feed rates

A much better p-value was achieved when the effect of feed rate is compared. Figure 8-29 illustrates the results obtained from cases 41 and 42. A p-value of 0.069 was achieved, which proved the parameter feed rate to be significant. The mean microchannel depth is almost half of that of case 41, which is to be expected when using twice the feed rate.

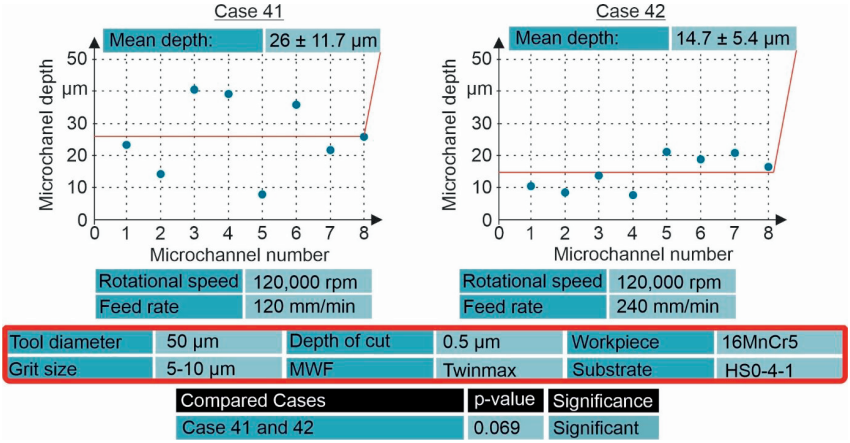

Figure 8-29: Endurance test analysis for different feed rates

8.6.3 Conclusions

A pendulum grinding process was combined with the previously introduced submerged cutting process to conceive an endurance test for this type of micro grinding process. In this process, a smaller depth of cut of 0.5 µm was used to produce 50 µm deep and 5 mm long microchannels. The parameters tested were: the effect of MWF, grit size, rotational speed, effect of a cavity,

and the effect of higher rotational speeds with higher feed rates. So far, the process proved to have high deviations, which is why each case was performed eight times.

The effect of MWFs

As previously discussed, viscosity influences the formation of adhesions on the abrasive layer; this is underlined by the experiments conducted in section 8.5. In section 8.5, the two MWFs that caused the least adhesions had the highest viscosity. *Twinmax*, which happens to have the highest viscosity, outperformed all the other MWFs. Both their mean microchannel depth and the p-value indicate that the process performs equally well, using either of the two MWFs, however, a higher number of MPGTs sustained the experiment using *Twinmax* than when using *Lubrimax Edel C*.

The effect of grit size

In section 8.3, it became evident that a larger grit size outperforms a smaller grit size. Larger grit sizes are generally more resistant to impacts and can endure machining with larger chip thicknesses that would completely engulf smaller grits. However, at a certain grit size, the size of the grits reduces the grit density on MPGTs, so much, that tool life is reduced again; an example of such a case was the MPGTs with a grit size of 8-16 µm presented in Chapter 6. While MPGTs with a grit size of 6-12 µm seemed to have a relatively decent grit density, the machining results proved that a grit size of 5-10 µm is superior. MPGTs with a grit size of 4-8 µm had a higher grit density than MPGTs with a grit size of 5-10 µm but had a much worse tool life than the other two. As it seems, the best grit size for MPGTs with a diameter of 50 µm is 5-10 µm.

The effect of a cavity

The results showed that a cavity reduces the tool life of MPGTs. Just as with MPGTs that employ a grit size of 6-12 µm, a minimal number of active grits are required for the process to perform well. A cavity at the pivot of the tool reduced the area grits can populate, increasing the process forces for the grits on the remaining substrate area. When SDS was used, the cavity reduced adhesions in the process, however, since the MWF *Twinmax* has the same effect on the process, this is no longer an advantage.

The effect of rotational speed

In section 8.3, it appeared that when using higher rotational speeds, the tool performed worse. Despite having smaller chip thicknesses, the abrasive layer was clogged with a layer of adhesions. This layer of adhesions was the result of a lack of lubrication. Now that a suitable MWF is used, tool life improved with progressing rotational speeds. In order to test higher rotational speeds, a different machine tool was used. The NGC uses a spindle with an automatic clamping system, which adds a large clamping error to the process. Additionally, different axes with different resolutions have been used in the comparison.

Feed rates of 120 mm/min (case 41) and 240 mm/min (case 42) were attempted with a rotational speed of 120,000 rpm. Compared to a previous case (case 34) in which 30 mm/min was used with a rotational speed of 30,000 rpm, the tool life decreased despite having the same speed ratio at 120 mm/min. Apart from the obvious machine tool differences, a probable cause for the high difference in performance is that higher feed rates and higher rotational speeds add higher process forces and higher process temperatures, which may cause MPGTs to fail sooner

than in case 34. Besides, as mentioned in section 2.4, the tool is surrounded by a boundary layer made of air that increases in strength as rotational speed increases. In other words, as rotational speed increases, the amount of MWF that is dragged into the machining zone decreases.

The difference in tool life between case 41 and case 42 is proportional to the feed rate.

Discussions and outlook

The results show that the best performance with MPGTs with diameters of 50 µm can be achieved using high rotational speeds, a grit size of 5-10 µm, without a cavity. *Twinmax* is the recommended MWF from the selection of MWFs tested; this does not mean that a new MWF could not improve performance even further.

Now that adhesions have a much smaller influence on the process, a few deciding factors determine the performance of MPGTs. Chip thickness per grit, for instance, is lower with a higher rotational speed and a higher grit density. Grit density decreases with a cavity at the bottom of MPGTs, when an inclination angle is applied to the tool, or when a larger grit size is used. In turn, a larger grit size increases the resilience of individual grits, as higher process forces are possible. As it stands right now, a grit size of 5-10 µm is the perfect balance between grit density and grit size.

A larger feed rate increases chip thickness per grit directly and, in turn, the process forces. However, a larger feed rate decreases machining time, a parameter that is desired. To increase possible feed rates while sustaining a functional tool, other process parameters and tool specifications have to be optimized. By changing the composition of the NI-P layer that binds the abrasive grits, higher retention forces are possible, making it far more resilient. Those parameters require a large-scale investigation that will be conducted in future works, however, as of now, the easiest most obvious way to increase feed rate is increasing the cutting speed. This can either be achieved by increasing the tool diameter, or by increasing rotational speed. There are of course faster spindles than the ones introduced so far, like the one manufactured at our institute during the dissertation of MÜLLER. The spindle can reach rotational speeds of over 450,000 rpm [Müll19] and can be installed into any of the two machine tools introduced. With such rotational speeds, feed rates of up to 1000 mm/min can be attempted. However, during the final investigations of this dissertation, the spindle was unavailable.

In the next sections, the method behind the formation of various substructures is elaborated upon. And finally, a method to produce complex microchannel structures is introduced.

8.7 Manufacturing Complex Structures

Using the micro pendulum grinding process, several microchannels were machined. Various shapes were machined: A pineapple, a pint of beer, a platypus, an Axolotl, and a microchannel that closely resembles the author of this dissertation. Figure 8-30 shows these complex microchannels. As usual, the parameters used to manufacture these structures are added to the image. A feed rate of 45 mm/min was successfully attempted here.

In section 8.1.3 a microchannel in a U-form has been attempted to test the capability of MPGTs to change feed direction. The shape of a house in section 8.3.4 expanded on that by machining a channel in all eight straight and diagonal directions. In this section, a number of geometries were machined using computer-aided manufacturing (CADCAM) techniques. Corel draw was used to draw lines over the original images of the desired shape. The line structure was exported

to the computer-aided design program (CAD) Unigraphics NX 10.0. In NX 10.0 the drawn lines were converted to a CNC program, saving the user a lot of time writing the CNC program.

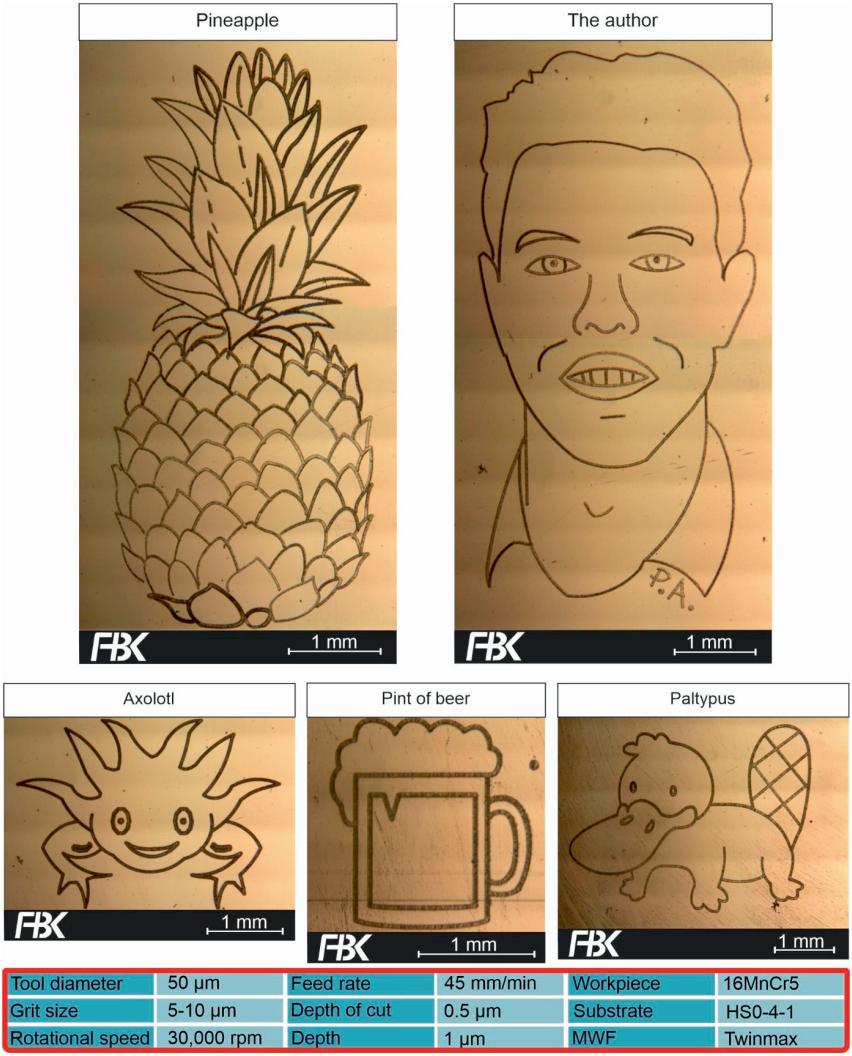

Tool diameter	50 µm	Feed rate	45 mm/min	Workpiece	16MnCr5
Grit size	5-10 µm	Depth of cut	0.5 µm	Substrate	HS0-4-1
Rotational speed	30,000 rpm	Depth	1 µm	MWF	Twinmax

Figure 8-30: Complex micro structures machine in 16MnCr5 (665 HV30)

As a final challenge in this dissertation, a more complex structure was chosen to demonstrate the capabilities of the process: text. Text is a collection of different shapes that need to be small enough to fit on a certain template but large enough so it can be read. As mentioned in the introduction, physicist Richard Feynman challenged scientists around the world to write a large quantity of information in a small area. While we can't write the entire Encyclopedia Britannica on the head of a pin, writing a text on a small area is possible.

Figure 8-31 depicts the introduction to Richard Feynman's „There's Plenty of Room at the bottom." Two workpieces were used to encompass an area that is 17 mm wide and 16.5 mm long. Six MPGTs in total were used to minimize the effect of tool wear. The depth of each letter ranges from a few hundred nanometers to 2 µm. Tool wear, axial run-out, and surface defects on the workpiece caused the variations in channel depth. A camera was used to capture the images, and a filter was used to highlight the text further.

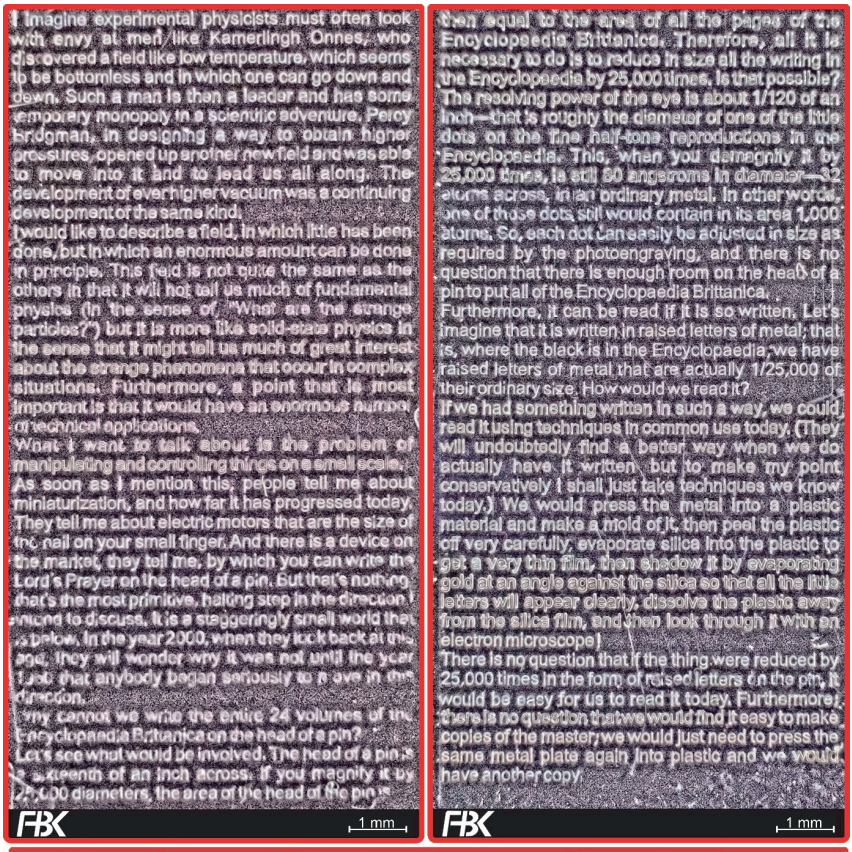

Tool diameter	50 µm	Feed rate	40 mm/min	Workpiece	16MnCr5
Grit size	5-10 µm	Depth of cut	0.5 µm	Substrate	HS0-4-1
Rotational speed	120,000 rpm	No. of passes	2	MWF	Twinmax

Figure 8-31: Introduction to Richard Feynman's „There's Plenty of Room at the bottom " [Feyn59]

9 Conclusions and Outlook

The trend for the miniaturization of components has been a central theme in product development, provoking the development of new manufacturing processes. These manufacturing processes included non-contact methods like laser beam machining, electrical discharge machining or lithographic processes in which workpieces are covered with a light-sensitive resist layer that is microstructured with an ultraviolet light beam or an electron beam. The microstructured area on the resist layer is used to remove material from the workpiece by wet etching or add material via electroplating processes.

With improving manufacturing techniques, another trend emerged: manufacturing micro tools for micromachining operations. Micro tools have the advantage of being able to machine complex microchannels with a computerized numerical control method with minimal workpiece preparation. Micromachining processes are, therefore, suitable for small-batch manufacturing operations. These micro tools include micro end mills, micro drills, dicing blades, and micro pencil grinding tools (MPGTs).

MPGTs comprise a cylindrical shaft and superabrasives that are bound with a metallic layer made of nickel. These micromachining tools use their bottom surface as well as their circumference to machine microchannels in hard and brittle materials. MPGTs are capable of machining any type of closed structure with a number of different microchannel-cross-sections that even make undercutting possible.

Due to their rather small diameters, MPGTs are known to have rather low cutting speeds, limiting their feed rate as well as their tool life when compared to larger grinding tools like dicing blades or conventional grinding wheels. The objective of this dissertation was to find ways to improve both the tool life and the achievable feed rates. To achieve this objective, the manufacturing process starting from the substrate, its manufacturing process, its form, and the coating process have been revised. Metalworking fluid (MWF) supplying methods and new MWFs have been adapted to the process from literature research to achieve both higher tool life and higher surface quality. Optimized machining methodologies, as well as numerous parameter studies, have been conducted.

An electroless plating process has been developed to replace the electroplating process that was previously used to manufacture MPGTs. The process involved a surface treatment that consisted of electrolytic degreasing, electrochemical machining, a pickling process, and an electroplating precoating process. The main coating process was conducted on a magnetic stirrer, that heated the electroless plating solution to a temperature of 87 °C ± 1 °C. The superabrasives were added to the solution and were embedded into the abrasive layer whilst electroless plating was ongoing. The superabrasives reached the surface of the substrates by whirling the solution up via magnetic stirrer – the substrate was rotating via a small electric motor. The solution consisted of 30 g/L nickel sulfate hexahydrate, 20 g/L sodium hypophosphite, 20 g/L sodium acetate, 0.4 mg/L thiourea, and hydrochloric acid.

The thiourea concentration was determined via a parameter study, a range of 0.4-0.5 mg/L was considered to be the range with the highest, most consistent nickel growth; a nickel growth of 21 µm/h was measured for a thiourea concentration of 0.4 mg/L. Substrate rotational speed was also inspected, as a too high rotational speed was found to increase nonuniform nickel growth.

MPGTs with various diameters and various grit sizes were coated with this process; for conducted machining experiments, a diameter of 50 µm was chosen.

Hardened steel workpieces made of 16MnCr5 that have a hardness of approximately 665 HV30 were used for the machining experiments. It was determined early on, that dry machining is almost impossible, which is why a MWF study was required. A MQL-system was developed and used a MWF made of distilled water and sodium dodecyl sulfate (SDS). Initially, a concentration of 0.02 g/L SDS was used in the MWF. The cutting path achieved with dry machining and machining with sprayed distilled water was almost zero. MPGTs used with SDS successfully machined 0.5 mm long and 5 µm deep microchannels, using a rotational speed of 30,000 rpm at feed rates of 0.05 mm/min and 0.1 mm/min – MPGTs were coated with a grit size of 2-4 µm. Building on these initial results a larger parameter study was conducted and evaluated using analysis of variance (ANOVA). This parameter study consisted of a full factorial parameter study that tested the effect of feed rate (0.1 mm/min and 0.2 mm/min), rotational speed (30,000 rpm and 50,000 rpm), grit size (1-2 µm and 3-6 µm), and tool inclination (0° and 2°) on the process. The SDS concentration in the MWF was increased to 1 wt.%, the microchannels were 1 mm long, and 5 µm deep. The most prominent results were:

- A larger grit size increased tool life, a tilt angle reduced tool life, and, to our surprise, a larger rotational speed reduced tool life. A higher rotational speed means that each grit on the tool bottom removes less material per rotation, reducing the process forces and, therefore, increasing tool life. In this particular case, however, it was determined by analyzing the abrasive layer of MPGTs after the process via a scanning electron microscope (SEM) and energy-dispersive X-ray spectroscopy, that the bottom surface of the abrasive layer is clogged with iron adhesions. Adhesions are a sign of a lack of lubrication, therefore, the used MWF is insufficient for the process.
- The surface quality of the microchannels fluctuated due to the formation of so-called substructures. Substructures are smaller microchannels that form at the bottom of the microchannel and occur due to different protrusions at the bottom of MPGTs. The formation of substructures might compromise the function of the microchannels because it reduces the overall channel depth.

To fix the problem with the substructures an electrical discharge machining process that was previously developed at our institute was used to produce a cavity at the pivot of MPGTs – a cavity with diameters of 20-25 µm. This increased the minimal width and decreases the depth of substructures, reducing the effect they have on roughness values. Results were also compared to a tool, tilted with a 2° angle. MPGTs with cavities produced wide substructures that were only a few hundred nanometers deep, tilted MPGTs produced concave structures. The adhesions produced during the process were almost completely focused on the cavity, improving the tool life when compared to the old process.

To increase the tool life further, a new MWF supplying method was introduced: submerged micro grinding. A Machining process that takes place in a pool of MWF. Using this MWF supplying method, a case study was initiated in which seven different MWFs were tested. MPGTs with a grit size of 5-10 µm were used to machine 3 mm long and 5 µm deep microchannels. The rotational speed was kept at 30,000 rpm with a feed rate of 1 mm/min Cases were mainly evaluated by the concentration of adhesions the tools have after machining. The MWFs

Twinmax and *Lubrimax Edel C*, two plant-based, highly viscose, and oil-based MWF from the company *Steidle GmbH* provided the best results, reaching adhesion concentrations of less than 10% on some of the specimens.

A pendulum grinding methodology was adapted to the process. Instead of machining the entire depth of cut in one step, the required microchannel depth is machined in multiple much smaller depth of cut steps of 0.5 µm. The feed rate can be increased to values of 30-60 mm/min for an MPGT with a grit size of 5-10 µm that rotates with a rotational speed of 30,000 rpm. Simultaneously the tool moves in a rectangular fashion when machining the full length of the microchannel, increasing the width of the channel by 4 µm to increase the flow of MWF. The Z-axis only moves downwards during the process to diminish backlash errors from the axis. An endurance test was developed using pendulum grinding combined with the submerged cutting method. In this endurance test, 5 mm long and 50 µm deep microchannels were machined varying several parameters. Each test was repeated eight times because previous experiments showed a rather high standard deviation. A small experimental series was conducted with the base parameters: a rotational speed of 30,000 rpm, a grit size of 5-10 µm, a feed rate of 30 mm/min, and the MWF *Twinmax*. The following tests were conducted with this method:

- *Twinmax* and *Lubrimax Edel C* the two best MWFs from the previous study were compared in an endurance test. The mean values achieved were 35.9 µm ± 13.2 µm for *Twinmax* and 33.3 µm ± 10.4 µm for *Lubrimax Edel C*. Statistically insignificant, however, four tools used with *Twinmax* completed the experiment while still intact and only one tool did so with *Lubrimax Edel C*.
- Rotational speeds 10,000 rpm, 30,000 rpm, and 50,000 rpm were compared. The test clearly showed that the higher rotational speed was best suited.
- The grit sizes 4-8 µm, 5-10 µm, and 6-12 µm were tested. The result was that for a diameter of 50 µm, the grit size 5-10 µm was best suited.
- Finally, MPGTs with a cavity were compared to MPGTs without a cavity. The results show that a cavity reduced the tool life to about a third of the tool life (14.5 µm ± 9.8 µm).

A different machine tool with a spindle that allows for higher rotational speeds was used. A rotational speed of 120,000 rpm was configured to test a feed rate of 120 mm/min and 240 mm/min. The results of a feed rate of 120 mm/min was first compared to that of a 30 mm/min and 30,000 rpm rotational speed from the previous case study to see if the feed rate/rotational speed ratio can be upscaled; while this was not achieved completely, the results were within the margin of error from one to the other. The upscaling functioned better when comparing feed rates that were used with the same rotational speed. When compared in achieved microchannel depth, the feed rate of 240 mm/min, achieved almost half the depth achieved with a 120 mm/min.

Outlook

Now that a completely functional process is presented, a large-scale parameter study is required to test the full capabilities of these tools. What became apparent from the final case study was that feed rate and rotational speed can simultaneously be increased correspondingly to the feed per rotation parameter of a single-edged cutting tool. This feed per rotation relationship can be

explored further with higher rotational speeds. In addition, the micro pendulum grinding parameters can be optimized to different values than the ones chosen here – the depth of cut and width of the channel that is. Furthermore, different MWFs could increase tool life even further. The MWF studies in this dissertation concluded that viscosity is an important factor.

In addition, further tool development could increase tool life and decrease the process duration even further. Those developmental steps could involve looking for a more adhesive substrate material, a better tool form than a cylinder, heat treatment for the Ni-P layer, and further plating solution developments like manipulating the phosphorus content of the Ni-P layer to improve mechanical properties.

10 Appendix

10.1 A list of experimental cases

Case	MWF	Grit size in µm	Feed rate in mm/min	Rotational speed in rpm	Inclination angle in °	Depth of cut in µm	Channel length in mm	Channel depth in µm	Cavity
Case 1	None	2-4	0.05	30,000	0	5	0.5	5	None
Case 2	None	2-4	0.1	30,000	0	5	0.5	5	None
Case 3	Water	2-4	0.05	30,000	0	5	0.5	5	None
Case 4	Water	2-4	0.1	30,000	0	5	0.5	5	None
Case 5	SDS (0.02 wt.%)	2-4	0.05	30,000	0	5	0.5	5	None
Case 6	SDS (0.02 wt.%)	2-4	0.1	30,000	0	5	0.5	5	None
Case 7	SDS (1 wt.%)	1-2	0.1	30,000	0	5	1	5	None
Case 8	SDS (1 wt.%)	3-6	0.1	30,000	0	5	1	5	None
Case 9	SDS (1 wt.%)	1-2	0.2	30,000	0	5	1	5	None
Case 10	SDS (1 wt.%)	3-6	0.2	30,000	0	5	1	5	None
Case 11	SDS (1 wt.%)	1-2	0.1	30,000	2	5	1	5	None
Case 12	SDS (1 wt.%)	3-6	0.1	30,000	2	5	1	5	None
Case 13	SDS (1 wt.%)	1-2	0.2	30,000	2	5	1	5	None
Case 14	SDS (1 wt.%)	3-6	0.2	30,000	2	5	1	5	None
Case 15	SDS (1 wt.%)	1-2	0.1	50,000	0	5	1	5	None
Case 16	SDS (1 wt.%)	3-6	0.1	50,000	0	5	1	5	None
Case 17	SDS (1 wt.%)	1-2	0.2	50,000	0	5	1	5	None
Case 18	SDS (1 wt.%)	3-6	0.2	50,000	0	5	1	5	None
Case 19	SDS (1 wt.%)	1-2	0.1	50,000	2	5	1	5	None
Case 20	SDS (1 wt.%)	3-6	0.1	50,000	2	5	1	5	None
Case 21	SDS (1 wt.%)	1-2	0.2	50,000	2	5	1	5	None
Case 22	SDS (1 wt.%)	3-6	0.2	50,000	2	5	1	5	None
Case 23	SDS (1 wt.%)	3-6	0.2	50,000	0	5	1	5	None
Case 24	SDS (1 wt.%)	5-10	1	30,000	0	5	-	5	None
Case 25	SDS (1 wt.%)	5-10	2	30,000	0	5	-	5	None
Case 26	SDS (1 wt.%)	5-10	4	30,000	0	5	-	5	None
Case 27	*Twinmax*	5-10	1	30,000	0	5	3	5	None
Case 28	*Lubrimax Edel C*	5-10	1	30,000	0	5	3	5	None
Case 29	*Canola oil*	5-10	1	30,000	0	5	3	5	None
Case 30	*DiaMond 80*	5-10	1	30,000	0	5	3	5	None
Case 31	*Petrofer Iso-cut R – 10 HM*	5-10	1	30,000	0	5	3	5	None
Case 32	SDS (1 wt.%)	5-10	1	30,000	0	5	3	5	None

Case	MWF	Grit size in µm	Feed rate in mm/min	Rotational speed in rpm	Inclination angle in °	Depth of cut in µm	Channel length in mm	Channel depth in µm	Cavity
Case 33	SDS (5 wt.%)	5-10	1	30,000	0	5	3	5	None
Case 34	*Twinmax*	5-10	30	30,000	0	0.5	5	50	None
Case 35	*Lubrimax Edel C*	5-10	30	30,000	0	0.5	5	50	None
Case 36	*Twinmax*	4-8	30	30,000	0	0.5	5	50	None
Case 37	*Twinmax*	6-12	30	30,000	0	0.5	5	50	None
Case 38	*Twinmax*	5-10	30	10,000	0	0.5	5	50	None
Case 39	*Twinmax*	5-10	30	50,000	0	0.5	5	50	None
Case 40	*Twinmax*	5-10	30	30,000	0	0.5	5	50	Cavity
Case 41	*Twinmax*	5-10	120	120,000	0	0.5	5	50	None
Case 42	*Twinmax*	5-10	240	120,000	0	0.5	5	50	None

11 References

[Anan12] K.P. Anandan, A.S. Tulsian, A. Donmez, O.B. Ozdoganlar: A Technique for measuring radial error motions of ultra-high-speed miniature spindles used for micromachining. Precision Engineering 36/1 (2012): S. 104-120.

[Arra16a] P.A. Arrabiyeh, V. Raval, B. Kirsch, M. Bohley, J.C. Aurich: Electroless Plating of Micro Pencil Grinding Tools with 5-10 µm sized cBN Grits. Advanced Materials Research 1140 – Proceedings of the WGP Congress 2016 – Progress in Production Engineering, 2016.

[Arra16b] P.A. Arrabiyeh, B. Kirsch, J.C. Aurich: Development of Micro Pencil Grinding Tools via an Electroless Plating Process. Volume 1: Processing, (2016): V001T02A006.

[Arra17a] P.A. Arrabiyeh, M. Bohley, F. Ströer, B. Kirsch, J. Seewig, J.C. Aurich: Experimental Analysis for the Use of Sodium Dodecyl Sulfate as a Soluble Metal Cutting Fluid for Micromachining with Electroless-Plated Micropencil Grinding Tools. Inventions 2/29 (2017).

[Arra17b] P.A. Arrabiyeh, B. Kirsch, J.C. Aurich: Development of Micro Pencil Grinding Tools Via an Electroless Plating Process. Journal of Micro and Nano-Manufacturing 5/1 (2017): 011002-1-011002-6.

[Arra18] P.A. Arrabiyeh, B. Kirsch, J.C. Aurich: Electroless plating and application of micro pencil grinding tools with a diameter of ~5 µm. euspen's 18th International Conference, 2018.

[Arra19a] P.A. Arrabiyeh, D. Setti, S. Basten, B. Kirsch, J.C. Aurich: Micro grinding 16MnCr5 hardened steel using micro pencil grinding tools with diameters ∼50 µm. CIRP Journal of Manufacturing Science and Technology (2019).

[Arra19b] P.A. Arrabiyeh, M. Heintz, B. Kirsch, J.C. Aurich: Custom made electroless plated dicing blades for micro machining operations. euspen's 19th International Conference & Exhibition, Bilbao, Spain: 2019.

[Arra19c] P.A. Arrabiyeh, M. Dethloff, C. Müller, B. Kirsch, J.C. Aurich: Optimization of Micropencil Grinding Tools Via Electrical Discharge Machining. Journal of Manufacturing Science and Engineering 141/3 (2019): 31005-1-31005-9.

[Arra20] P.A. Arrabiyeh, M. Heintz, S. Kieren-Ehses, M. Bohley, B. Kirsch, J.C. Aurich: Submerged micro grinding: a metalworking fluid application study. International Journal of Advanced Manufacturing Technology 107 (2020): 3807-3815.

[Auri08] J.C. Aurich, R. Haberland, G.M. Schüler, J. Engmann: Mikroschaftwerkzeuge für die Fräs- und Schleifbearbeitung. Neue Wege zur Herstellung und Anwendung. Wt Werkstattstechnik Online 98/11-12 (2008): S. 944-949.

[Auri09] J.C. Aurich, J. Engmann, G.M. Schueler, R. Haberland: Micro grinding tool for manufacture of complex structures in brittle materials. CIRP Annals 58/1 (2009): S. 311-314.

[Auri10a] J.C. Aurich, J. Engmann, G.M. Schüler, M. Walk: Micro-EDM-device for machining tungsten carbide in a desktop machine tool. Proceedings of the 10th International Conference of the Eurpean Society for Precision Engineering and Nanotechnology, 2010.

[Auri10b] J.C. Aurich, J. Engmann, M. Walk: Zerspanen mit Mikroschleifstiften - Zylindrische und formoptimierte Mikroschaftschleifstifte bei der Hartmetallzerspanung – Untersuchung und Vergleich. Wt Werkstattstechnik Online 100/11/12 (2010).

[Auri12] J.C. Aurich, I.G. Reichenbach, G.M. Schüler: Manufacture and application of ultra-small micro end mills. CIRP Annals 61/1 (2012): S. 83-86.

[Auri17] J.C. Aurich, M. Bohley, I.G. Reichenbach, B. Kirsch: Surface quality in micro milling - Influences of spindle and cutting parameters. CIRP Annals 66/1 (2017): S. 101-104.

[Aziz12a] M. Aziz, O. Ohnishi, H. Onikura: Innovative micro hole machining with minimum burr formation by the use of newly developed micro compound tool. Journal of Manufacturing Processes 14/3 (2012): S. 224-232.

[Aziz12b] M. Aziz, O. Ohnishi, H. Onikura: Innovative micro hole machining with minimum burr formation by the use of newly developed micro compound tool. Journal of Manufacturing Processes 14/3 (2012): S. 224-232.

[Bamb09] E. Bamberg, S. Heamawatanachai: Orbital electrode actuation to improve efficiency of drilling micro-holes by micro-EDM. Journal of Materials Processing Technology 209/4 (2009): S. 1826-1834.

[Bifa88] T.G. Bifano: Ductile-regime grinding of brittle materials. North Carolina State University, (1988).

[Bill57] J. Billiter: Galvanotechnik. 2. Aufl. Springer-Verlag, (1957).

[Bobz13] K. Bobzin: Oberflächtentechnik für den Maschinenbau. 1. Auflage Wiley-VCH Verlag GmbH & Co. KGaA, (2013).

[Bohl16] M. Bohley, I.G. Reichenbach, Müller Christopher, J.C. Aurich: Development of a desktop machine tool for integrated ultra-small micro end mill production and application. Proceedings of the 11th International Conference on Micro Manufacturing, 2016.

[Bren47] A. Brenner, G. Riddell: Deposition of nickel and cobalt by chemical reduction. Journal of Research of the National Bureau of Standards 39/5 (1947): S. 385.

[Brie14] H. Briehl: Chemie der Werkstoffe. 3., überarb. und erw. Aufl. Springer Vieweg, (2014).

[Brin10] E. Brinksmeier, Y. Mutlugünes, F. Klocke, J.C. Aurich, P. Shore, H. Ohmori: Ultra-precision grinding. CIRP Annals 59/2 (2010): S. 652-671.

[Brud06] G. Brudek, J.P. Wulfsberg: Kühlschmierung beim Mikrofräsen - Einfluss der Kühlschmierfahren und -stoffe auf die erzeugte Oberflächengüte beim Mikrofräsen. Werkstattstechnik online 96/1 (2006): S. 6-11.

[Buhl17] M. Buhlert: Electropolishing - Electrolytic brightening, smoothing and deburring of stainless steel, steel, brass, copper, aluminium, titanium and magnesium. 1st edition with 111 pictures and 3 tables Leuze Verlag, (2017).

[Carr16] M. Carrella: Zerspanungsmechanismen beim Mikroschleifen von einkristallinem Silizium. Technische Universität, (2016).

[Chen13] K. Cheng, D. Huo: Micro cutting - Fundamentals and applications. Wiley, (2013).

[Chen14] J. Cheng, Y.D. Gong: Experimental study of surface generation and force modeling in micro-grinding of single crystal silicon considering crystallographic effects. International Journal of Machine Tools and Manufacture 77 (2014): S. 1-15.

[Cheo04] W.J. Cheong, B.L. Luan, D.W. Shoesmith: The effects of stabilizers on the bath stability of electroless Ni deposition and the deposit. Applied Surface Science 229/1-4 (2004): S. 282-300.

[Degn15] W. Degner, H. Lutze, Smejkal Erhard: Spanende Formung - Theorie - Berechnung - Richtwerte. 17. Aufl. Carl Hanser Verlag GmbH & Co., (2015).

[Denk11] B. Denkena, H.K. Tönshoff: Spanen - Grundlagen. Springer-Verlag Berlin Heidelberg, (2011).

[Diam10] N.N: Firmenschrift Diametal AG/SA www.diametal.ch/diametal/images/stories/downloads/Kat_ 2 d e.pdf, 2010.

[DiBa10] G.A. DiBari: Electrodeposition of Nickel. Modern Electroplating, Hoboken, NJ, USA: John Wiley & Sons, Inc, 2010.

[DiBi89] D.D. DiBitonto, P.T. Eubank, M.R. Patel, M.A. Barrufet: Theoretical models of the electrical discharge machining process. I. A simple cathode erosion model. Journal of Applied Physics 66/9 (1989): S. 4095-4103.

[DIN00]: DIN 50150:2000-10 Testing of metallic materials - Conversion of hardness values, 2000.

[DIN09]: Geometrical product specifications (GPS) – Surface texture: Profile method – Terms, definitions and surface texture parameters, 2009.

[DIN12]: DIN EN ISO 16610-21: Geometrical product specifications (GPS) – Filtration – Part 21: Linear profile filters: Gaussian filters, 2012.

[DIN13]: DIN 51385:2013-12: Lubricants - Processing fluids for forming and machining of materials - Terms, 2013.

[DIN85]: DIN 50133:1985-02 Testing of metallic materials; Vickers hardness test, HV 0,2 to HV 100, 1985.

[DIN97]: DIN EN ISO 11562: Geometrical product specifications (GPS) – Surface texture: Profile method – Metrological characteristics of phase correct filters, 1997.

[DIN98]: DIN EN 10084:1998-06 Case hardening steels - Technical delivery conditions; German version EN 10084:1998, 1998.

[DIN99]: DIN EN ISO 4957 Tool steels (ISO 4957:1999); German version EN ISO 4957:1999, 1999.

[Disc18] Disco: Resin Bond Blades P1A-Series. URL: <https://www.disco.co.jp /eg/products/catalog/pdf/p1a.pdf>.

[Dorn06] D. Dornfeld, S. Min, Y. Takeuchi: Recent Advances in Mechanical Micromachining. CIRP Annals 55/2 (2006): S. 745-768.

[Dröd19] Dröder K., H.-W. Hoffmeister, Tounsi T.: Structured CVD coated diamond abrasive tools. euspen's 19th International Conference & Exhibition, 2019.

[Ebbr00] S. Ebbrell, N.H. Woolley, Y.D. Tridimas, D.R. Allanson, W.B. Rowe: The effects of cutting fluid application methods on the grinding process. International Journal of Machine Tools and Manufacture 40/2 (2000): S. 209-223.

[Ecks87] H.-J. Eckstein: Technologie der Wärmebehandlung von Stahl. 2. Aufl. Deutscher Verlag für Grundstoffindustrie, (1987).

[Egas02] K. Egashira, Mizutani K.: Micro-drilling of monocrystalline silicon using a cutting tool. Precision Engineering 26 (2002): S. 263-268.

[Egas11a] K. Egashira, S. Hosono, S. Takemoto, Y. Masao: Fabrication and cutting performance of cemented tungsten carbide micro-cutting tools. Precision Engineering 35/4 (2011): S. 547-553.

[Egas11b] K. Egashira, S. Hosono, S. Takemoto, Y. Masao: Fabrication and cutting performance of cemented tungsten carbide micro-cutting tools. Precision Engineering 35/4 (2011): S. 547-553.

[Ekme07] B. Ekmekci: Residual stresses and white layer in electric discharge machining (EDM). Applied Surface Science 253/23 (2007): S. 9234-9240.

[Engi92] F. Engineer: Experimental Measurement of Fluid Flow Through the Grinding Zone. Journal of Manufacturing Science and Engineering 114/1 (1992): S. 61.

[Engm11] J. Engmann: Galvanisch gebundene Mikroschleifstifte - Entwicklung, Herstellung und Einsatz. Techn. Univ, (2011).

[Feng10] J. Feng: Microgrinding of ceramic materials. (2010).

[Ferr07] J.C. Ferreira: A study of die helical thread cavity surface finish made by Cu-W electrodes with planetary EDM. The International Journal of Advanced Manufacturing Technology 34/11-12 (2007): S. 1120-1132.

[Feyn59] R.P. Feynman: There's Plenty of Room at the Bottom. An Invitation to Enter a New Field of Physics, 1959, Annual American Physical Society meeting at California Institute of Technology (Caltech).

[Feyn91] R.P. Feynman: There's Plenty of Room at the Bottom. Science 254/11 (1991): S. 1300-1301.

[Feyn95] R.P. Feynman, C. Sykes: No ordinary genius - The illustrated Richard Feynman. Norton, (1995, 1994).

[Fisc01] U. Fischer: Tabellenbuch Metall. 41., neubearb. und ew. Aufl., 7. Dr Verl. Europa-Lehrmittel Nourney Vollmer, (2001).

[Fond08] P. Fonda, Z. Wang, K. Yamazaki, Y. Akutsu: A fundamental study on Ti–6Al–4V's thermal and electrical properties and their relation to EDM productivity. Journal of Materials Processing Technology 202/1-3 (2008): S. 583-589.

[Frie96] C.R. Friedrich, M.J. Vasile: The micromilling process for high aspect ratio microstructures. Microsystem Technologies 2/3 (1996): S. 144-148.

[Frit08] A.H. Fritz, G. Schulze: Fertigungstechnik. 8., neu bearbeitete Aufl. Springer-Verlag Berlin Heidelberg, (2008).

[Gäbl03] J. Gäbler, L. Schäfer, B. Menze, H.-W. Hoffmeister: Micro abrasive pencils with CVD diamond coating. Diamond and Related Materials 12/3-7 (2003): S. 707-710.

[Gäbl10] J. Gäbler, S. Pleger: Precision and micro CVD diamond-coated grinding tools. International Journal of Machine Tools and Manufacture 50/4 (2010): S. 420-424.

[Gäbl99] J. Gäbler, L. Schäfer, A. Wenda, H.-W. Hoffmeister: Development and application of CVD diamond micro tools for milling and grinding. euspen's 1st International Euspen Conference, Bremen, 1. Aufl. Aachen, Germany: Shaker Verlag, 1999.

[Gaid12] B. Gaida: Einführung in die Galvanotechnik - Grundlagen der chemischen, elektrochemischen, physikalischen und elektrotechnischen Begriffe ; mit 21 Tabellen. 10., neu überarb. Aufl. Leuze, (2012).

[Godd12] W.A. Goddard: Handbook of nanoscience, engineering, and technology. 3rd ed. CRC Press, (2012).

[Gran17] Granta Design Ltd.: CES EduPack Software . In: J.C. Aurich (Hrsg.): Produktionstechnische Berichte aus dem FBK. Band 2012, Granta Design Ltd.: Cambridge, UK,: Techn. Univ., 2017.

[Grig09] A.E. Grigorescu, C.W. Hagen: Resists for sub-20-nm electron beam lithography with a focus on HSQ: state of the art. Nanotechnology 20/29 (2009): S. 1-31.

[Guo02] D.C. Guo, V.Y. Karelin: Abrasive Erosion & Corrosion of Hydraulic Machinery. Imperial College Press, (2002).

[Gvin05] V. Gviniashvili, J. Webster, B. Rowe: Fluid Flow and Pressure in the Grinding Wheel-Workpiece Interface. Journal of Manufacturing Science and Engineering 127/1 (2005): S. 198-205.

[Haef17] Haefeli Diamantwerkzeugfabrik AG: Product catalog for internal grinding. (2017).

[Hess02] Hesselbach, J.(Hrsg.): MikroPRO - Untersuchung zum internationalen Stand der Mikroproduktionstechnik. Essen: Techn. Univ., Vulkan-Verl., 2002.

[Hoff00] H.-W. Hoffmeister, A. Wenda: Novel Grinding Tools for Machining Precision Micro Parts of Hard and Brittle Materials. Proceedings of the 15th annual meeting of ASPE, 2000.

[Hoff02] H.-W. Hoffmeister, M. Hlavac: Schleifen von Mikrostrukturen. Tagungsband des 10. Feinbearbeitungskolloqiums in Braunschweig 2002 (2002): 7.1–7.24.

[Jand03] G. Jander, K.F. Jahr, G. Schulze: Maßanalyse - Theorie und Praxis der Titrationen mit chemischen und physikalischen Indikationen ; [mit 21 Tabellen]. 16. Aufl. De Gruyter, (2003).

[Japp05] J.W. Jappes, B. Ramamoorthy, P.K. Nair: A study on the influence of process parameters on efficiency and crystallinity of electroless Ni–P deposits. Journal of Materials Processing Technology 169/2 (2005): S. 308-313.

[Joch16] N. Jochum: Zerspanung ultraharter Keramik am Beispiel einer dreigliedrigen Zahnbrücke. 1. Auflage Shaker, (2016).

[Kana07] N. Kanani: Chemische Vernicklung - Nickel-Phosphor-Schichten : Herstellung, Eigenschaften, Anwendungen. 1. Aufl. Leuze, (2007).

[Kass69] G. Kassen: Beschreibung der elementaren Kinematik des Schleifvorganges. Rheinisch-Westfälische Technische Hochschule Aachen, (1969).

[Kier18] S. Kieren-Ehses, M. Bohley, P.A. Arrabiyeh, B. Kirsch, J.C. Aurich: Influence of different metal working fluids when micro machining cp-titanium with 50 µm diameter micro end millsArticle. 4th CIRP Conference on Surface Integrity (CSI 2018), 2018.

[Kirs17] B. Kirsch, M. Bohley, P.A. Arrabiyeh, J.C. Aurich: Application of Ultra-Small Micro Grinding and Micro Milling Tools - Possibilities and Limitations. Micromachines 8/9 (2017): S. 261-279.

[Kloc09] F. Klocke: Manufacturing Processes 2 - Grinding, Honing, Lapping. Springer-Verlag Berlin Heidelberg, (2009).

[Kloc16] F. Klocke, C. Wirtz, S. Mueller, P. Mattfeld: Analysis of the Material Behavior of Cemented Carbides (WC-Co) in Grinding by Single Grain Cutting Tests. Procedia CIRP 46 (2016): S. 209-213.

[Köni80] W. König: Schleifen, Honen, Läppen. VDI-Verlag, (1980).

[Lach06] F. Lacharme, M.A.M. Gijs: Pressure injection in continuous sample flow electrophoresis microchips. Sensors and Actuators B: Chemical 117/2 (2006): S. 384-390.

[Laue80] H. Lauer-Schmaltz, W. König: Phenomenon of Wheel Loading Mechanisms in Grinding. CIRP Annals 29/1 (1980): S. 201-206.

[Lawn75] B.R. Lawn, Wilshaw Rodney: Indentation fracture: principles and applications. Journal of material science 10 (1975): S. 1049-1081.

[Lee05] S.B. Lee, Y. Tani, T. Enomoto, H. Sato: Development of a Dicing Blade With Photopolymerizable Resins for Improving Machinability. CIRP Annals 54/1 (2005): S. 293-296.

[Liao05] Y.-S. Liao, S.-T. Chen, C.-S. Lin, T.-J. Chuang: Fabrication of high aspect ratio microstructure arrays by micro reverse wire-EDM. Journal of Micromechanics and Microengineering 15/8 (2005): S. 1547-1555.

[Lin02] K.-L. Lin, J.-W. Hwang: Effect of thiourea and lead acetate on the deposition of electroless nickel. Materials Chemistry and Physics 76/2 (2002): S. 204-211.

[Lou06] H.H. Lou, Y. Huang: Electroplating. Encyclopedia of chemical processing, New York NY: Marcel Dekker, 2006.

[Luo98] Y.F. Luo: An evaluation of spark mobility in electrical discharge machining. IEEE Transactions on Plasma Science 26/3 (1998): S. 1010-1016.

[Ma16] X. Ma, H. Zheng, M. Tian: Optimize the shape of curved-Fresnel lens to maximize its transmittance. Solar Energy 127 (2016): S. 285-293.

[Mahe10] S. Mahendran, R. Devarajan, T. Nagarajan, A. Majdi: Review of Micro-EDM. Proceedings of the International Multiconference of Engineers and Computer Scientists, 2010.

[Malk08] S. Malkin, C. Guo: Grinding technology - Theory and applications of machining with abrasives. 2. ed. Industrial Press, (2008).

[Mall90] Mallory, G.O.; Hajdu, J.B.(Hrsg.): Electroless plating - Fundamentals and applications. Orlando, Fla.: Techn. Univ., The Society, op. 1990.

[Mars09] E. Marsh: Precision Spindle Metrology, Second Edition. DEStech Publications, Incorporated, (2009).

[Mars83] D.B. Marshall, A.G. Evans, B.T. Khuri Yakub, J.W. Tien, G.S. Kino: The nature of machining damage in brittle materials. The royal society London 385, 1789. Aufl. 1983.

[Mars86] D.B. Marshall, B.R. Lawn: Indentation of Brittle Materials, Microindentation Techniques in Materials Science and Engineering. ASTM STP 889, 1986.

[Masu00] T. Masuzawa: State of the art of micro machining. CIRP Annals 49/2 (2000): S. 473-488.

[Masu85] T. Masuzawa, M. Fujino, K. Kobayashi, T. Suzuki, N. Kinoshita: Wire Electro-Discharge Grinding for Micro-Machining. CIRP Annals 34/1 (1985): S. 431-434.

[May00] P.W. May: Diamond thin films: a 21st-century material. Philosophical Transactions of the Royal Society A: Mathematical, Physical and Engineering Sciences 358/1766 (2000): S. 473-495.

[Morg05] C. Morgan, R.R. Vallance, E.R. Marsh: Micro Grinding Blind Holes in Hard Tungsten Carbide with Polycrystalline Diamond Micro Tools. (2005).

[Morg07] C.J. Morgan, R.R. Vallance, E.R. Marsh: Specific Grinding Energy While Microgrinding Tungsten Carbide with Polycrystaline Diamond Micro Tools. International Conference on Micromanufacturing 2, 2007.

[Müll19] C. Müller: Kompakte Luftlagerspindeln für die spanende Mikrobearbeitung auf Desktop-Werkzeugmaschinen. (2019).

[Nam15] J.S. Nam, D.H. Kim, H. Chung, S.W. Lee: Optimization of environmentally benign micro-drilling process with nanofluid minimum quantity lubrication using response surface methodology and genetic algorithm. Journal of Cleaner Production 102 (2015): S. 428-436.

[Nano18] Nanofocus: Technologie - optische Messtechnik URL: <https://www.nanofocus.de/technologie/messprinzipien/usurf-technologie/>. <URL: <https://www.nanofocus.de/technologie/messprinzipien/usurf-technologie/>> -.

[Oelh18] Oelheld GmbH.: http://www.oelheld.de/.

[Oert11] H. Oertel, M. Böhle: Strömungsmechanik - Grundlagen - Grundgleichungen - Lösungsmethoden - Softwarebeispiele. 6. Aufl. Vieweg + Teubner, (2011).

[Okan93] K. Okano, T. Waida, T. Suto, J. Mizuno, T. Kobayashi: Micro-grinding of Micromachine Parts. 1st international ABTEC conference in Seoul, Korea, 1. Aufl. 1993.

[Osen65] C. van Osenbruggen, G. Luimes, A. van Dijk, J.G. Siekman, N.V. Philips': Micro-Spark Erosion as a Technique in Micro-miniaturization. IFAC Proceedings Volumes 2/3 (1965): S. 485-493.

[Park10] H.-K. Park, H. Onikura, O. Ohnishi, A. Sharifuddin: Development of micro-diamond tools through electroless composite plating and investigation into micromachining characteristics. Precision Engineering 34/3 (2010): S. 376-386.

[Park97] R. Parkinson: Properties and applications of electroless nickel deposits. Technical Series No. 10081, Nickel Development Institute (1997).

[Pate89] M.R. Patel, M.A. Barrufet, P.T. Eubank, D.D. DiBitonto: Theoretical models of the electrical discharge machining process. II. The anode erosion model. Journal of Applied Physics 66/9 (1989): S. 4104-4111.

[Pauc08] E. Paucksch, S. Holsten, M. Linß, F. Tikal: Zerspantechnik - Prozesse, Werkzeuge, Technologien ; mit 45 Tabellen. 12., vollst. überarb. und erw. Aufl. Vieweg + Teubner, (2008).

[Petr18] Petrofer Chemie H. R. Fischer GmbH + Co. KG.: https://www.petrofer.com/de/.

[Pham14] M.-Q. Pham, H.-S. Yoon, V. Khare, S.-H. Ahn: Evaluation of ionic liquids as lubricants in micro milling – process capability and sustainability. Journal of Cleaner Production 76 (2014): S. 167-173.

[Pica03] Y.N. Picard, D.P. Adams, M.J. Vasile, Ritchey M. B.: Focused ion beam-shaped microtools for ultra-precision machining of cylindrical components. Precision Engineering 27 (2003): S. 59-69.

[Ratn16] C. Ratnam, K. Arun Vikram, B.S. Ben, B.S.N. Murthy: Process monitoring and effects of process parameters on responses in turn-milling operations based on SN ratio and ANOVA. Measurement 94 (2016): S. 221-232.

[Reic17] I.G. Reichenbach: Beitrag zur Beherrschung der Mikrofräsbearbeitung von Polymethylemethacrylat. Als Manuskript gedruckt Technische Universität Kaiserslautern, Lehrstuhl für Fertigungstechnik und Betriebsorganisation, (2017).

[Roul17] E. Rouly, R.J. Bauer, A. Warkentin: An investigation into the effect of nozzle shape and jet pressure in profile creepfeed grinding. Proceedings of the Institution of Mechanical Engineers, Part B: Journal of Engineering Manufacture 231/7 (2017): S. 1116-1130.

[Rowe09] W.B. Rowe: Principles of modern grinding technology. William Andrew, (2009).

[Rowe18] W. Rowe: Towards High Productivity in Precision Grinding. Inventions 3/2 (2018): S. 24.

[Rügg19] M. Rüggeberg: Zerspanuntersuchungen an technischen Keramiken mit Mikroschleifprozessen. [1. Auflage] Vulkan-Verlag GmbH, (2019).

[Sail09] V. Saile: LIGA and its applications. Wiley-VCH, (2009).

[Sait08] Y. Saito, S. Okamoto, A. Miki, H. Inomata, T. Hidaka, H. Kasai: Fabrication of micro-structure on glass surface using micro-indentation and wet etching process. Applied Surface Science 254/22 (2008): S. 7243-7249.

[Salj87] E. Saljé, H. Möhlen: Prozessoptimierung beim Schleifen keramischer Werkstoffe. IDR 21 4 (1987): S. 243-247.

[Salv72] G. Salvago, P.L. Cavalotti: Characteristics of the chemical reduction of nickel alloys with hypophosphite. Plating 59/7 (1972): S. 665-671.

[Schl01] S. Schlautmann, H. Wensink, R. Schasfoort, M. Elwenspoek, A.-v.-d. Berg: Powder-blasting technology as an alternative tool for microfabrication of capillary electrophoresis chips with integrated conductivity sensors. Institute of Physics, (2001).

[Schl06] H. Schlichting, K. Gersten: Grenzschicht- theorie. 10., überarbeitete Aufl. Springer, (2006).

[Schl10a] Schlesinger, M.; Paunovic, M.(Hrsg.): Modern Electroplating. Hoboken, NJ, USA: Techn. Univ., John Wiley & Sons, Inc, 2010.

[Schl10b] M. Schlesinger: Electroless Deposition of Nickel. Modern Electroplating, Hoboken, NJ, USA: John Wiley & Sons, Inc, 2010.

[Schm06] K. Schmidt: Mikrofräswerkzeuge aus Hartmetall. (2006).

[Schm08] C. Schmidt: Koordinatenschleifen dentalkeramischer Werkstoffe mit kleinen Diamantwerkzeugen. Shaker, (2008).

[Schw03] C. Schwietering: Technologische Aspekte der mikromechanischen Fräsbearbeitung mit Schaftwerkzeugen. Vulkan-Verl., (2003).

[Sett15] D. Setti, M.K. Sinha, S. Ghosh, P. Venkateswara Rao: Performance evaluation of Ti–6Al–4V grinding using chip formation and coefficient of friction under the influence of nanofluids. International Journal of Machine Tools and Manufacture 88 (2015): S. 237-248.

[Sett18] D. Setti, B. Kirsch, P.A. Arrabiyeh, J.C. Aurich: Visualization of geometrical deviations in micro grinding by kinematic simulations. Proceedings of the 13th Manufacturing Science and Engineering Conference, 2018.

[Sett19] D. Setti, B. Kirsch, J.C. Aurich: Characterization of micro grinding tools using optical profilometry. Optics and Lasers in Engineering 121 (2019): S. 150-155.

[Sett20] D. Setti, P.A. Arrabiyeh, B. Kirsch, M. Heintz, J.C. Aurich: Analytical and experimental investigations on the mechanisms of surface generation in micro grinding. International Journal of Machine Tools and Manufacture 149 (2020): S. 103489.

[Shab11] M. Shabgard, H. Kakolvand, M. Seyedzavvar, R.M. Shotorbani: Ultrasonic assisted EDM - Effect of the workpiece vibration in the machining characteristics of FW4 Welded Metal. Frontiers of Mechanical Engineering 43/13 (2011): S. 1287.

[Sing12] V. Singh, P. Venkateswara Rao, S. Ghosh: Development of specific grinding energy model. International Journal of Machine Tools and Manufacture 60 (2012): S. 1-13.

[Sing78] E. Singer, E. Strauss: Korrosion und Oberflächenbehandlung. Schroedel, (1978).

[Smul00] E. Smulders, W.-V. Rybinski, E. Sung, W. Rähse, J. Steber, F. Wiebel: Ullmann's Encyclopedia of Industrial Chemistry. Wiley-VCH Verlag GmbH & Co. KGaA, (2000).

[Somm14] K. Sommer, R. Heinz, J. Schöfer: Verschleiß metallischer Werkstoffe - Erscheinungsformen sicher beurteilen ; mit zahlreichen Tabellen. 2., korrigierte und erg. Aufl. Springer Vieweg, (2014).

[Spic07] U. Spicher, M. Lüft: Optimierung der Kraftstoffstrahlausbreitung für Pflanzenöl, insbesondere natürliches Rapsöl, bei der Verwendung moderner Diesel-Einspritzsysteme. Institut für Kolbenmaschinen, (2007).

[Spur89] G.e.a. Spur: Keramikbearbeitung. Hanser, (1989).

[Stei18] Steidle GmbH: https://www.steidle-gmbh.de/.

[Stra87] A. Strauch: Galvanotechnisches Fachwissen - Mit 59 Tabellen. 2., überarb. Aufl. Dt. Verl. für Grundstoffindustrie, (1987).

[Stra90] A. Strauch: Galvanotechnisches Fachwissen. 3. Aufl. VEB, (1990).

[Suzu01] H. Suzuki, T. Higuchi, Nishioka Masahiko, Kitajima Takayuki, Yui Akinori, Okuyama Shigeki, Shibutani Hideo, Horiuchi Osamu: Precision Grinding of Micro Fresnel Shape and Precision Glass Molding of Micro Fresnel Lens. Proceedings of the 16th Annual Meeting of the ASPE, 25. Aufl. 2001.

[Tara50] L.P. Tarasov: Some Metallurgical Aspects of Grinding, Machining - Theory and Practice. ASM (1950): S. 409-464.

[Tiny86] N.N: Tiny Tale Gets Grand. Engineering & Science (1986): S. 24-26.

[Töns93] H.K. Tönshoff: Werkzeuge für die moderne Fertigung - Möglichkeiten zur Rationalisierung in der spanenden Fertigung : mit 176 Bildern und 123 Literaturstellen. expert-Verl., (1993).

[Vasi96] M.J. Vasile, C.R. Friedrich, B. Kikkeri, R. McElhannon: Micrometer-scale machining: tool fabrication and initial results. Precision Engineering 19/2-3 (1996): S. 180-186.

[Walk14] M. Walk, J.C. Aurich: Integrated Desktop Machine Tool for Manufacturing and Application of Ultra-small Micro Pencil Grinding Tools. Procedia CIRP 14 (2014): S. 333-338.

[Walk16] M. Walk: Integriertes Desktopmaschinensystem für die Herstellung und Anwendung ultrakleiner Mikroschleifwerkzeuge. Als Manuskript gedruckt Technische Universität, (2016).

[Ward15] F. Wardle: Ultra precision bearings. Woodhead Publishing, (2015).

[Wass16] R.L. Wasserstein, N.A. Lazar: The ASA's Statement on p -Values - Context, Process, and Purpose. The American Statistician 70/2 (2016): S. 129-133.

[Wats89] Watson S. A.: Electroless Nickel Coatings. Technical Series No. 10055, 1989.

[Watt16] O.P. Watts: Rapid Nickel Plating. 29th general meeting of the American Electrochemical Society, 1916.

[Wegs13] C.W. Wegst, M. Wegst: Stahlschlüssel - Key to Steel = La clé des aciers. 23. Aufl. Verl. Stahlschlüssel Wegst, (2013).

[Wein07] K. Weinert, T. Jansen: Bohrungsfertigung mit Schleifstiften faserverstärkte Keramik effizient bearbeiten. Diamond business 46/2 (2007).

[Wein99] K. Weinert: Trockenbearbeitung und Minimalmengenkühlschmierung - Einsatz in der spanenden Fertigungstechnik. Springer Berlin Heidelberg, (1999).

[Wend02] A. Wenda: Schleifen von Mikrostrukturen in sprödharten Werkstoffen. Vulkan-Verl., (2002).

[Wens02] H. Wensink: Fabrication of microstructures by powder blasting. University of Twente [Host], (2002).

[Wern71] G. Werner: Kinematik und Mechanik des Schleifprozesses. Rheinisch-Westfälische Technische Hochschule Aachen, (1971).

[Worl60] N.N: The World's smallest Motor. The Times from San Mateo, California (1960): S. 25.

[Yama04] Y. Yamamoto, H. Suzuki, T. Okino, Y. Hijikata, Moriwaki Toshimichi: Ultra Precision Grinding of Micro Aspherical Surface - Development of a Three-Axes Controlled Single Point Inclined Grinding Method. Proceedings of the 13th Annual Meeting of the ASPE, 34. Aufl. St. Louis, USA: 2004.

[Yeh01] L.-Y. Yeh: Einfluss von Bearbeitungsparametern auf die Oberflächen- und Werkstoffeigenschaften von laserbearbeiteten Mikrobauteilen. Shaker, (2001).

[Yu09] Z.Y. Yu, Y. Zhang, J. Li, J. Luan, F. Zhao, D. Guo: High aspect ratio micro-hole drilling aided with ultrasonic vibration and planetary movement of electrode by micro-EDM. CIRP Annals 58/1 (2009): S. 213-216.

[Zeid12] H. Zeidler: Schwingungsunterstützte Mikro-Funkenerosion. Verlag Wissenschaftliche Scripten, (2012).

[Zhan04] Q. Zhang: Study on technology of ultrasonic vibration aided electrical discharge machining in gas. Journal of Materials Processing Technology (2004).

Directory of supervised student research projects:

Dethloff, Maximilian:	Weiterentwicklung und Inbetriebnahme einer Mikro-Erodiereinheit für die Optimierung von Mikroschleifstiften, 2017. (german thesis)
Gröls, Jens:	Optimization of the electroplating process of tungsten carbide micro pencil grinding tools for the machining in 16MnCr5, 2016. (german thesis)
Heintz, Marius:	Electroless plating of tungsten carbide micro pencil grinding tools for machining in 16MnCr5, 2016. (german thesis)
	Design and implementation of a splash lubrication system for micromachining 2018. (german thesis)
Hembel, Julian:	Der Einfluss von Natriumdodecylsulfat als Schmierstoff in der Mikrozerspanung, 2018. (german thesis)
Hertel, Christian:	Investigation on the influence of cooling lubricants during the micro grinding process with micro pencil grinding tools, 2016. (german thesis)
Krafczyk, Nico:	Application of electroless plated micro pencil grinding tools with diameters ~5 µm for the machining of hardened 16MnCr5, 2018. (german thesis)
	Electroplating of micro pencil grinding tools made of high speed steel for the machining of hardened 16MnCr5, 2018. (german thesis)
Leismann, Markus	A parameter study on microgrinding with a submerged cutting unit, 2019. (german thesis)
Lenz, Lukas:	A parameter study for machining with micro pencil grinding tools in hardened 16MnCr5, 2017. (german thesis)
	Investigation of the influence of tool parameters for micro pencil grinding tools on the micro grinding process, 2018. (german thesis)
Patel, Anil	An investigation on the influence of up and down grinding on the surface topography in micro grinding, 2019.
Shaikh, Allauddin	Experimental investigations on the influence of the micro pencil grinding tools topography in micro grinding process, 2019.
Zeuner, Valerie:	Study on the application of electroplating and electroless plating in the manufacturing process of grinding tools, 2016. (german thesis)

Lebenslauf

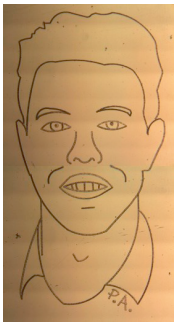

Persönliche Daten:

Name:	Peter Amer Arrabiyeh
Geburtsort:	Bamberg
Eltern:	Mahmoud und Elke Monika Arrabiyeh
Familienstand:	Verheiratet

Schule:

09/1995 – 06/2004	Technisches Gymnasium Don Bosco in Nazareth, Israel Zeugnis der allgemeinen Hochschulreife vom 01.06.2004

Studium:

10/2005 – 02/2013	TU Kaiserslautern, Fachbereich Maschinenbau und Verfahrenstechnik Vertiefungsrichtung: Anlagenbau Diplomzeugnis vom 11.02.2013

Berufstätigkeit:

08/2004 – 08/2005	Lehrling in der Musak Ahim Arrabiyeh Kfz Reparaturwerkstatt in Nazareth, Israel
04/2012 – 03/2013	Wissenschaftliche Hilfskraft beim Lehrstuhl für Messtechnik und Sensorik, TU Kaiserslautern
08/2012 – 03/2013	Wissenschaftliche Hilfskraft beim Lehrstuhl für Thermische Verfahrenstechnik, TU Kaiserslautern
04/2013 – 08/2013	Wissenschaftlicher Mitarbeiter im Bereich Betriebsfestigkeit, Hochschule Kempten
11/2013 – 11/2014	Angestellter bei der Firma Bauer Gear Motor GmbH in Esslingen als Trainee Programm in der Konstruktionsabteilung
12/2014 – 03/2020	Wissenschaftlicher Mitarbeiter am Lehrstuhl für Fertigungstechnik und Betriebsorganisation, TU Kaiserslautern
04/2020 –	Wissenschaftlicher Mitarbeiter am Institut für Verbundwerkstoffe GmbH in Kaiserslautern

Produktionstechnische Berichte aus dem FBK

bereits veröffentlicht wurden

01/09 Aurich, J. C.: Radio Frequency Identification (RFID) in der Fertigung – Handbuch zur Einführung in neue Anwendungsfelder.
2009, ISBN 978-3-941438-08-8 **€ 30,–**

02/09 Stürenburg, B.: Optimierung der Spanbildung und Minimierung des Späneeintrages in das Werkstück für das Bohren von Al-Legierungen.
2009, ISBN 978-3-941438-13-2 **€ 30,–**

03/09 Eyrisch, T.: Optimierung der Herstellung von Vollhartmetallwerkzeugen – Strategie zur Vermeidung von Oberflächenschädigungen.
2009, ISBN 978-3-941438-12-5 **€ 30,–**

04/09 von Killisch-Horn, G.: Erfahrungsbasierte Implementierung von APS-Systemen in der Einzel- und Kleinserienproduktion.
2009, ISBN-978-3-941438-17-0 **€ 30,–**

05/09 Naab, C.: Auslaufmanagement – Konzept zur Abwicklung des Serienauslaufs in der Produktion.
2009, ISBN-978-3-941438-26-2 **€ 35,–**

06/09 Herzenstiel, P.: Hochleistungsplanschleifen mit einer definiert gesetzten CBN-Schleifscheibe.
2009, ISBN-978-3-941438-28-6 **€ 35,–**

07/09 Aurich, J.C.: Lebenszyklusorientierte Konfiguration von Produkt-Service Systemen – Ein Leitfaden für die Praxis.
2009, ISBN-978-3-941438-27-9 **€ 30,–**

01/10 Aurich, J.C.: Organisationsveranstaltung und Kompetenzaufbau bei der Gestaltung und Realisierung investiver Produkt-Service Systeme – Ein Leitfaden für die Praxis.
2010, ISBN-978-3-941438-37-8 **€ 35,–**

02/10 Aurich, J.C.: Gestaltung investiver Produkt-Service Systeme – Ein Leitfaden für die Praxis.
2010, ISBN-978-3-941438-38-5 **€ 35,–**

03/10 Aurich, J.C.: Realisierung investiver Produkt-Service Systeme – Ein Leitfaden für die Praxis.
2010, ISBN-978-3-941438-39-2 **€ 35,–**

04/10 Franke, V.: Einfluss der Werkzeugschneidkante auf die Bohrungsqualität bei der spanenden Bearbeitung langfaserverstärkter Kunststoffe.
2010, ISBN-978-3-941438-53-8 **€ 35,–**

05/10 Sudermann, H.: Gratbildung beim Schleifen – Experimentelle Analyse und Modellierung der Gratbildung sowie Ansätze zur Gratminimierung.
2010, ISBN-978-3-941438-54-5 **€ 35,–**

06/10 Shahzad, M.A.: Analysis of the Machinability of an Aluminum Matrix Composite Material.
2010, ISBN-978-3-941438-56-9 **€ 35,–**

07/10 Gómez Kempf, F.A.: Flexibilitätsorientierte Produktionssysteme – Modulare Gestaltung, Einführung und Nutzung.
2010, ISBN-978-3-941438-58-3 **€ 35,–**

01/11 Engmann, J.: Galvanisch gebundene Mikroschleifstifte – Entwicklung, Herstellung und Einsatz.
2011, ISBN-978-3-941438-59-0 **€ 35,–**

02/11 Leitz, L.: Beitrag zur Beherrschung der Gratbildung bei Bohrungsverschneidungen.
2011, ISBN-978-3-941438-72-9 **€ 35,–**

03/11 Siener, M.: Sicherung der Qualitätsfähigkeit von Produktionsprozessen.
2011, ISBN-978-3-941438-79-8 **€ 35,–**

04/11 Wolf, N.: Modell zur Unterstützung der Analyse von Ausfallursachen bei komplexen mechatronischen Systemen.
2011, ISBN-978-3-941438-89-7 **€ 35,–**

01/12 Faltin, M.: RFID-Einsatz in fertigungstechnischen Prozessketten – Identifikation und Beurteilung von Einsatzpotentialen.
2012, ISBN-978-3-941438-97-2 **€ 35,–**

01/13 Lauer, C.: Integriertes Modell zur Materialflusssimulation und zur Visualisierung in der Virtuellen Realität.
2013, ISBN 978-3-943995-19-0 **€ 35,–**

02/13 Aurich, J.C.: Qualitätsorientierte Instandhaltungsplanung und -steuerung in produktionstechnischen Prozessketten Handbuch für die Praxis.
2013, ISBN 978-3-943995-21-3 **€ 35,–**

03/13 Kirsch, B.: Wirkmechanismen der Kühlschmierstoff-Zufuhr beim Schleifen – Analyse externer und interner Kühlschmierstoff-Zufuhrmethoden.
2013, ISBN 978-3-943995-25-1 **€ 35,–**

04/13 Schweitzer, E.J.: Prozessorientiertes Dienstleistungsproduktionssystem.
2013, ISBN 978-3-943995-30-2 **€ 35,–**

05/13 Malak, R. C.: Methode zur softwarebasierten Planung technischer Änderungen in der Produktion.
2013, ISBN 978-3-943995-34-3 **€ 35,–**

06/13 Yang, X.: Sound Simulation and Visualization in virtual Manufacturing Systems.
2013, ISBN 978-3-943995-39-8 **€ 35,–**

07/13 Kranz, J.-N.: Konzept zur Vermeidung von Produkt-Piraterie Risiken – Ein Ansatz für die Ersatzteile der Investitionsgüterindustrie –
2013, ISBN 978-3-943995-46-6 **€ 35,–**

01/14 Mannweiler, C.: Konfiguration investiver Produkt-Service Systeme.
2014, ISBN 978-3-943995-61-9 **€ 35,–**

02/14 Aurich J.C. (Hrsg.): Produktivität und Qualität von Serviceprodukten – Ein Leitfaden für die Praxis.
2014, ISBN 978-3-943995-65-7 **€ 35,–**

03/14 Waltemode S.: Qualitätsbewertung technischer Produkt-Service Systeme.
2014, ISBN 978-3-943995-68-8 **€ 35,–**

04/14 Bohr C. L.: Vermeidung struktureigener Produktpiraterie bei Ersatzteilen.
2014, ISBN 978-3-943995-69-5 **€ 35,–**

05/14 Olenburg A.: Tribologisches Prozessverhalten beim Bearbeiten von Feinsteinzeug-Fliesen.
2014, ISBN 978-3-943995-76-3 **€ 35,–**

01/15 Zimmermann M.: Drehen von Aluminium-Matrix-Verbundwerkstoffen - Analyse thermischer und mechanischer Einflüsse auf die Fertigungsgenauigkeit bei der Trockenbearbeitung.
2015, ISBN 978-3-943995-94-7 **€ 35,–**

01/16 Adam M.: Konzept zum Umgang mit scheinbar zufälligen Fehlern an technischen Systemen – eine Systematik.
2016, ISBN 978-3-95974-008-1 **€ 35,–**

02/16 Walk M.: Integriertes Desktopmaschinensystem für die Herstellung und Anwendung ultrakleiner Mikroschleifwerkzeuge.
2016, ISBN 978-3-95974-021-0 **€ 35,–**

03/16 Carrella M.: Zerspanungsmechanismen beim Mikroschleifen von einkristallinem Silizium.
2016, ISBN 978-3-95974-032-6 **€ 35,–**

01/17 Reichenbach I. G.: Beitrag zur Beherrschung der Mikrofräsbearbeitung von Polymethylmethacrylat.
2017, ISBN 978-3-95974-042-5 **€ 35,–**

02/17 Fallenstein F.: Kühlkanalaustrittsbedingungen bei VHM-Wendelbohrern - Analyse der Einflüsse von Kühlkanalaustrittsposition und KSS-Volumenstrom auf die Temperatur im Schneidkeil.
2017, ISBN 978-3-95974-056-2 **€ 35,–**

03/17 Winkes P.: Vorgehensmodell für den systematischen Einsatz der Virtuellen Realität zur Unterstützung des Montageplanungsprozesses.
2017, ISBN 978-3-95974-057-9 **€ 35,–**

04/17 Schneider F.: Analyse der Spanbildung und Oberflächenmorphologie beim Mikrospanen von Titanwerkstoffen
2017, ISBN 978-3-95974-059-3 **€ 35,–**

05/17 Mert G.: Kumulierter Energieaufwand technischer Produkt-Service Systeme
2017, ISBN 978-3-95974-074-6 **€ 35,–**

06/17 Weidig C.: Konzept zum prozessgetriebenen Anforderungsmanagement für die Entwicklung mobiler Fabrikplanungs-Apps
2017, ISBN 978-3-95974-075-3 **€ 35,–**

07/17 Cichos D.: Physikalische Modellierung technischer Änderungen in der Produktion
2017, ISBN 978-3-95974-073-9 **€ 35,–**

01/18 Effgen C.: Schneidkantenpräparation mit elastisch gebundenen Schleifwerkzeugen – Konzeptionierung, Entwicklung und Bewertung am Beispiel von Vollhartmetallfräswerkzeugen
2018, ISBN 978-3-95974-089-0 **€ 35,–**

02/18 Kasakow G.: Entwicklung einer ereignisdiskreten Produktionssteuerung
2018, ISBN 978-3-95974-090-6 **€ 35,–**

03/18 Mayer P.: Verformungsinduzierte Martensitbildung beim kryogenen Drehen von metastabilem austenitischem Stahl
2018, ISBN 978-3-95974-098-2 **€ 35,–**

04/18 Herder C.: Konzept zur impliziten Identifikation und Planung von Technologien für die Produktion
2018, ISBN 978-3-95974-101-9 **€ 35,–**

01/19 Müller C.: Kompakte Luftlagerspindeln für die spanende Mikrobearbeitung auf Desktop-Werkzeugmaschinen
2019, ISBN 978-3-95974-105-7 **€ 35,–**

01/20 Meissner H. M.: Integrierte Arbeitsplanung und Produktionssteuerung cyber-physischer Produktionssysteme
2020, ISBN 978-3-95974-125-5 **€ 35,–**

02/20 Sinnwell C.: Methode zur Produktionssystemkonzipierung auf Basis früher Produktinformationen – Ein Beitrag zur Integration von Produktionssystemplanung und Produktentwicklung unter Einsatz des MBSE
2020, ISBN 978-3-95974-127-9 **€ 35,–**

03/20 Bohley M.: Prozess-Maschine-Interaktion beim Mikrofräsen von cp-Titan
2020, ISBN 978-3-95974-130-9 **€ 35,–**

01/21 Hotz H.: Kryogenes Drehen metastabiler austenitischer Stähle – Analyse der Wirkzusammenhänge zwischen Einstellgrößen, Prozessgrößen und Oberflächenmorphologie
2021, ISBN 978-3-95974-146-0

02/21 Arrabiyeh P. A.: Electroless Plated Micro Pencil Grinding Tools: Conception, Manufacturing, and Application
2021, ISBN 978-3-95974-158-3

Lehrstuhl für Fertigungstechnik und Betriebsorganisation

ISBN 978-3-95974-158-3
ISSN 0937-9061

TECHNISCHE UNIVERSITÄT
KAISERSLAUTERN